"NG2 cells" in adult neural plasticity

A thesis submitted for the degree of Doctor of Philosophy in the Faculty of Biomedical Sciences, University College London

By

Konstantina Psachoulia

Wolfson Institute for Biomedical Research
University College London

I, Konstantina Psachoulia, confirm that the work presented in this thesis is my own. Where information has been derived from other sources, I confirm that this has been indicated in the thesis.

Signed

Printed

Abstract

During development oligodendrocyte progenitor cells (OLPs) are responsible for the production of oligodendrocytes. Cells with similar antigenic properties to developmental OLPs persist throughout postnatal life, beyond the cessation of "developmental" myelination. These postnatal cells are often referred to as "NG2 cells" because they (and their perinatal counterparts) express the NG2 proteoglycan, but little is known about their function in the adult brain.

Experiments documented in this Thesis use transgenic lineage tracing technology to characterize the *in vivo* behavior of OLPs in the brain at various ages. Fate mapping of OLPs revealed that they give rise to oligodendrocytes throughout life. In addition, OLPs were shown to generate a small proportion of the projection neurons present in the posterior piriform cortex, while no evidence for astrogliogenesis from OLPs was found.

Cumulative in vivo labelling of OLPs with thymidine analogues (BrdU and EdU) showed that they proliferate continuously throughout life with an increasing cell cycle time with age. At all ages examined, there was a proportion of OLPs that

never underwent cell division, indicating that there are cycling and non-cycling populations of OLPs in the mouse brain that persist throughout life.

The observed contribution of adult-born oligodendrocytes to myelinating the brain was surprisingly large, and raised intriguing questions as to the necessity and function of these new myelinating cells. To investigate this directly, I generated a new transgenic mouse line that when crossed to a transgenic mouse that expresses an inducible form of Cre, can be used to selectively ablate the myelinating oligodendrocytes produced in adult life.

Table of Contents

List of Figures and Tables

Acknowledgments

First and foremost, I would like to thank Kaylene for her supervision, help and support as well as her continuous encouragement and belief in my capabilities during the 3 years of my PhD. I am extremely grateful to her as my PhD experience would not have been the same without her. Without doubt I will miss having such a stimulating and unique person next to me. I would also like to thank Bill Richardson for supervision and for giving me the opportunity to work in his lab. I also benefited from working with Ian and I am thankful to him for his supervision and assistance. All people in the lab welcomed me and assisted me throughout my PhD and most importantly they created a friendly and joyful lab environment that I was very fortunate to work in. In particular, Joanna was always supportive and congenial during the last 3 years.

During these 3 years all my friends and especially Flora had an important role in my life during my PhD. Thank you, Flora, for all the discussions about my PhD in periods of joy and frustration.

Last but not least, I am really grateful to my parents. Without their constant guidance, love and support throughout my whole life, I would not have been able to to acquire my PhD. For this, I dedicate my PhD to them.

Special thanks to my sister Emi, to whom I owe a lot and I would therefore like to dedicate this degree to her as well. She always believed in me and encouraged me to do great things in life. Emi, this is just the first step. I promise I will do my best not to disappoint you in the future.

Abbreviations

AEP	Anterior Entopenducular Area
AMPA	a-amino-3-hydroxy-5-methyl-4-isoxazole propionate
ANOVA	Analysis of Variance
ATP	Adenosine TriPhosphate
BAC	Bacterial Artificial Chromosome
BDNF	Brain Derived Neurotrophic Factor
bHLH	basic helix-loop-helix
bp	base pairs
bFGF	bovine Fibroblast Growth Factor
BrdU	5-bromo-2-deoxyuridine
BSA	Bovine Serum Albumin
Cb	Calbindin
CC	Corpus Callosum
CGE	Caudal Ganglionic Eminence
CNP	2',3'-cyclic nucleotide 3'-phosphodiesterase
CNS	Central Nervous System
Cre	Cre Recombinase
$CreER^{T2}$	Cre Recombinase Estrogen Receptor fusion

Ct	Calretinin
Ctx	Cortex
CY	Cyanine
DAPI	4’,6’-Diamidino-2-phenylidole
dATP	deoxyribo Adenosine Triphosphate
dCTP	deoxyribo Cytosine Triphosphate
DEPC	Diethylpyrocarbonate
dGTP	deoxyribo Guanine Triphosphate
dH_2O	distilled H_2O
DMEM	Dulbecco’s Modified Eagle’s Medium
DNA	DeoxyriboNucleic Acid
DNase	Deoxyribonuclease
dNTPs	Deoxyribonucleotide Triphosphates
DPX	Di-N-Butyle Phthalate in Xylene
DT	Diphtheria Toxin
DTR	Diphtheria Toxin Receptor
dTTP	deoxyribo Thymidine Triphosphate
E	Embryonic day
EBSS	Earles Buffered Saline Solution
E. coli	*Escherichia coli*
EDTA	EthyleneDiamineTetraacetic Acid
EdU	5’-ethynyl-2’-deoxyuridine
EGF	Embryonic Growth Factor
ER	Estrogen Receptor

EtOH	Ethanol
FGF2	Basic fibroblast Growth Factor
FGFR3	Fibroblast Growth Factor Receptor 3
FITC	Fluoroscein isothiocynate
GABA	Gamma-Aminoburytic Acid
GF	Growth Fraction
GFAP	Glial Fibrillary Acidic Protein
GFP	Green Fluorescent Protein
HCl	Hydrochloric Acid
hCG	human chorionic gonadotrophin
HEM	HEPES bufferd essential medium
iCre	improved Cre recombinase
IGF-1	Insulin like Growth Factor-1
IgG	Immunoglobulin G
IgM	Immunoglobulin M
i.p.	intraperitoneal
IPTG	Isopropyl-Beta-d-Thiogalactopyranoside
Kan	Kanamycin
kb	kilobases
KCl	Potassium Chloride
KO	Knock Out
LB	Luria Broth
LGE	Lateral Ganglionic Eminence
LMP	Low Melting Point

MABT	Maleic acid buffered Tween
MAG	Myelin Associated Glycoprotein
MBP	Myelin Basic Protein
MGE	Medial Ganglionic Eminence
MOG	Myelin Oligodendrocyte Glycoprotein
MRI	Magnetic Resonance Imaging
NaCl	Sodium Chloride
NaOH	Sodium Hydroxide
NBT	4-nitro blue tetrazolium chloride
NeuN	Neuronal Nuclear Antigen
NG2	Neuro-Glial Proteoglycan 2
NMDA	N-methyl-D-aspartate
NPY	Neuropeptide Y
OCT	Optimal Cutting Temperature
OD_{600}	Optical Density at 600 nm
OLP	Oligodendrocyte Progenitor
P	Postnatal day
p	Passage number
PBS	Phosphate Buffered Saline
PAC	Phage Artificial Chromosome
PC	Piriform Cortex
PCNA	Proliferating Cell Nuclear Antigen
PCR	Polymerase Chain Reaction
PDGF	Platelet Derived Growth Factor

PDGFRα	Platelet Derived Growth Factor Receptor alpha
PFA	Paraformaldehyde
PFGE	Pulse Field Gel Electrophoresis
PLP	Proteolipid Protein
PNS	Peripheral Nervous System
PSA-NCAM	Polysialylated – Neural Cell Adhesion Molecule
Pv	Palvalbumin
R26-YFP	ROSA26 - Yellow Fluorescent Protein
RNA	RiboNucleic Acid
RNase	Ribonuclease
RT	Room Temperature
SDS	Sodium Dodecyl Sulfate
SSC	Sodium Chloride-Sodium Citrate Buffer
SST	Somatostatin
SVZ	Subventricular Zone
TAE	Tris-Acetate EDTA buffer
TBE	Tris-Borate EDTA Buffer
Tc	Cell cycle time
TE	Tris – EDTA
TENPA	Tris – EDTA NaCl Polyamines
TH	Tyrosine Hydroxylase
TM	Tamoxifen
TRITC	Tetramethylrhodamine isothiocynate
UV	Ultraviolet

VZ	Ventricular Zone
w/v	weigth/volume
WIBR	Wolfson Institute for Biomedical Research
v/v	volume/volume
YFP	Yellow Fluorescent Protein

Chapter 1: Introduction

1.1 Oligodendrocyte morphology and function

The central nervous system (CNS) contains 3 major neural cell types: neurons, astrocytes and oligodendrocytes (**Fig. 1.1**). Oligodendrocytes are found throughout the CNS. However, as they are the myelinating cells of the CNS, it follows that they are in greatest abundance in the white matter, where the necessity for myelination is greatest. Their cell bodies are small in size but they can form as many as 50 separate myelin segments, each wrapping an axon in multispiral membrane myelin (Bunge *et al*., 1961; Bunge *et al*., 1968; Simons and Trotter, 2007; **Fig. 1.2**).

In addition to myelin formation, oligodendrocytes provide mechanical protection for axons and trophic support for neurons (reviewed in McTigue and Tripathi, 2008). For instance, it has been shown that oligodendrocytes promote survival of developing cortical neurons by secreting insulin-like growth factor (IGF)-1 and that they modulate phosphorylated neurofilament levels by secreting glial cell line-derived neurotrophic factor (GDNF) (Wilkins et *al*., 2001; Wilkins *et al.,* 2003). Furthermore, the secretion of brain-derived growth factor (BDNF) and neurotrophin-3 (NT-3) by oligodendrocytes has been shown to promote the survival of cholinergic neurons of the basal forebrain (Dai *et al*., 2003). Dai *et al*. (2001) provided evidence

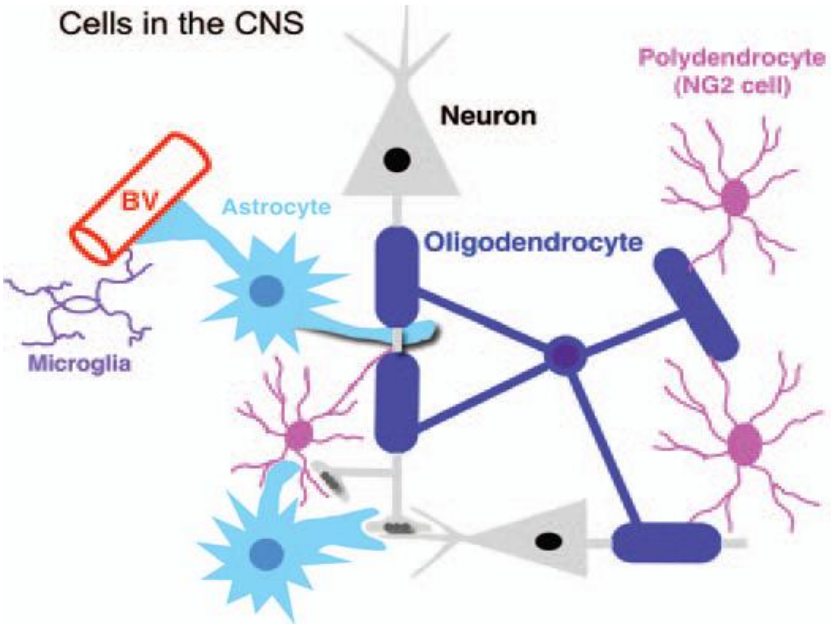

Figure 1.1 *Cells in the CNS. Oligodendrocytes form myelin sheaths. Astrocytes extend processes that surround the vasculature, the synapse, and the node of Ranvier. Oligodendrocyte precursors (NG2 cells) extend processes to nodes of Ranvier in white matter and form synapses with axons in gray matter. In addition to these neuroectoderm-derived cells, resting ramified microglia are thought to originate in the mesoderm and subsequently take up residence in the CNS. (Diagram taken from: Nishiyama et al., 2007)*

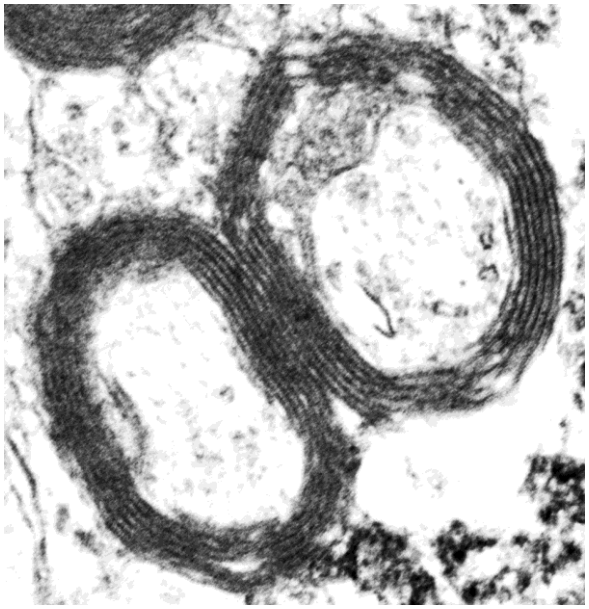

Figure 1.2 *Transmission electron micrograph of a myelinated axon (image provided by Kaylene M. Young)*

that K^+ channels present in neurons and glutamate and carbachol secreted by neurons influence the amount of the nerve growth factor (NGF), BDNF and NT-3 that is secreted by oligodendrocytes (Dai *et al*., 2001), suggesting that the expression of neurotrophic factors by oligodendrocytes depends on neuron-derived signals.

Oligodendrocytes also support neuronal function by secreting soluble mediators that cause channel clustering along the axon (Kaplan *et al*., 2001). Sodium channel clustering is vital for rapid saltatory conduction (Kaplan *et al*., 1997; Dupree *et al*., 2004). Therefore, oligodendrocytes are essential for the rapid propagation of neuronal signals and are hence hugely important for the maintenance and proper functioning of the CNS.

1.2 Myelination

Myelin consists of ~70% lipids and ~30% proteins by mass, of which the proteolipid protein (PLP), the myelin basic protein (MBP), the myelin oligodendrocyte glycoprotein (MOG), the 2', 3'-cyclic nucleotide 3'-phosphodiesterase (CNPase) and the myelin associated glycoprotein (MAG) are the most abundant (reviewed in Dubois-Dalcq *et al*., 1986).

Myelination starts at birth in the mouse spinal cord and occurs rostrocaudally, while in the brain developmental myelination starts in the hindbrain region and extends caudally and rostrally from there (Baumann and Pham-Dinh, 2001). Myelination is initiated after glial processes have attached to the axon and polarization of the plasma membrane has been triggered (Simons and Trotter, 2007). Though it has been shown

that the presence of axons is necessary to trigger the expression of myelin genes in oligodendrocytes and myelin formation *in vivo* (Goto *et al.*, 1990), evidence from *in vitro* studies suggest that oligodendrocytes are able to express myelin genes and form myelin-like structures in the absence of neurons (Dubois-Dalcq *et al*., 1986; Saneto and de Vellis, 1985; Knap *et al.*, 1987; Zeller *et al*., 1985; Hudson *et al.*, 1989; Nussbaum *et al.*, 1988). Nevertheless, myelination *in vivo* requires neuron-glia cell recognition, which in turn triggers myelin formation. The constituents of the nodal and paranodal junctions are well understood, but the molecules involved in myelin initiation and nodal formation and the way these molecules get targeted to the appropriate domains is still unclear (reviewed in Sherman and Brophy, 2005).

There are several molecules present on naked axons that are proposed to be involved in initiating myelination, including cell adhesion molecules, such as integrins, neurofascins and laminins. So far none have been shown to directly drive myelin formation, but the downregulation of the polysialic acid neural cell adhesion molecule and the adhesion molecule Lingo-1 is required for initiating axonal myelination (Sherman and Brophy, 2005; Laursen and ffrench-Constant, 2007). Park *et al*. (2008) have also reported that the Nectin-Like 1 adhesion molecule is crucial for axon-oligodendrocyte recognition and adhesion at the initial stages of myelin formation in the CNS (Park *et al*., 2008). The role of laminin signalling via integrin receptors is well established for PNS myelination, and, while its role is less clear for the CNS (Sherman and Brophy, 2005; Laursen and ffrench-Constant, 2007), it appears to promote oligodendrocyte differentiation and survival (Sherman and Brophy, 2005; Taveggia *et al*., 2010). In addition to cell adhesion molecules, other

signalling systems are important in this process, for example, neuregulin signalling has been linked with the decision to myelinate a particular axon and the number of myelin wraps that will surround it (Sherman and Brophy, 2005; Laursen and ffrench-Constant, 2007). Initiating myelination also requires glial recruitment and differentiation, which may involve semaphorins and netrins present on axons, interacting with their receptors present on oligodendroglial cells (Taveggia *et al*., 2010). Fyn kinase is associated with Tau and α-Tubulin and has been reported to promote oligodendroglial process growth and to initiate myelin wrapping (Klein et al., 2002). Therefore, multiple parallel signalling pathways appear to coordinate in order to initiate CNS myelination and there are distinct from those regulating PNS myelination.

1.3 Developmental Oligodendrogenesis

During CNS development, oligodendrocytes are generated by oligodendrocyte progenitor cells (OLPs), which are in turn derived from ventricular zone (VZ) stem cells in the embryonic brain and spinal cord (reviewed by Woodruff *et al*., 2004; Richardson *et al*., 2006). OLPs are characterized by the expression of the NG2 proteoglycan and the mitogenic growth factor receptor, platelet-derived growth factor receptor (alpha subtype, PDGFRα). In the spinal cord, most (~80%) of OLPs are produced by a specialized group of SOX10+/OLIG2+ progenitors in the ventral VZ (the same progenitors that earlier generate motor neurons). The other ~20% are produced from more dorsal parts of the VZ (Vallstedt *et al*. 2005; Cai *et al*., 2005; Fogarty *et al*., 2005; reviewed by Richardson *et al*., 2006).

NG2 is a chondroitin sulphate proteoglycan, first identified in the late 1970's (Wilson *et al*., 1981). It is a highly conserved protein expressed by a range of cells including glial cells, vascular mural cells, such as pericytes in the brain, cells of mesenchymal lineages, such as immature chondrocytes, osteoblasts and myoblasts, and stem cells in the skin (Levine *et al*., 1986; reviewed in Trotter *et al*., 2010). NG2 has been widely used as a marker for oligodendrocyte progenitor cells in the mammalian CNS and it is down-regulated when cells start to differentiate (Stallcup *et al*., 1987; Nishiyama *et al*., 1996).

The human platelet-derived growth factor (PDGF) is a 30kDa cationic transmembrane protein, which stimulates the proliferation of various cultured cells, including oligodendrocyte progenitors (OLPs; Richardson et al., 1988), and a number of connective tissue-derived cells, e.g., arterial smooth muscle cells and human fibroblasts (Heldin *et al*., 1981; reviewed by Hoch and Soriano, 2003). In the CNS, the alpha receptor for platelet-derived growth factor (PDGFRα) is preferentially expressed in OLPs and not in neurons or astrocytes (Pringle *et al*., 1992) and it is down-regulated very rapidly following cell differentiation (Hall *et al*., 1996; Nishiyama *et al*., 1996b). Loss of PDGF-A in PDGF-A knockout mice results in significant loss of PDGFRα+ cells and subsequently of oligodendrocytes and myelin, though not uniformly throughout the brain (Fruttiger *et al*., 1999). It is important to note that PDGF-A does not directly affect oligodendrogenesis and myelination. Overexpression of PDGF-A causes increased production of OLPs but does not affect the final number of postmitotic, differentiated oligodendrocytes (Calver *et al*., 1998; van Heyningen *et al*., 2001). This is because PDGF-A only affects the proliferation

of OLPs, while oligodendrocyte differentiation and survival is influenced by other factors, including axon-derived factors (Barres and Raff, 1999).

Another marker protein expressed by OLPs, as well as primary Schwann cells and mature oligodendrocytes, is the transcription factor SOX10 (Kuhlbrodt *et al*., 1998). SOX10 is characterized by a high-mobility-group DNA-binding domain (Wegner *et al*., 2001). Expression of SOX10 starts early in oligodendrocyte lineage development and, once turned on, it persists throughout life in all cells of the lineage (Wegner *et al*., 2001).

OLIG1 and OLIG2 are basic helix-loop-helix (bHLH) transcription factors expressed very early in development under the control of the extracellular ventralizing signal, Sonic hedgehog (Shh) (Lu *et al*., 2000). They are the only cell type-specific bHLH proteins known to be expressed by oligodendrocyte lineage cells (Wegner *et al*., 2001) and their expression is strongly restricted to cells of this lineage throughout life. The OLIG proteins are not thought to be expressed outside of the CNS (Rowitch et al., 2002).

1.3.1 Oligodendrogenesis in the Spinal Cord

Pdgfra transcripts (and OLPs), are first detected at the ventricular surface of the cervical spinal cord on embryonic day 12.5 (E12.5) in the mouse (E14 in rat, E7 in chick) (Pringle and Richardson, 1993; Pringle *et al*., 1996). OLPs are therefore generated after neurogenesis is complete (motor neurons in the mouse are generated from ~E9-E12, for example). Most OLPs are generated in the ventral VZ under the influence of sonic hedgehog secreted from the notochord and floor plate (Poncet *et*

al., 1996; Pringle *et al*., 1996; Orentas *et al*., 1999). At first, there are only a few OLPs on each side of the central canal, but they soon increase in number and migrate from the midline into the parenchyma of the cord. By E17 (in the mouse), PDGFRα+ OLPs are distributed more-or-less evenly throughout the spinal cord and their number reaches an approximate steady-state (Richardson *et al*, 2000). A study by Nishiyama *et al*. (1996) has shown that NG2 expression is detectable on PDGFRα+ cells outside the VZ but not on PDGFRα+ cells in the VZ, suggesting that PDGFRα expression precedes NG2 expression during OLP development in the spinal cord (Nishiyama *et al*., 1996). Just before birth, spinal cord OLPs begin to generate oligodendrocytes and they continue to do so during the first few postnatal weeks (Richardson *et al*., 2000). This process requires the cell to pass through several distinct stages of maturation. The cells down-regulate PDGFRα and NG2 when they start to differentiate. They maintain their expression of markers such as the transcription factors SOX10 and OLIG2, but they additionally begin to produce the myelin proteins CNPase, MBP and MOG. These myelinating oligodendrocytes are generated from P0/P1 and later (Richardson *et al*., 2000), peaking in the second and third postnatal weeks in mice. It is during postnatal life that the CNS becomes mature and functional.

1.3.2 Oligodendrogenesis in the Brain

Oligodendrocyte development has also been studied in the forebrain and its embryonic predecessor the telencephalon. The process of OLP development is similar, albeit more complex with OLPs being generated from most parts of the embryonic neuroepithelium in a temporal wave from ventral to dorsal. In the mouse,

the first OLPs are generated from the medial ganglionic eminence (MGE) and anterior entopeduncular area in the ventral telencephalon from E11.5, then from the lateral and caudal ganglionic eminences (LGE and CGE) from E15 and finally from the cortex after birth (Kessaris *et al*, 2006). OLP specification in the ventral telencephalon depends on sonic hedgehog as in the ventral spinal cord (Kessaris et al., 2001). Consistent with the timing of NG2/PDGFRα expression in the spinal cord, NG2 is expressed in the postnatal brain by PDGFRα+ cells outside the SVZ but not in the SVZ (Nishiyama *et al*., 1996). The time course of oligodendrocyte differentiation and maturation is similar in the brain and spinal cord.

1.4 Adult OLPs ("NG2 cells")

Adult OLPs were first identified in the rat optic nerve and later in other parts of the adult mammalian CNS (ffrench-Constant and Raff, 1986; Wolswijk and Noble, 1989, Engel and Wolswijk, 1996; Reynolds and Hardy, 1997; Chang *et al.*, 2000; Horner *et al.*, 2000; Reynolds *et al.*, 2002). In vitro studies have shown that adult OLPs are able to generate either oligodendrocytes, GFAP+ "type-2 astrocytes" or neurons, depending on the composition of the culture medium (Raff et al., 1983; Kondo and Raff 2000). Both perinatal and adult OLPs are characterized by the expression of NG2 and PDGFRα (Shi *et al.*, 1998). PDGF-A also controls the number of OLPs in the adult CNS as it does during development (van Heyningen *et al*., 2001; Woodruff *et al*., 2004). In addition, like perinatal OLPs, adult OLPs respond to PDGF-A by dividing and migrating in vitro (Wolswijk and Noble, 1989; Shi *et al.*, 1998). Conversely, a few prominent differences were identified when adult OLPs were compared to their perinatal counterparts. These include their

morphology, cell cycle length and their migration and differentiation rates (Wolswijk and Noble, 1989). However, if their intracellular levels of cAMP are elevated, OLPs can be induced to divide as rapidly as perinatal OLPs when cultured with PDGF and the glial growth factor (GGF), suggesting that adult OLPs have the capacity to proliferate and differentiate faster under the right conditions (Shi *et al*., 1998).

Because of their obvious similarities to perinatal OLPs, adult OLPs have been widely presumed to be glial precursors, playing a role in CNS maintenance, replacing oligodendrocytes and possibly astrocytes that might die as a result of injury or disease or as a natural part of the ageing process. However, they exist in significant numbers in the adult brain, comprising ~5% of all cells in the mature CNS (Pringle *et al.*, 1992; Dawson *et al.*, 2003). In addition, in the spinal cord grey and white matter, the ratio of OLPs to myelinating oligodendrocytes was found to be 1:4, while in the grey matter forebrain it was found to be 1:1, suggesting that OLPs in the adult brain may yet make a greater contribution to oligodendrogenesis than in the spinal cord (Dawson *et al*., 2003), or else might fulfil another role(s) unrelated to myelination.

OLPs are mitotically active throughout life as shown in studies using the thymidine analogue bromo-deoxyuridine (BrdU) (Levison *et al*., 1999; Horner *et al*., 2000; Dawson *et al*., 2003; Lasiene *et a*l., 2009; Psachoulia *et al*., 2009). Following single BrdU injections to adult rats, BrdU+ OLPs have been shown to persist in the adult brain (Dawson *et al.*, 2003) and spinal cord (Horner *et al*., 2000) and to constitute the major cycling population of the adult rodent (Dawson *et al.*, 2003) and human (Geha *et al.*, 2010) CNS. Apoptosis of these cells was minimal (Dawson *et al.*, 2003). This

observation and the fact that the number of BrdU+ OLPs was decreasing in parallel to the increasing number of BrdU+ oligodendrocytes in rats that received a single BrdU injection suggests that adult OLPs differentiate into oligodendrocytes in the adult CNS (Dawson *et al*., 2003; Horner *et al*., 2000; Gensent and Goldman, 1997).

This presumed oligodendrogenic role does not preclude the possibility that OLPs might perform another more 'physiological' role besides. OLPs have a complex morphology in the adult CNS and they contact neurons at synapses and nodes of Ranvier, which is not what one might expect of a simple precursor cell, making the question of their adult function even more intriguing. The finding that postnatal OLPs express ligand- and voltage-gated ion channels and receive synaptic input from neurons has encouraged the idea that OLPs participate in neural processing during adulthood (Gallo *et al*., 1996; Bergles *et al*., 2000; Lin and Bergles, 2002, 2004; Lin *et al*., 2005; Karadottir *et al*., 2005; Salter and Fern, 2005). OLPs form glutamatergic synapses with unmyelinated axons in white matter tracts (Kukley *et al*., 2007; Ziskin *et al*., 2007) and there is evidence that OLPs are able to fire action potentials in response to an initial depolarizing trigger (Chittajallu *et al*., 2004; Karadottir *et al*., 2008), though this is still controversial (e.g. Lin and Bergles, 2002). Taking all of this evidence together, it seems possible that OLPs might participate in neural processing, by sensing neuronal activity and reporting this activity to neighbouring neurons or glia.

Alternatively, or in addition, OLPs might be 'listening in' to the electrical activity of their associated axons, which at some threshold might trigger their myelination

programme. This could ensure that only active circuits are myelinated and might even contribute to circuit plasticity during adulthood (Fields, 2008). It has been reported that only around 30% of corpus callosal axons are myelinated even in eight month-old mice (Sturrock, 1980). This suggests that there is still plenty of scope for de novo myelination of axons to occur throughout life. It has been observed that extensive piano practise during childhood can cause long-term changes to the structure of white matter tracts, including parts of the corpus callosum (Bengtsson *et al.*, 2005). Furthermore, both cognitive ability and white matter volume increase in parallel until the fourth decade of life, when both start to decline (Bartzokis *et al.*, 2001; Mabbott *et al.*, 2006; Hasan *et al.*, 2008; Ullen *et al.*, 2008; Bartzokis et al., 2008; Zahr *et al.*, 2009), suggesting a causative link. As there is a growing body of evidence to indicate that CNS plasticity and repair decreases with age, it is possible that this might result from an age-related decline in the ability of OLPs to proliferate and generate new oligodendrocytes (Rivers et al., 2008; Psachoulia et al., 2009; Lasienne et al., 2009; this Thesis).

In addition to their putative role in normal neural plasticity, OLPs are thought to be crucial for remyelination following demyelinating injury or disease. For example, during cytotoxin-induced focal demyelination and subsequent re-myelination of the mouse spinal cord, the dynamic behaviour of OLPs in and around the lesion suggests that they are a major source of remyelinating oligodendrocytes (Keirstead *et al.*, 1998; Watanabe *et al.*, 2002; Dawson *et al.*, 2003). The efficiency of remyelination following experimental demyelination decreases with age, which might be attributed to an age-related decline in the regenerative properties of OLPs (Sim *et al.*, 2002).

Therefore, OLP function is probably crucial, not only during normal healthy adulthood but also for tissue regeneration following demyelinating insults to the CNS. The factors that cause these age-related changes are unknown but they could possibly be related to changes in the ability of OLPs to proliferate and generate new oligodendrocytes as the brain matures and ages. How and why the behaviour of OLPs alters with age is a very important question, because it might become possible to manipulate the properties of OLPs in the mature and ageing brain so as to improve their regenerative capacity.

Adult OLPs/NG2 cells have been described as the "4th major CNS cell type" (after neurons, oligodendrocytes and astrocytes; see polydendrocytes Fig. 1.1). Despite their prominence in the adult CNS, many questions regarding their fate, behaviour and function have yet to be answered. This is the focus of my PhD Thesis. The major questions that I have addressed are the following:

1. What are the fates and functions of OLPs in the young adult and ageing brain?
2. Are there different functional subsets of OLPs in the adult brain?
3. What is the function of adult-born myelinating oligodendrocytes?

A major theme in my research has been to use the tools of mouse genetics and transgenesis to mark, follow and manipulate OLPs/NG2 cells in the adult mouse brain.

Chapter 2: Materials and Methods

General

General chemicals and reagents were purchased from Sigma-Aldrich Co Ltd, unless otherwise stated.

All water used was purified using the Milli-Q system (Millipore).

Sterilization of solutions was performed by autoclaving at 15lb/sq.in. for 15 minutes or by filtration through a 0.22μm filter (Millipore). All solutions were stored at room temperature unless otherwise stated.

Falcon sterile plastic-ware was purchased from Marathon Ltd unless otherwise stated.

RNase/DNase free microcentrifuge tubes were purchased from Starlab.

2.1 DNA extraction and Amplification

2.1.1 Small scale plasmid preparation

Small quantities of purified plasmid DNA (1-2mg) were obtained by inoculating 5ml of Luria broth (LB) containing the appropriate antibiotic with a single colony of

transformed bacteria (see **2.4.3**) and incubating overnight in a shaking incubator at 37ºC. 1.5ml of the bacterial culture was transferred to a Microcentrifuge tube and centrifuged for 1 minute at maximum speed (13000rpm) in a microfuge. The supernatant was removed, another 1.5ml of the culture was added and centrifugation repeated. The bacterial pellet was resuspended in 100µl Solution 1 (50mM glucose, 25mM Tris-HCl, pH 8.0 and 10mM EDTA, pH 8.0) by vortexing. 200µl of fresh Solution 2 (0.2N NaOH, 1% w/v SDS) was added and the cells lysed by gentle mixing. 150µl of Solution 3 (3M potassium acetate and 11.5% v/v glacial acetic acid) was added and after gentle mixing, the tube was centrifuged at 13,000rpm for 10 minutes. The supernatant was next transferred to a new Microcentrifuge tube containing 900µl of absolute ethanol (-20ºC), and centrifuged at 13,000rpm for 10 minutes. The precipitated DNA was subsequently washed with 200µl of 70% ethanol and centrifuged for 1 minute. The ethanol was removed and the DNA pellet was resuspended by adding 50µl of MilliQ water and incubating at 55ºC in a water bath for 10 minutes. The purified DNA was stored at -20ºC.

Alternatively, plasmid DNA (excluding BAC DNA) was isolated using the QIAGEN® MiniPrep kit according to the manufacturer's instructions. The bacterial cells were pelleted as previously described, resuspended in 250µl Buffer P1 (RNase A solution added) and transferred to a 1.5ml microcentrifuge tube. 250µl Buffer P2 was added and mixed thoroughly to lyse the cells. 350µl of Buffer N3 was added, mixed and centrifuged at 13,000rpm for 10 minutes. The supernatant was transferred to a QIAprep spin column, which was then centrifuged at 13,000rpm for 1 minute. The flow-through was discarded and the column was washed with 0.5ml of Buffer

PB, followed by a 1 minute centrifugation at 13,000rpm. 0.75ml of Buffer PE was added to the column, before a 1 minute centrifugation at 13,000rpm. The flow-through was discarded and the column was centrifuged again to remove residual wash buffer. DNA was eluted from the column by the addition of 50µl of MilliQ water to the centre of the column, incubation for at least 1 minute at room temperature and centrifugation for 1 minute. The spin column was transferred to a new microcentrifuge tube.

2.1.2 Large scale plasmid preparation

Large quantities of plasmid DNA (≥ 1mg) were prepared using one of the two following methods. For the first method, 400ml of LB media containing chloramphenicol was inoculated with 500µl of a starting culture (grown overnight at 32ºC, 225rpm) and grown overnight, shaking at 32ºC, 225rpm overnight. The culture was transferred to a 50ml falcon tube and centrifuged at 3,750rpm for 10 minutes at 4ºC. The supernatant was removed and the pellet resuspended in 8ml of P1 solution (50mM glucose, 25mM Tris pH8.0 and 10mM EDTA pH8.0) with 100 µg/ml RNase A. 8ml of freshly prepared P2 solution (0.2N NaOH and 1% w/v SDS) was then added and the mixture was gently mixed by inversion and incubated for 5 minutes at room temperature. 8ml of P3 solution (0.3M Potassium Acetate and 11.5% v/v glacial acetic acid) was added, mixed and centrifuged at 3,750rpm for 15 minutes at 4ºC. The supernatant was passed through a double sheet of autoclaved muslin before the DNA was precipitated by the addition of an equal volume (~24ml) of ice-cold isopropanol. After mixing and spinning at 3,750rpm for 15 minutes at 4ºC, the pelleted DNA was washed with ~5ml of 70% ethanol (v/v in MQ water) and

centrifugation at 3,750rpm for 1 minute. The supernatant was removed, and the DNA resuspended in 1ml of Tris-EDTA (TE) and then pooled into 4 x 1.5ml microcentrifuge tubes using cut autoclaved P1000 tips to avoid DNA shearing. 500µl of Phenol/Chloroform pH7.9 was added to each tube and the contents mixed gently by inverting ~8 times. They were then centrifuged for 5 minutes at 13,000rpm and the top phase was transferred to a new 1.5ml tube. The phenol-chloroform extraction was repeated. 500µl of Chloroform:IAA was next added and the tube inverted 8 times before centrifugation for 5 minutes at maximum speed. The top phase of the supernatant was removed to a new 1.5ml microcentrifuge tube, 1ml of ice-cold absolute ethanol was added to each tube and mixed by inverting. At this stage, 3 tubes were stored at -20ºC and the fourth tube was centrifuged for 10 minutes at 13,000rpm at 4ºC. The pelleted DNA was next washed with 70% ethanol and centrifuged for a further 5 minutes. The supernatant was removed and the DNA pellets air dried at room temperature. Finally, 100µl of MilliQ water was added and the DNA resuspended by incubation in a 55ºC water bath for 30 minutes before storing at 4ºC, until the DNA completely dissolved.

Alternatively, DNA purification was performed using the QIAGEN® Plasmid Midi Kit (25) (Cat no. 12143) according to the manufacturer's instructions. The pelleted bacteria were resuspended in 20ml of Buffer P1, followed by the addition of 20ml of Buffer P2. The tube was inverted vigorously 4-6 times before incubating at room temperature for 5 minutes. 20ml of chilled Buffer P3 was added and mixed immediately and thoroughly. The tubes were then incubated for 30 minutes on ice and were next centrifuged for 30 minutes at 20,000g at 4ºC. The supernatant was

passed through a double sheet of autoclaved muslin and was then precipitated by the addition of 42ml of isopropanol. After centrifugation at 15,000g for 30 minutes at 4ºC, the DNA pellet was redissolved in 500µl TE buffer, pH8.0. 4.5ml of Buffer QBT was added and the solution was centrifuged for 15 minutes at 6,000g and the supernatant applied to a QIAGEN-tip, already equilibrated with Buffer QBT. The DNA solution was allowed to enter the resin by gravity flow, before washing twice with 10ml of Buffer QC. The DNA was removed from the column with 5ml of Buffer QF (65ºC) and was precipitated with 3.5ml of isopropanol and centrifugation at 15,000g for 30 minutes at 4ºC. The DNA pellet was washed with 70% ethanol (v/v) in MQ water and centrifuged at 15,000g for 10 minutes. Once the supernatant was removed, the DNA pellet was air-dried at room temperature and then dissolved in 50µl of MilliQ water by incubating for 15 minutes in a 55ºC water bath. DNA was subsequently stored at -20ºC.

2.1.3 DNA gel extraction

QIAquick gel extraction Kit was used according to the manufacturer's instructions. DNA fragments were separated by agarose gel electrophoresis (see **2.3.1**) and the required bands were illuminated by UV excitation. The required DNA band was excised from the agarose gel using a clean scalpel blade, and placed inside a 1.5ml microcentrifuge tube. The agarose was solubilized by the addition of a volume (ml) of Buffer QG equal to 3x the weight of the agarose fragment (mg), and incubation at 55ºC in a water bath for 15 minutes. The liquid sample was then transferred to the QIAquick column and centrifuged at 13,000rpm for 1 minute. The flow-through was discarded and the column was washed with 0.5ml of Buffer QG, followed by a

further 1 minute centrifugation. The column was further washed with 0.75ml of Buffer PE and centrifuged twice for 1 minute. The DNA was eluted with the addition of 40µl of MilliQ water to the centre of the column, incubation for at least 1 minute at room temperature and centrifugation at 13,000rpm for 1 minute.

2.1.4 Extraction of genomic DNA from mouse tails

Mouse genomic DNA was extracted from mouse tail tips. Each sample was collected into a 1.5ml microcentrifuge tube and was incubated overnight in a 55ºC water bath with 250µl of DNA Extraction buffer (100mM Tris-HCl, pH8.5, 5mM EDTA, pH8.0, 200mM NaCl, 0.2% w/v SDS) containing 0.48mg/ml Proteinase K. The following day, 100µl 0f 6M ammonium acetate was added and the tube vortexed, before incubating on ice for 15 minutes. The samples were then centrifuged at 4ºC for 10 minutes at 13,000rpm. The supernatant was transferred to a new tube with 250µl of isopropanol, vortexed and centrifuged for 3 minutes at 13,000rpm. The isopropanol was removed, 250µl of 70% v/v ethanol in MQ H_2O was added and the tubes were centrifuged for 3 minutes at 13,000rpm. The ethanol was removed with a P200 pipette and the DNA pellets allowed to dry at room temperature. 50µl of MilliQ water was added before incubating in a 37ºC water bath for ~2 hours. The genomic DNA was stored at 4ºC.

2.2 Polymerase chain reaction (PCR)

2.2.1 Amplification of genomic DNA

PCR was used to amplify regions of genomic DNA. Reactions were carried out in 0.2ml PCR tubes, each reaction containing 2.5µl 10x PCR buffer (500mM KCl, 100mM Tris-HCl pH 9.0, 1% (v/v) Triton X-100; Promega), 25mM $MgCl_2$, 0.2mM dNTPs (dATP, sCTP, dGTP, dTTP; Amersham Pharmacia Biotech), 10pmol of each primer, 0.5µl of TAQ DNA Polymerase (purified by Matthew Grist) and MQ water to give a final volume of 23µl, to which 2µl of genomic DNA (prepared as above) was added. Tubes were then placed in either a Microcentrifuge Mastercycler Gradient or an MWG-Biotech Primus 96 PCR machine. Reactions were initially denatured at 94ºC for 4 minutes, followed by 35 cycles of denaturing for 30 seconds at 94ºC, then annealing for 45 seconds at 62ºC (this varies according to the optimum annealing temperature for each primer - see **Table 2.1**), and finally an extension of 45 seconds at 72ºC. The final extension step of 10 minutes at 72ºC was stopped by cooling to 4ºC.

2.2.2 Amplification of vector DNA

To amplify a DNA sequence for cloning, PCR was carried out using a DNA polymerase with proof reading compatibility. The PCR reaction included 5x PfuUltraII Buffer (contains 10mM Mg^{2+}), 0.56mM dNTPs, 0.1µl each primer, 1µl of PfuUltra II HS DNA Polymerase (Roche), ~100ng of purified template DNA and MQ water up to 25µl. The amplification program comprised a 2 minute denaturation step at 95ºC, 35-38 cycles through a program of 95ºC for 20 seconds, 62ºC (±5ºC

Transgene	Forward Primer 5' to 3' direction	Reverse Primer 5' to 3' direction	Annealing temperature	Product size
IresVenus	GCGTATTCAACAAGGGGCTG	CCTTGATGCCGTTCTTCTGCTTGT	62°C	700bp
DsRed	TCTAGATAATATTGGCCACAACCATGGCCTCC	CTCGAGCCCCAGGAACAGGTGGTGGCGGC	66°C	700bp
GFP	CCCTGAAGTTCATCTGCACCAC	TTCTCGTTGGGGTCTTTGCTC	62°C	
iCre	GAGGGACTACCTCCTGTACC	TGCCCAGAGTCATCCTTGGC	62°C	630bp
Cre	CAGGTCTCAGGAGCTATGTCCAATTTACTGACCGTA	GGTGTTATAAGCAATCCCCAGAA	59°C	500bp
Rosa26	AAAGTCGCTCTGAGTTGTTAT	GGAGCGGGAGAAATGGATATG	59°C	550bp
	GCGAAGAGTTTGTCCTCAACC	AAAGTCGCTCTGAGTTGTTAT	59°C	250bp
Olig2	GCCAGCTATCAACTCGCGCCC	GTGGAAGACGTGGCCGCC	61°C	400bp

Table 2.1 *Table showing the primer sequences used to genotype the transgenic mice used and also the annealing temperature and the size of the amplified DNA product obtained required.*

according to primer T_m) for 45 seconds and 15 seconds at 72ºC, before a final extension step of 10 minutes at 72ºC, followed by cooling to 4ºC.

2.3 Analysis of DNA

2.3.1 Agarose gel electrophoresis

The gel tray and combs used were from peqlab Biotechnologie GmbH. 1% Agarose w/v in 1x TAE buffer (0.04M Tris, 1mM EDTA, 0.35% v/v glacial acetic acid) was microwaved until all agarose was dissolved and cooled to 55ºC before adding 0.5µg/ml ethidium bromide. Once the gel was set, the sample DNA was diluted 5:1 with loading buffer (Bioline Cat no. BIO-37045) was loaded into the wells of the gel alongside 10µl of Hyperladder 1 (Bioline Cat no. HYPL1500), which is a mixture of a variety of DNA fragments of known sizes (200bp-10kb) and known amounts (15ng-100ng). Agarose gel electrophoresis was performed using a horizontal gel tank by peqlab Biotechnologie GmbH powered by a BioRad Power Pac 300 at 150V. Visualization of DNA within the gel by the presence of ethidium bromide was performed using a MultiImage™ Light Cabinet and processed by the AlphaImage™ 1220 Documentation & Analysis system.

2.3.2 Pulse Field Gel Electrophoresis of BAC DNA

Pulse field gel electrophoresis (PFGE) was performed to separate DNA fragments larger than 10kb, e.g. BAC DNA. It was conducted in a Bio-Rad contour-clamped homogenous electric field electrophoresis cell connected to a CHEF DR II control module and CHEF DR II drive module, both from Bio-Rad. Electrophoresis of DNA

samples was carried out using 1% w/v agarose gels in 0.5x TBE (stock: 45mM Tris-borate, 1mM EDTA, pH8.0). Prior to electrophoresis, 2mm of Pulse Marker™ (0.1-200kb) was placed in the first lane and sealed with additional 1% w/v agarose to act as a standard marker. The DNA was loaded with loading buffer (see above). Gels were run for 12 hours in approximately 2 litres of 0.5x TBE which was kept recirculating via a peristaltic pump. Electrophoresis was at 4ºC in a 6V/cm field with an initial switch time of 2.1 seconds and a final switch time of 10 seconds. Gels were stained in 0.5µg/ml ethidium bromide in MQ H_2O for 10 minutes and rinsed once with MQ water before being visualized on a UV transilluminator.

2.3.3 Quantification of DNA

The concentration of DNA was estimated by matching the intensity of the sample band DNA band to the intensity of bands of known quantity within the Hyperladder I on the same agarose gel. Alternatively, DNA concentration was determined by measuring the absorbance of UV light by a DNA solution at a wavelength of 260nm using a UV Mini 1240 uv-vis spectrophotometer from Simadzu. At this wavelength 50mg of DNA free from RNA and protein contaminants has an absorbance of 1.0. The value obtained was used to calculate the DNA concentration.

2.3.4 DNA Sequencing

DNA sequencing was carried out by the Wolfson Institute for Biomedical Research (WIBR) Scientific Support Services on the Beckman Coulter CEQ 8000 Genetic Analysis System. For sequencing, DNA prepared by Mini-Prep was produced at a

concentration of 9-16fmoles/µl and was used in conjugation with the Beckman Coulter DTCS quick start kit (Cat no. 608120) and the appropriate primers.

2.3.5 Restriction Enzyme Digestion of DNA

Restriction enzymes, buffers and 100xBSA solution were obtained from New England Biolabs. DNA digestions were carried out using 1µl of restriction enzyme with 5µl of the appropriate buffer and 1xBSA if specified by the enzyme's manufacturer. For analytical purposes, around 50ng of plasmid DNA was digested (10-15µl digest volume), while for cloning purposes, up to 1µg of DNA (15µl digest volume) was digested. The reaction was incubated for 2 hours in a 37ºC water bath and was subsequently analysed by agarose gel electrophoresis or pulse field gel electrophoresis.

2.4 Bacterial Biology

2.4.1 Bacterial strains, growth and storage

All plasmids were maintained in *Escherichia coli (E. coli)* strain XL1-Blue (*recA1, endA1, gyrA96, thi-1, hsdR17, supE44, relA1, lac [F' proAB, lacl^{q}ZΔM15, Tn10 [Tet^R]*]). *E. coli* were grown in Luria Broth (LB; 10g bacto-tryptone, 5g yeast extract, 10g NaCl per litre) at 37ºC and 225rpm incubator (New Brunswick scientific; innova 4300, shaking incubator). Alternatively, cells were grown on LB-agar plates (LB + 15g/l bacto-agar). When selecting with ampicillin (Ampicillin sodium salt; Cat no A9518) or kanamycin (Kanamycin Solution; Cat no K0129), these were added to the LB or molten LB-agar at a final concentration of 100µg/ml

(ampicillin; 100mg/ml stock in water stored at -20ºC). When selecting with chloramphenicol, this was added at a final concentration of 44 µg/ml (34mg/ml stock in ethanol at -20ºC).

For long term storage of bacterial strains and clones, glycerol was added to the overnight cultures at a final concentration of 15% (v/v) and 1ml aliquots were stored at -80ºC.

2.4.2 Preparation of electro-competent bacteria

E. coli strain XL1-Blue was made electro-competent as follows: 1ml of an overnight liquid culture of bacteria (grown from a single colony) was used to inoculate 1 litre of LB until it was in mid-log growth phase (OD_{600} of ~0.6; OD: Optical Density). The culture was then chilled on ice for ~10 minutes, and then centrifuged at 3000g, at 4ºC for 10 minutes. The bacterial pellet was resuspended in 1ml of ice-cold autoclaved MQ water, centrifuged and finally resuspended in 200µl of ice-cold 10% (v/v) sterile glycerol in LB. 50µl aliquots were snap frozen in liquid nitrogen and stored at -80ºC.

2.4.3 Transformation of electro-competent bacteria

E. coli bacteria aliquots were thawed on ice, mixed with 2-6µl of purified DNA (see **2.5.1.3** and **2.1.3**) and transferred to a chilled disposable 0.1cm electroporation cuvette (Bio-Rad Laboratories Ltd). Bacteria were electroporated using a Gene Pulser electroporator equipped with Pulse Controller (Bio-Rad Laboratories Ltd) set to 2500V, 200Ω, 25µF, producing a time constant of between 4.5-6 seconds. The

bacteria were then incubated in a 37ºC water bath for 1 hour with 250µl of LB before plating on LB-agar plates with suitable antibiotic. Plates were incubated in a 37ºC oven overnight to allow colonies of transformed bacteria to grow. The plates used had Kanamycin or Ampicillin resistance, as well as a mixture containing 90µl MilliQ water, 10µl Isopropyl-Beta-d-Thiogalactopyranoside (IPTG) and 20µl Xgal. White colonies (negative for ß galactosidase product) were selected.

2.4.4 Preparation and transformation of electrocompetent EL250 cells

The *E. coli* EL250 strain (available via MTA from Neal G. Copeland) is a modified DH10B strain [Gibco] containing a replication defective lambda prophage (Yu et al., 2000) coding for the arabinose *flpe* gene (Lee et al., 2001). *E. coli* EL250 bacteria were grown in 5ml of LB with no antibiotic at 32ºC, 225rpm in a shaking incubator overnight. 1ml of this culture was added to 50ml of fresh LB with no antibiotic and grown in a shaking incubator in an autoclaved flat bottom conical flask at 32ºC, 225rpm until reaching an OD_{600}= 0.5-0.8. The flask containing the culture was then placed in ice water for 5 minutes to cool down, and centrifuged at 2,200rpm at 4ºC for 8 minutes. The bacterial pellet was resuspended in 1ml of autoclaved MQ water, transferred to a microcentrifuge tube and centrifuged for 20 seconds at 13,000rpm. The pellet was washed thrice with MQ water before finally been resuspended in 50µl of sterile MQ water (or 50µl of 10% (v/v) glycerol in LB for long term storage at -80ºC). 2-8µl of purified BAC DNA was added to the bacteria before the mix was transferred to a chilled 0.1cm disposable cuvette, which was then electroporated with1.8kV using a Bio-Rad gene pulser, 25uF with pulse controller set to 200Ohms [Ec1]. The cells were recovered by adding 250µl of LB and incubating at 32ºC in a

shaking incubator for 2 hours. 20% of the bacterial solution was spread onto one, and the remaining 80% onto a second LB-agar plate containing chloramphenicol (44µg/ml). The plates were incubated overnight at 32ºC.

2.5 Generation of transgenic mice

2.5.1 Generation and characterization of Bacterial Artificial Chromosomes (BACs)

2.5.1.1 Choosing the appropriate BAC

The ermin gene is located on chromosome 2 in mice, has 3 exons and 2 introns and is distributed over 7.7kb (**Fig. 5.1**). Using the BAC Map provided by Ensemble (www.ensemble.org; **Fig. 5.1**), 3 BACs were chosen that included the coding sequence for ermin. Bacteria containing the BACs inside the pBACe3.6 vector were obtained from the CHORI BACPAC resources center (http://bacpac.chori.org). The bacteria were cultured and DNA, extracted as previously described (see **2.1.2**), was restriction enzyme digested and the DNA fragment sizes were analyzed by PFGE to confirm the identity of the BAC received. The BAC DNA inside the pBACe3.6 vector was subsequently electroporated into EL250 bacteria as described (see **2.4.4**).

2.5.1.2 Cloning/Purifying DNA fragments for the targeting vector

DNA fragments for cloning were obtained by direct restriction digest of existing plasmid DNA, or following PCR amplification and cloning. Fragments of interest

were then isolated by agarose gel electrophoresis followed by band purification as previously described.

PCR amplified gel purified DNA was incorporated into the pCRII-TOPO® vector using the TOPO TA cloning® kit (Invitrogen Cat no. K4600-01). This vector uses a backbone topoisomerase enzyme that rapidly links any PCR fragment into its covalently bound vector. PCR amplified DNA was incubated for 10 minutes at 72ºC with 2mM dNTPs and 0.5µl DNA Polymerase. DNA was then run on 1% (w/v) agarose gel in TAE and the DNA was purified (see **2.1.3**). 2µl of the DNA, 0.25µl salt solution (provided in the kit), 1µl pCRII-TOPO® vector and 2µl MilliQ water were incubated for 10 minutes at room temperature. 2µl of the TOPO cloning reaction was used directly to transform *E. coli* cells (see **2.4.3**).

2.5.1.3 Ligation of DNA fragments

Band purified fragments of DNA were digested with restriction enzymes that generated overhanging "sticky" ends. Where specified, DNA fragments were blunt using T4 DNA polymerase (restriction enzyme digested DNA was incubated at 12ºC water bath for 15 minutes with 0.2mM dNTPs and 1µl of T4 DNA Polymerase followed by addition of 0.5µl EDTA and purification – see **2.1.3**). Ligation reactions were carried out using 50ng of vector DNA. The amount of insert DNA required was calculated to give (insert DNA):(vector DNA) molar ratio of 3:1. This could be calculated by applying the equation X = ((50/V) x I) x 3 where X is the amount of insert in ng, V is the length of the vector in base pairs and I is the length of the insert in base pairs. The reaction mixture containing the calculated amounts of vector and

insert DNA in a total volume of 10µl with 40 cohesive end units/µl of T4 DNA ligase (New England Biolabs), 1x T4 DNA ligase buffer and 0.5 nM ATP, was incubated either at 16ºC overnight or at room temperature for 1 hour.

2.5.2 BAC recombination

2.5.2.1 Induction of recombination in EL250 cells

EL250 cells that contained the BAC DNA were grown on LB agar plates supplemented by kanamycin (12.5µg/ml) at 32ºC overnight. A single colony was selected and used to inoculate a 5ml starter culture that was again grown overnight, shaking at 32ºC (with kanamycin). 4ml of this overnight culture was used to inoculate 50ml of LB (without kanamycin) which was grown until OD_{600} reached 0.5-0.8. Recombination was induced by transferring 10ml of this culture to a 42ºC water bath for 15 minutes. This culture was then cooled rapidly in ice water for 5 minutes, alongside a 10ml of the non-induced (32ºC only) culture. The non-induced culture acts as a negative control for the recombination. Both induced and non-induced cultures were spun at 1100g at 4ºC for 8 minutes and the bacterial pellets were resuspended in 1ml of ice cold autoclaved MQ water and transferred to a 1.5ml microcentrifuge tube and centrifuged at 13,000rpm for 20 seconds. This was repeated three times and after the final wash, the pellets were resuspended in 100µl of autoclaved MQ water. 50µl of the induced and non-induced cells were electroporated with 100-300ng of the linear targeting vector DNA. After transformation 500µl of warm LB was added to the cells and they were incubated at 32ºC in a shaking incubator for 90 minutes. Cells were then placed on LB agar

plates containing 20µg/ml ampicillin and LB agar plates containing 12.5µg/ml kanamycin as a control to demonstrate the presence of live cells in both the induced and non-induced cultures regardless of whether recombination had been successful. Colonies that have grown on the ampicillin plates from the induced cultures were used to inoculate overnight mini cultures. BAC DNA was then purified (see **2.1.3**), digested with restriction enzymes and PFGE was used to confirm that recombination had occurred.

In addition to the temperature-inducible recombination events, it was also necessary to remove the kanamycin resistance cassette, prior to inserting the recombinant DNA into the mice. To allow this the kanamycin resistance cassette was flanked by *frt* sites. The EL250 bacteria contain an arabinose inducible *flpe* gene that can be used to excise the cassette. To achieve this, 300µl of recombinant EL250 bacterial culture were used to inoculate 15 ml of fresh LB broth. The bacteria were grown to an OD_{600} of 0.5-0.8 and the sterile arabinose was added to a final concentration of 0.2% (v/v). The cultures were then incubated for 1 hour at 32ºC. 1ml of this culture was then used to inoculate 10ml of fresh LB broth and this was incubated for 2 hours at 32ºC before plating on the appropriate selective LB agar, with ampicillin (20µg/ml) for recombinant bacteria and with kanamycin (15µg/ml) to indicate the efficiency of that recombination. In theory, the recombination should be very efficient giving no colonies on the kanamycin-containing LB agar plate. Again recombination was further verified by carrying out restriction enzyme digests and PFGE.

2.6 Creation of Transgenic Mice

2.6.1 Linearization and Purification of recombinant BAC DNA

Linear recombinant BAC DNA was used for *in ovo* injections. This was obtained by firstly carrying out a large scale preparation of BAC DNA as described (see **2.1.2**). The resulting DNA (100µl) was digested overnight with the restriction enzyme PISceI. The BAC DNA fragments were subjected to PFGE by running 90% of the digested BAC DNA across 3-5 merged lanes, with additional lanes containing 2mm of Pulse Marker and 5% of the digested BAC DNA respectively were loaded. After PFGE the marker lane, the 5% BAC DNA digest and ~1mm of the 90% BAC DNA were cut away from the gel with a scalpel blade and stained with 0.2µg of ethidium bromide in MQ H_2O. This revealed the relative locations of the liberated BAC DNA and the vector backbone without ethidium staining the DNA required for microinjection. Using the stained BAC DNA as a guide, the vector DNA and the insert DNA were excised from the large lane and placed in a mini gel tray as shown in figure 2.1a. 4% (w/v) low melting point (LMP) agarose in TAE was poured into the tray until it just covers the bands. The gel was allowed to set and was then run at 50V for 9 hours at 4ºC (**Fig. 2.1b**). The portion of the mini gel containing the vector band and ~1mm of the BAC insert band was then excised and stained with ethidium bromide to confirm that the DNA had accumulated into the 4% LMP agarose. It was also used to determine the position of the insert DNA (**Fig. 2.1c**).

A small block of LMP agarose containing the concentrated insert DNA of interest was equilibrated in TENPA buffer (1M Tris-HCL pH 7.5, 0.5 EDTA pH 8.0, 5M

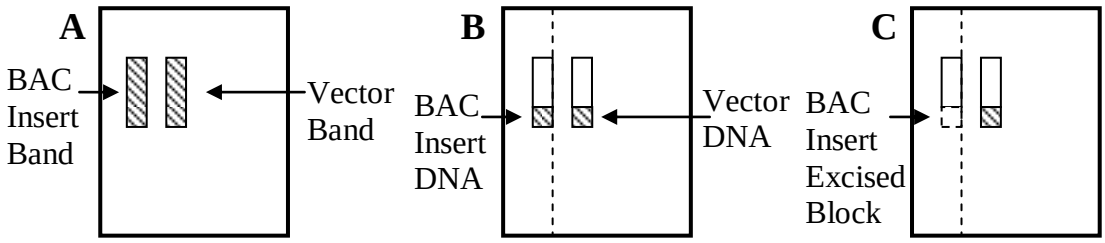

Figure 2.1 *(A) The arrangement of the excised bands in the mini gel tray. Hashed area indicates the location of the DNA. (B) After running the DNA becomes concentrated in a small region of the 4% LMP agarose immediately adjacent to the original excised PFGE band. The dashed line indicates where the vector DNA section of the mini gel should be cut away to allow it to be stained with ethidium bromide. (C) Visualization of the vector band by UV illumination allows localization and removal of the BAC DNA of interest.*

NaCl) containing 30μM spermine and 70μM spermidine while being agitated for 1.5 hours. The gel block was then placed in a microcentrifuge tube, incubated in a 65ºC water bath for 3 minutes, centrifuged briefly and incubated for a further 5 minutes. The tube was then transferred to a 42ºC water bath for 5 minutes. Without removing the molten agarose from the water bath, 2 units of β-Agarase (New England Biosciences) was added per 100μl of molten agarose and the solutions were mixed by pipetting up and down with a wide bore pipette. Agarose digestion took 3 hours at 42ºC and then the mixture was placed at room temperature. If all agarose had fully digested the solution did not set. In a 60x15mm Petri dish, 3 dialysis membranes (Millipore, pore size 0.025μm) were placed floating on a solution of microinjection buffer (1M Tris-HCL pH 7.5, 0.5M EDTA pH 8.0, 5M NaCl, filter sterilized) containing 30μM spermine and 70μM spermidine. The DNA solution was pipetted directly on top of the three filters in equal volumes and the solutions were allowed to dialyse for 1 hour at room temperature. The purified insert DNA was recovered from the top of the filters and stored at 4ºC. A small volume of the DNA was analysed by PFGE along with an equivalent volume of control BAC DNA of which a known quantity had previously been microinjected and produced founder transgenic mice. This gel was stained with 0.5μg/ml ethidium bromide in H_2O and was used as a rough means of quantifying the DNA and checking its purity. The stained DNA was microfuged and diluted in microinjection buffer (1:3000-1:100) on the day of microinjection. DNA was generally used for microinjection within a week of purification.

2.6.2 In ovo injection of BAC DNA and transplantation

Fertilized eggs were obtained from superovulated females. Superovulation was induced in 3-4 weeks old (B6 x CBA) F1 mice by injecting with 0.1ml of 50units/ml of follicle stimulating hormone (Folligon, from Intervet) in 0.9% NaCl at around 5pm on day 1. They were then injected with 0.1ml of 50units/ml of human chorionic gonadotrophin (hCG, Chorulon, from Intervet) in 0.9% NaCl around 45 hours later. After hCG injection, females were mated with (B6 x CBA) F1 fertile males. 4-6 females typically yielded 100-200 fertilized ova.

Microinjection of DNA was carried out by U. Dennehy (Richardson Lab, WIBR). Briefly, linear BAC DNA, suspended in microinjection buffer was injected into the pronuclei of the fertilized mouse ova. Surviving 2 cell stage embryos were then transplanted into the oviducts of pseudopregnant foster mothers (18-22 embryos per mother). Pseudopregnant mothers were prepared 24 hours previously by mating 6-24 week old females in natural oestrous with vasectomized males.

2.7 Neural Cell labelling, tracing and ablation

2.7.1 Transgene labelling, tracing and ablation

The following transgenic mice were bred and maintained:

PDGFRα-CreER^{T2} transgenic (Rivers *et al.*, 2008) express a tamoxifen inducible form of Cre recombinase under the regulation of the *pdgfrα* gene promoter. This transgenic line was maintained as a homozygous breeding colony.

Emx1-iCre (Kessaris *et al*., 2006), *Gsh2-iCre* (Kessaris *et al*., 2006) and *Olig2-Cre* (unpublished, Richardson laboratory) transgenic mice express a constitutively active form of Cre recombinase in Emx1-, Gsh2- and Olig2- expressing cells respectively. These transgenic lines were maintained as heterozygous breeding colonies and were genotyped for iCre and Cre as specified in table 2.1.

Fgfr3-iCreER^{T2} transgenic mice (Young *et al.*, 2010) were maintained as a heterozygous breeding colony and genotyped for expression of iCre (**Table 2.1**).

Rosa26-YFP transgenic reporter mice (Srinivas *et al.*, 2001), following recombination by Cre, express the yellow fluorescent protein (YFP) under the regulation of the ubiquitous Rosa26 promoter. This transgenic line was maintained as a homozygous breeding colony.

The *Tau-mGFP* transgenic reporter mice (Hippenmeyer *et al.*, 2006) contain a *lox-STOP-lox-mGFP-IRES-NLS-LacZ-pA* targeting cassette in exon 2 of the Tau genomic locus. Following recombination by Cre, these mice express a membrane targeted form of GFP under the control of the Tau promoter. They were maintained as a heterozygous breeding colony and genotyped using primers that identify the GFP coding sequence (**Table 2.1**).

The *Ermin-DTR* transgenic mice detailed in Chapter 5 were maintained as a heterozygous breeding colony and genotyped using primers that identify the DNA coding sequences of Venus and/or DsRed (**Table 2.1**).

All transgenic mice were housed under the standard animal housing conditions (23ºC, 48% humidity, 12h dark/12h light cycle) with food and water available ad libitum. When specified, mice were transferred to running wheel cages (Lafayette

Neuroscience) and their running performance was monitored using the Monitoring Software (Lafayette Neuroscience).

2.7.1.1 PCR Genotyping

Genomic DNA was extracted from tissue biopsy and used for PCR amplification as described (see **2.1.4**). The primers used for genotyping the animals were designed specifically to amplify only stretches of DNA within the targeting construct.

2.7.1.2 Cre mediated recombination

To generate mice for experimental use, *Ermin-DTR* transgenic mice were crossed to *Emx1-iCre* transgenic mice. iCre is expressed in all Emx1+ cells, e.g. stem cells in the embryonic VZ. iCre binds to the loxP sites in the *Ermin-DTR* transgene and recombines them, thus removing the stop sequence and allowing expression of the *Venus* and *DTR* genes.

2.7.1.3 CreER^{T2} mediated recombination

Mice expressing an inducible form of Cre were crossed with one of two reporter mouse lines: *Rosa26-YF*P, *Tau-mGFP* (see previous section) (**Fig. 2.2**). Cre recombination in adult *CreER^{T2}*/reporter mice was induced when Tamoxifen (TM), an estrogen analogue, is administered to transgenic mice. When the enzyme cre-recombinase is bound by the estrogen receptor (ER^{T2}), it is held inactive in the cell cytoplasm. Upon tamoxifen administration, tamoxifen will bind to the ER^{T2} allowing Cre to translocate from the cytoplasm into the nucleus. In the nucleus, activated Cre recognizes sequences in the DNA that correspond to lox-P sites and

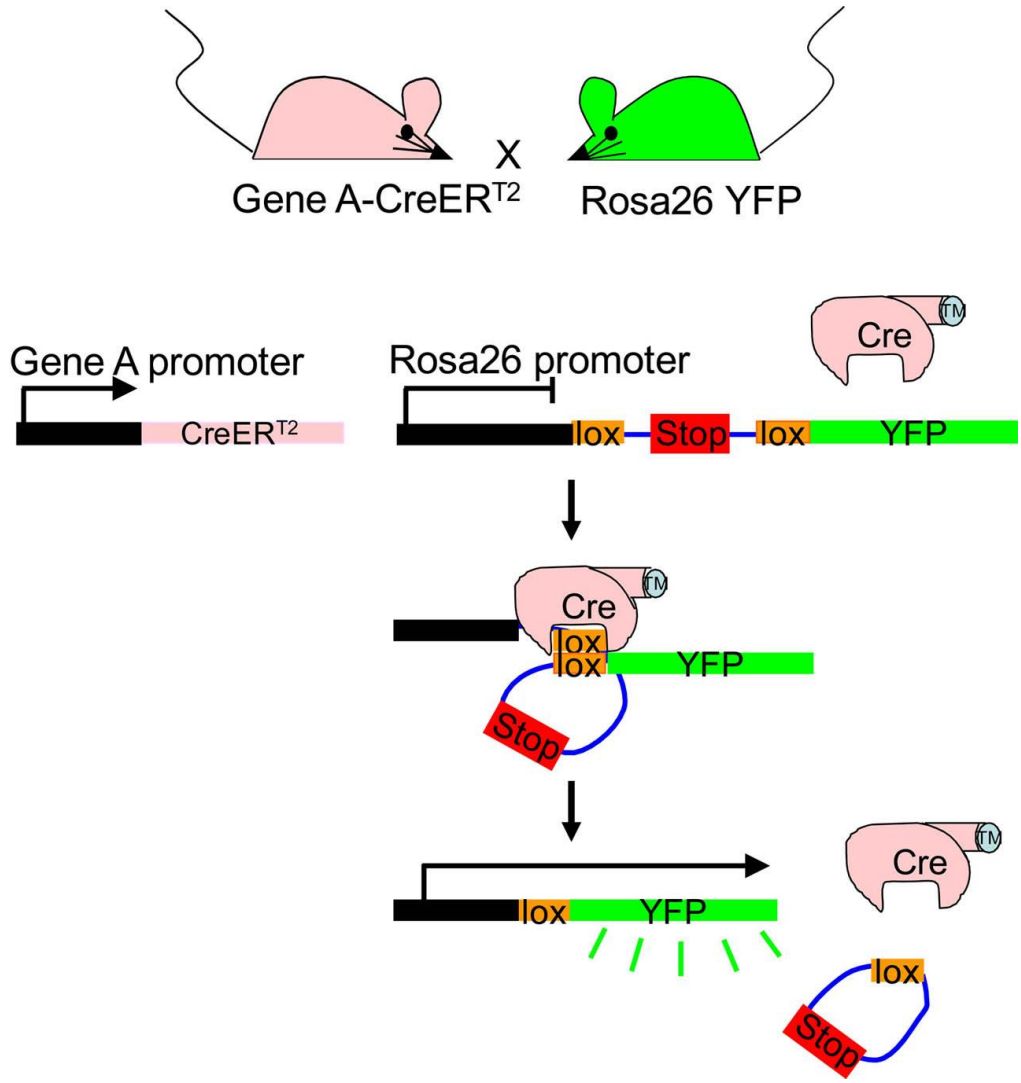

Figure 2.2 *Cre-mediated recombination of loxP sites in iCre(or)CreER^{T2}/Rosa26-YFP double transgenic mice. Orally administered tamoxifen to CreER^{T2}/Rosa26-YFP double transgenics binds to cytoplasmic CreER^{T2}, allowing it to translocate to the nucleous. CreER^{T2} locates loxP sites and recombines them, excising the stop sequence in between and thus switching on the expression of YFP. For iCre/Rosa26-YFP double transgenics, tamoxifen administration is not needed as iCre is expressed in all cells that express Gene A throughout life.*

recombines the lox-P sites, excising whatever DNA sequence lies between them (**Fig. 2.2**).

Tamoxifen was administered orally to *CreER*^{T2}/reporter mice. 40mg/ml TM was sonicated in corn oil for 55 minutes at 30ºC and administered by oral gavage into the stomach. Adult mice received 300mg/kg body weight TM daily for 4 consecutive days.

2.7.1.4 Diphtheria toxin (DT) administration

DT (Merck) was administered to adult (P50) mice twice per day for 3 consecutive days. 100µl were intraperitoneally (i.p.) injected to the mice at a concentration of 20µg/kg body weight.

2.7.2 BrdU labelling of proliferating cells in vivo

Bromodeoxyuridine (BrdU) is a thymidine analogue that is incorporated into the DNA of cells as they undergo DNA replication as part of the cell division process. BrdU was administered to P4 and to ≥ P60 mice by subcutaneous and i.p. injection respectively. Alternatively, for mice ≥ P60 BrdU was administered via the surgical implantation of mini osmotic pumps or through the drinking water (**Fig. 2.3**). For injections, BrdU (20mg/ml in PBS) was incubated for 60-90 minutes in a 55ºC water bath. Pups received serial injections of ~20µl at 120mg/kg body weight every 3 hours for up to 3 days, whereas adult mice were injected with a single dose of 100µl at 800mg/kg body weight. Osmotic minipumps were implanted subcutaneously into adult mice by Leanne Rivers as described by van-Heyningen et al. (2001). When BrdU was added to the drinking water of mice, BrdU was dissolved in MilliQ water

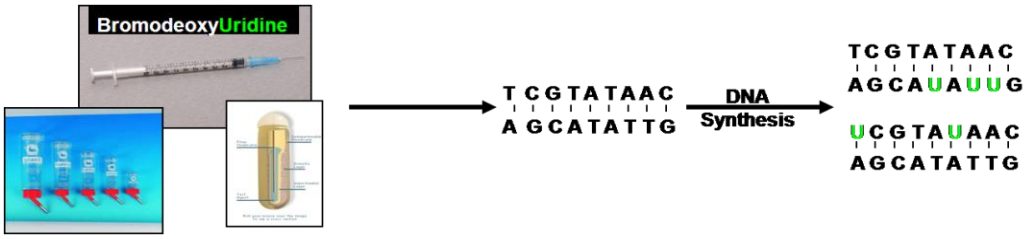

Figure 2.3 *BrdU incorporation during DNA synthesis: BrdU can be administered via various routes: injection, through the drinking water or via implanted osmotic mini-pumps. When a cell undergoes cell division the DNA strands are separated and new complementary strands are synthesized, resulting in two complete copies of the genome. Nucleotides are added to synthesize the new DNA strands, and when BrdU is present, it is incorporated into the newly synthesized DNA strand in the place of thymidine (green 'U's). The presence of BrdU in DNA can be detected by immunohistochemistry (see below).*

to a concentration of 10mg/ml by incubation at 55ºC for 60-90 minutes, or until completely dissolved. Once dissolved, tap water was added to make a final concentration of 0.8mg/ml, which was used to fill the water bottles. Water bottles were covered with foil as BrdU is light sensitive. The BrdU/water solution was replaced every 2-4 days.

2.7.3 EdU labelling of proliferating cells in vivo and in vitro

5-ethynyl-2'-deoxyuridine (EdU) (Invitrogen) is a second thymidine analogue that is incorporated into the DNA of cells as they undergo DNA replication as part of the cell division process.

EdU was administered to mice either i.p., or via the drinking water and in the cultured cells medium. Sterile filtered EdU (5µg/ml in PBS) was added into the SATO medium (Appendix I) to a final concentration of 10µM. 25% of the medium supplemented with new EdU was exchanged every 48 hours. For i.p. injections, EdU was made up to 1mg/ml w/v in PBS and was administered to mice at a dose of 25mg/kg body weight. EdU was added in to the drinking water of mice at either 1, 10, 100, 200, 500 or 1000µg/ml. The EdU was vortexed in a small volume of MilliQ water until completely dissolved. Once dissolved, tap water was added to dilute the EdU to its final concentration in the water bottles of mice. Water bottles were covered with foil as EdU is light sensitive, and the water was replaced every 2-3 days to ensure that the EdU was active throughout the experiment. EdU was used at 200µg/ml of H_2O for the majority of experiments.

2.8 Histology

2.8.1 Generation, maintenance and fixation of OLP primary cultures

Mice were euthanized by steadily increasing exposure to CO_2. Brains were removed into Earles Buffered Saline Solution without Ca+ or Mg+ (EBSS; Invitrogen). Olfactory bulbs were dissected away from the brain. Brains were then sliced coronally using a scalpel blade at the level of the optic chiasm. The septum was removed by pinching with forceps clearly exposing the edge of the corpus callosum. Cortex was dissected by pinching a small region from each hemisphere with forceps. The corpus callosum between the lateral ventricles was then dissected excluding all SVZ and adjacent cortical tissue. The collected tissue was transferred into sterile EBSS.

The isolated tissue was incubated at 37^{o}C for 40-50 minutes in EBSS with Trypsin (62.5ng/ml) and DNase (56.25ng/ml). To inactivate trypsin DMEM/10% FBS was added to the tube, which was then gently tapped to dissociate some of the cells. Most of the medium was removed after allowing the larger tissue pieces to settle to the bottom of the tube. More medium was then added and the tube tapped sharply. This medium was then pooled with the first and centrifuged for 5 minutes at 1000rpm. The medium was aspirated using glass pipette and the cells were resuspended in DMEM/10% FBS and bFGF before being poured through a 70µm cell sieve. The cell concentration was determined using a haemocytometer. 1.5 µl per well of cell suspension was plated at a concentration of 10^5 cells/µl in 300µl of

SATO medium (Appendix I) onto polyD-lysine coated 13mm glass coverslips. Cells were grown for up to 2 days in a humid incubator at 37ºC and 5% CO_2.

For antigen detection, the culture medium was poured off cells and gently replaced with 4% PFA for 10 minutes at RT followed by two PBS washes. Immunohistochemistry and EdU detection was performed as described in section **2.8.4** and **2.8.6**.

2.8.2 Perfusion fixation, tissue collection and freezing

Mice were anaesthetized with pentobarbitone (2ml/kg body weight). When they no longer reacted to applied pressure with scissor tips, an incision was made at the base of the sternum extending along the base of the rib cage and then up the side of the body through the ribs allowing the rib cage to lift up. The diaphragm and connective tissue around the heart was blunt dissected away and a small incision was made in the atrium. A needle (25g, 3/8'') connected to a peristaltic pump containing 4% paraformaldehyde (wt/vol, PFA, Sigma, in PBS) was inserted into the apex (left ventricle). 4% PFA was delivered at a rate of 5ml/minute until there was no blood exiting the right atrium. The brain was next dissected from the head and sliced using a cutting matrix. The first blade cut at the level of the optic chiasm and another two blades cut 2mm either side. The brain slices were then immersed in 4% PFA w/v in PBS for 45 min at 20–25 °C (for antibodies requiring short fixation) or else overnight at 4 °C (for antibodies requiring long fixation). Tissue was then cryoprotected by replacing the 4% PFA with diethylpyrocarbonate-treated 20% sucrose (wt/vol) in PBS. The issue was then incubated overnight at 4°C and subsequently embedded in

Tissue-Tek OCT (optimal cutting temperature) compound, frozen on dry ice and stored at –80 °C.

2.8.3 In situ hybridization

Tissue blocks were sectioned using a Bright OTF5000 cryostat. 20µm sections were cut and transferred into DEPC-treated PBS. Sections were collected onto SuperFrost® Plus slides (VWR International) and dried for 30 minutes. The slides were placed onto a nescofilm and laid in a hybridization chamber, the base of which contained 2 sheets of Whatman paper wetted with a 50% formamide 1x SSC solution. DIG and FITC RNA probe aliquots were thawed on ice before diluting in 1/1000 in hybridization buffer containing 50% formamide, 100 mg/ml dextran sulphate, 1 mg/ml tRNA, 1x Denhardt's solution (50x stock, 1% Ficoll 400, 1% polyvinylpyrrolidone, 1% BSA), and 1x salt solution (10x salt stock, 2M NaCl, 50mM EDTA, 100mM Tris-HCl pH 7.5, 50mM $NaH_2PO_42H_2O$, 50mM Na_2HPO_4, DEPC treated). The diluted probe was denatured by placing in a 70ºC heat block for 5 minutes before applying to the slides. After application of 200µl of the probe solution, each slide was covered with a coverslip. The hybridization box was sealed closed and incubated in a 65ºC oven overnight.

After hybridization, slides were placed in wash solution (50% formamide, 1x SSC, 0.1% Tween-20) in a coplin jar for 15 minutes at 65ºC to remove the coverslips. The slides were then washed twice for 30 minutes each at 65ºC, before continuing to wash at room temperature in 1x MABT (5x stock, 0.5M maleic acid, 0.75M NaCl, 1M NaOH, 0.5% Tween-20) twice for 30 minutes. The sections were then blocked

in blocking solution (8g blocking reagent, Roche cat no 1-096-176, 100ml 5x MABT, 200ml distilled water, heated to 65ºC to dissolve, 80ml heat inactivated sheep serum added and MQ water to 400ml) was applied to slides for one hour at room temperature. Next, an anti-Digoxigenin alkaline phosphatase conjugated antibody (Roche) was diluted 1/1500 in blocking solution and applied to the sections overnight at 4ºC. The sections were then washed thrice for 20 minutes in 1 x MABT, followed by 2x 10 minute washes in staining buffer (0.1M NaCl, 0.05M $MgCl_2$, 0.1M Tris pH 9.5, 0.01% Tween-20). The color reaction was developed by placing the slides in a solution containing 20ml staining buffer, 0.025M $MgCl_2$, 87µl NBT (1g 4-nitro blue tetrazolium chloride crystals, plus 7ml dimethyl formamide and 3ml distilled water), 67µl BCIP (BCIP from Roche, 1g plus 20 ml dimethyl formamide), and 20ml of a 10% w/v polyvinyl alcohol in MQ water. Reactions were incubated in the dark at 37ºC and periodically checked for the development of a blue precipitate on the sections. For less abundant transcripts, reactions were allowed to proceed at 32 ºC overnight. Once cells could be clearly visualized, the reaction was quenched by immersing the slides in tap water. After this, the sections were dehydrated through an alcohol series before being treated with xylene and mounted with DPX mountant (Fluka) and coverslipped.

2.8.4 Immunohistochemistry

Frozen tissue was sectioned on a cryostat (Leica, Bright) to produce 30µm coronal brain sections. These were collected with a damp paint brush and floated onto the surface of PBS. Alternatively, sections were collected directly on SuperFrost® Plus slides and air dried. Immunohistochemistry followed.

Non-specific binding sites were blocked by tissue exposure to blocking (10% (v/v) sheep or cow serum/0.1% (v/v) Triton X-100 (BDH)/PBS) for 1 hour at room temperature. Sections were incubated overnight at 4ºC in primary antibody diluted in blocking solution. Sections were washed 3 times in PBS for 10 minutes each. Secondary antibody diluted in blocking solution was applied for 2-4 hours at room temperature. Sections were again washed thrice in PBS. Floating sections were then transferred onto Superfrost® Plus glass slides and dried. All slides were then coverslipped with mounting medium (Dako) and stored in the dark at 4°C. When staining to detect CC1, sections were collected in TBS (Tris buffered saline: 10x TBS is 0.5M Tris, 9% NaCl), the blocking solution was replaced with TBS/0.5% triton/10% fetal calf serum blocking solution and all washes performed in TBS instead of PBS.

2.8.5 BrdU Detection

The detection of BrdU in tissue sections followed staining with any other primary and secondary antibodies as described in **2.8.4**. Sections transferred onto slides and dried were then fixed with 70% (v/v) EtOH/20% (v/v) acetic acid/MQ water for 10 minutes at room temperature, followed by 20 minutes at -20ºC in 70% EtOH in MQ water. Sections were next incubated for 15 minutes at room temperature, first in 1% (v/v) Triton-X100/PBS and then in 6M HCl/1% Triton-X100/PBS, and were subsequently washed 3 times for 5 minutes in PBS. Anti-BrdU (**Table 2.2**), diluted in blocking solution was incubated overnight at 4ºC. Washing, secondary antibody and mounting was carried out as above.

Primary Antibody	Supplier	Dilution
Rat anti-PDGFRα	BD Pharmingen™	1:400
Rabbit anti-GFP	AbCam	1:6000
Rat anti-GFP	Fine Chemical Products LTD	1:3000
Guinea pig anti-SOX10	Gift from M. Wegner	1:2000
Mouse anti-NeuN	Chemicon	1:500
Mouse anti-PSA-NCAM IgM	Chemicon	1:1000
Mouse anti-CNPase	Chemicon	1:2000
Rabbit anti-Ng2	Chemicon	1:500
Rabbit anti-Olig2	Chemicon	1:1000
Rat anti-MBP	AbD Serotec	1:100
Mouse anti-BrdU	American Type Culture Collection (Manassas, VA)	1:10
Rat anti-BrdU	AbD Serotec	1:500
Mouse anti-GFAP	Sigma	1:2000
Rabbit anti-Tmem10/Opalin	Gift from Or. Peles, Weissmann Institute	1:1000
Rabbit anti-Ermin	Gift from Or. Peles, Weissmann Institute	1:400
Rabbit anti-Somatostatin	Peninsular	1:200
Rabbit anti-Calbindin	Swant, Bellinzona, Switzerland	1:1000
Rabbit anti-Calretinin	Swant	1:1000
Rabbit anti-Palvalbumin	Chemicon	1:1000
Mouse anti-Palvalbumin	Chemicon	1:1000
Mouse anti-Tyrosine hydroxylase	Chemicon	1:1000
Rabbit anti-NPY	Insight	1:1000
Mouse anti-CC1 IgG2	Calbiotech	1:250
Guinea pig anti-Doublecortin	Chemicon	1:3000
Secondary Antibody	**Supplier**	**Dilution**
Alexa 488 goat anti-rabbit IgG	Invitrogen	1:1000
Alexa 488 goat anti-rat IgG	Invitrogen	1:500
Alexa 568 goat anti-rabbit IgG	Invitrogen	1:1000
Alexa 568 goat anti-rat IgG	Invitrogen	1:500
Alexa 568 goat anti-mouse IgG1	Invitrogen	1:1000
Alexa 568 goat anti-mouse IgG H+L	Invitrogen	1:1000
Alexa 568 goat anti-mouse IgM	Invitrogen	1:1000
Alexa 647 goat anti-rabbit IgG	Invitrogen	1:1000
Alexa 647 goat anti-rat IgG	Invitrogen	1:500
Alexa 647 goat anti-mouse IgG1	Invitrogen	1:1000
Alexa 647 goat anti-mouse IgG H+L	Invitrogen	1:1000
Goat anti-guinea pig Cy3 conjugated	Chemicon	1:500

Table 2.2 *Table showing all the primary and secondary antibodies used for immunohistochemistry, their working solutions and sources.*

2.8.5 EdU Detection

In EdU the terminal methyl group is replaced with an alkyne group, which allows detection using a fluorescent azide that covalently binds to the alkyne group in a reaction called 'click chemistry' (Chehrehasa *et al*., 2009). Sections were collected and blocked as described for immunohistochemistry, followed by incubation at RT for 30 minutes in the dark. The EdU developing cocktail was washed off by three PBS washes. Non-specific binding sites were blocked with 10% (v/v) sheep or cow serum in 0.1% (v/v) Triton X-100 (BDH) in PBS for 1 hour at room temperature. Sections were then incubated in 0.5% (v/v) Triton X-100 in PBS for 15 minutes. EdU was detected using the Click-iT™ EdU Cell Proliferation Assay Kit according to the manufacturer's instructions. A reaction cocktail of 500µl was prepared using 43µl of 10x reaction buffer, 20µl of $CuSO_4$, 1.2µl of Alexa Fluor® 488 or 647 azide, 5µl of 10x reaction buffer additive and MQ H_2O. Sections (floating or on slides) were exposed to the reaction cocktail within 15 minutes of its preparation, and incubated for 30 minutes, at room temperature, in the dark. Sections were washed 3 times for 5 minutes in PBS, before continuing with immunohistochemistry as described previously.

2.9 Microscopy, quantification and statistics

2.9.1 Image collection

Slides were examined under a light microscope (Zeis Axioplan) with a Hamamatsu digital camera and/or under a confocal microscope (UltraView microscope, Perkin Elmer) using standard excitation and emission filters for visualizing DAPI, FITC

(Alexa Fluor 488), CY3, TRITC (Alexa Fluor 568) and Far Red (Alexa Fluor 647). Confocal z stacks were captured for each section with 0.5-2μm increments. Reconstruction of xz and yz views was carried out using the Volocity software (Perkin Elmer).

2.9.2 Quantification of histology

For quantification of immunohistochemical staining/ cell labelling, cells were manually counted from low (20x) magnification, non-overlapping confocal image-stacks, using Adobe Photoshop. Quantification of cells was concentrated in the anterior forebrain (neocortex, corpus callosum and piriform cortex) at Bregma levels 0-0.26 mm (**Fig. 2.4**) (Paxinos and Franklin, 2001)).

Generally, co-localization was expressed as a percentage, that is, as the ratio of cells expressing two markers divided by the total number of cells expressing a single marker multiplied by 100 (e.g. (PDGFRα+YFP)/YFPx100).

For all quantification a minimum of 2 sections from n=3 mice was examined. The proportion of labeled cells was determined per mouse. The average and standard deviation was then calculated for each group using Microsoft Excel. All statistical comparisons (two-tailed t tests or ANOVA) were made using Microsoft Excel.

2.9.3 Cell cycle calculation

For a homogeneous population of cycling cells, the fraction of cells that label with BrdU/EdU ("labelling index") is expected to increase linearly with the duration of

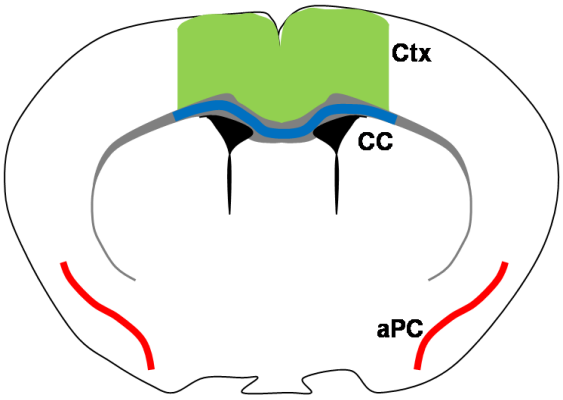

Figure 2.4 *Coronal section through adult mouse forebrain at the level of the SVZ. Images were collected at the coloured regions (Ctx in green, CC in blue, aPC in red).*

BrdU/EdU exposure until all dividing cells are labelled (phase 1). After this the labelling index cannot increase further and a plateau is reached (phase 2). The rate at which cells incorporate BrdU/EdU is given by the slope (m) of phase 1 and was calculated by performing a linear regression analysis in Microsoft Excel. This was an iterative process. The maximum labelling index (phase 2 plateau value) is known as the "growth fraction" (GF), which is expressed as a percentage of the total cell population. This was calculated only using points that were deemed not statistically significant from each other by ANOVA and not already included in the linear regression analysis. GF is the average of all mice analysed on the plateau.

From these data the length of the cell cycle Tc = GF/m was calculated (Nowakowski *et al.*, 1989; see **Fig. 2.5**). Since T_C depends on the reciprocal of m, the standard error ($s.e._{Tc}$) is not symmetrical about the mean. However, for simplicity $s.e._{Tc}$ is shown as ± half of the full range, calculated as follows:

$$s.e._{Tc} = [\{(GF + s.e._{GF}) / (m - s.e._{m})\} - \{(GF - s.e._{GF}) / (m + s.e._{m})\}] / 2$$

Similarly, S phase can be calculated as (labelling index at t=0)/m. This is equivalent to the intercept of the line (Phase 1) on the x-axis (labelled as Ts on the diagram, **Fig. 2.**5).

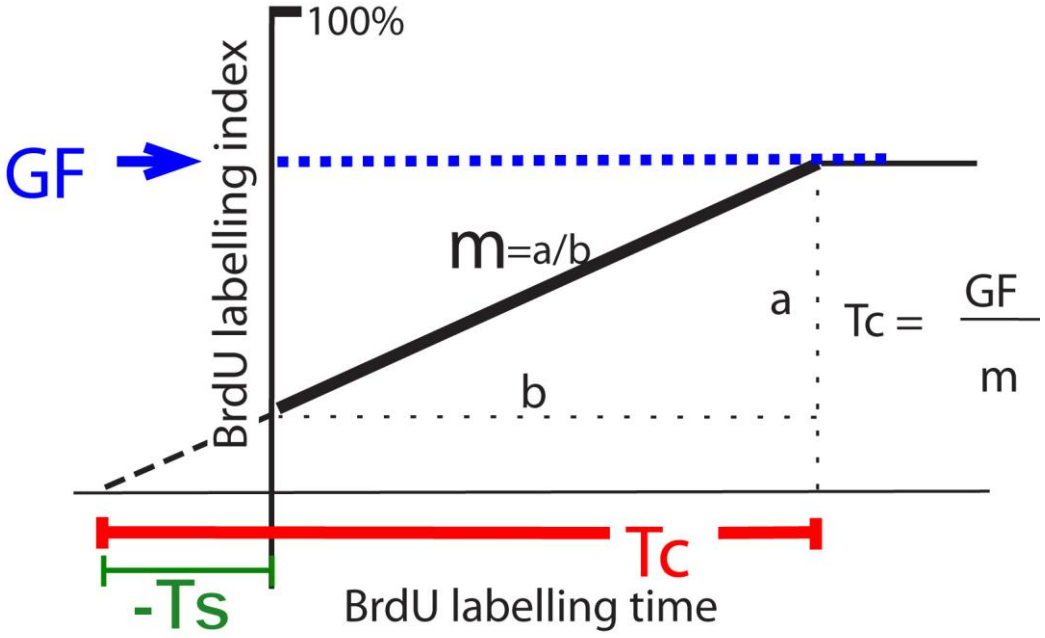

Figure 2.5 *Calculation of cell cycle time (T_C). The gradient (m) of the linear rising part of the graph (phase 1) was determined by the method of least squares (m=a/b). The labelling index at plateau (phase 2) is the fraction of the population that is actively cycling (the growth fraction, GF). If the whole population were cycling GF would be 100%. T_C was calculated as GF/m. Ts was calculated as (labelling index at t=0)/m.*

Chapter 3:

'Adult OLPs Generate New Myelinating Oligodendrocytes Throughout the Brain and New Projection Neurons in the Piriform Cortex'

3.1 Introduction

During CNS development, oligodendrocyte progenitor cells (OLPs) act as a source of oligodendrocytes, which in turn myelinate the neuronal circuits necessary for normal CNS function (Curtis *et al*., 1988; Levine *et al*., 1993; reviewed in McTigue and Tripathi, 2008). OLPs are characterized by their expression of specific markers, such as the proteoglycan NG2 and the platelet-derived growth factor for receptor alpha (PDGFRα), which they down-regulate as they differentiate into myelinating oligodendrocytes and gradually start to express myelin-associated markers (**Fig. 3.1;** reviewed in Trotter *et al*., 2010 and Nishiyama *et al*., 2010; Kippert *et al*., 2008; Brockschnieder *et al*., 2006).

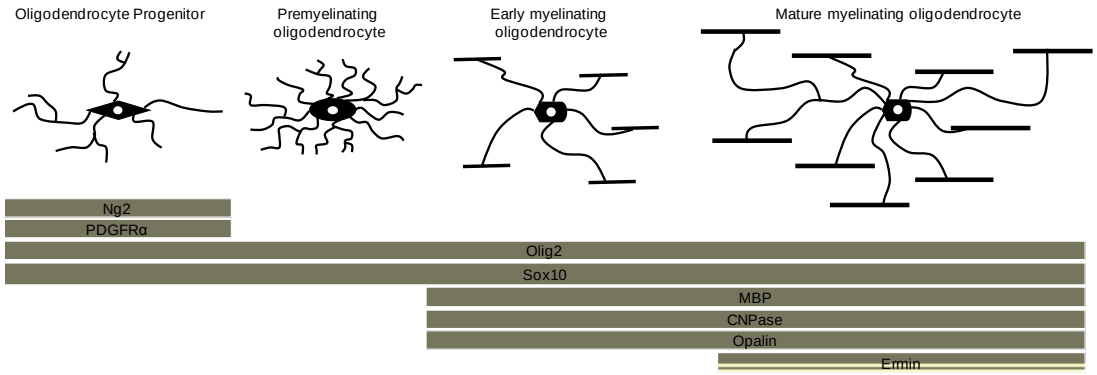

Figure 3.1 *Schematic of oligodendrocyte maturation from progenitor to fully myelinating cell. The antigenic properties of cells at the different maturation stages are depicted.*

During adulthood, the core function of OLPs is thought to be as a source of remyelinating cells in demyelinating lesions and to replace oligodendrocytes lost due to ageing, injury or disease (Keirstead *et al*., 1998; Watanabe *et al*., 2002; Dawson *et al*., 2003). Their abundance and distribution, however, have raised questions associated with alternative functions they might serve in the adult CNS (Chapter 1). To shed light on the fates and behaviour of OLPs in the normal adult brain, OLPs and their progeny were labelled and traced by "Cre-lox*"* technology in adult transgenic mice. This approach relies on expressing a tamoxifen-inducible version of Cre recombinase (CreER) under the transcriptional control of regulatory sequences associated with genes that are expressed specifically or preferentially in NG2 cells. When a Cre-conditional reporter transgene such as the *Rosa26-YFP* is also present (see **2.7.1**), brief administration of tamoxifen induces Cre recombination, activating the *yellow fluorescent protein (YFP)* reporter irreversibly in OLPs and all of their descendents (see Chapter 2 - **Fig. 2.4**).

For this study I used the *Pdgfrα-CreER*^{T2} transgenic mouse line (Rivers *et al*., 2008; see **2.7.1**), which, when crossed to the *R26-YFP* reporter mouse line, allowed me to follow the fates of OLPs in the adult mouse brain.

3.2 Results

3.2.1 Antigenic and proliferative properties of adult OLPs

Adult OLPs are usually characterized as NG2+, process-bearing cells in the grey and white matter. Expression of PDGFRα in NG2+ cells was confirmed by the

immunolabeling of adult brain sections, which showed that practically all nonvascular NG2-expressing cells co-express PDGFRα and vice versa (**Fig. 3.2**). In particular, 99.6% ± 0.4% of NG2+ OLPs in the corpus callosum co-expressed PDGFRα and 98.9% ± 2% of PDGFRα+ OLPs were also NG2+ (>1,000 cells total from three mice; **Fig. 3.2a**, **b**, **e**). These two OLP markers could therefore be used interchangeably depending on the specific experimental conditions (e.g. fixation conditions) required on each occasion. For example, the antibody to PDGFRα worked only in lightly-fixed tissue, whereas the antibody to NG2 could be used in short- or long-fixed material.

To further confirm that OLPs but not oligodendrocytes, express PDGFRα and NG2, cells were co-labelled with antibodies against CNP, an oligodendrocyte marker, and either PDGFRα or NG2. No PDGFRα+/CNP+ cell was detected in the corpus callosum or cortex (**Fig.3.2e**). Only a very small proportion of NG2+ cells (0.3% ± 0.4%) co-expressed CNP in the corpus callosum and none in the cortex (**Fig.3.2e**). CNP is an early myelination marker. The small proportion of NG2+/CNP+ cells observed could correspond to cells that had just started differentiation and had not yet fully down-regulated NG2 expression. Cells were also double-labelled with antibodies to NG2 and SOX10 (which works only in long-fixed tissue). I found that all nonvascular NG2+ cells co-expressed SOX10 (no SOX10– cells out of >1,000 NG2+ cells scored from three mice; **Fig. 3.2c**, **e**). There were, however, many SOX10+/NG2– cells, especially in white matter, that presumably correspond to differentiated oligodendrocytes (**Fig. 3.2c**, **e**). All SOX10+ cells were also OLIG2+ in the corpus callosum and cortex, which allowed the use of OLIG2 interchangeably

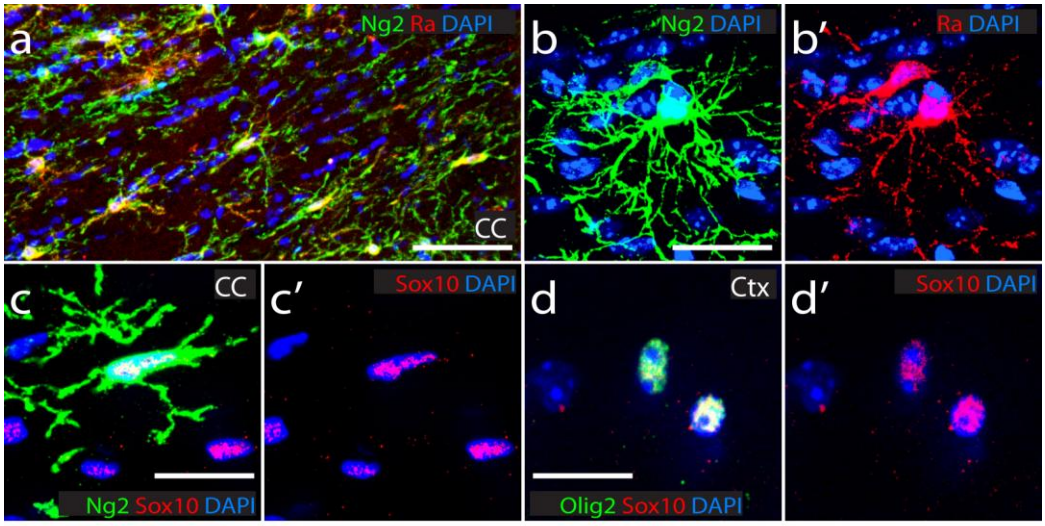

e

Percentage of labeled population coexpressing *second marker*

	Corpus callosum					Cortex				
	PDGFRa	NG2	OLIG2	SOX10	CNP	PDGFRa	NG2	OLIG2	SOX10	CNP
PDGFRa		99.6 ± 0.4			0 ± 0		98.9 ± 1.3			0 ± 0
NG2	99.6 ± 0.4			6.3 ± 0.6	0.3 ± 0.4	98.9 ± 2			32.7± 4.3	0 ± 0
OLIG2				99.7 ± 0.3	100 ± 0				98.1 ± 2.4	100 ± 0
SOX10		100 ± 0	98.6 ± 1.2		100 ± 0		100 ± 0	99.8 ± 0.3		100 ± 0
CNP	0 ± 0	0.9 ± 1.6				0 ± 0	0 ± 0			

Figure 3.2 *Antigenic properties of adult OLPs. (**a**–**e**) Cryosections of young adult (P45) brains were double-immunolabelled for different combinations of oligodendrocyte lineage markers PDGFRα (Ra), NG2, OLIG2, SOX10 and CNP. Representative images are shown in **a**–**d**, and cell counts (means ± s.d.) in **e**. Column headers refer to the labelled populations (e.g. PDGFRα/SOX10) and row headers refer to the co-expressed second marker. Certain antibody combinations were not possible because of incompatibilities between the required fixation conditions or the species origin of the antibodies. Kaylene M Young, Leanne E Rivers and Konstantina Psachoulia contributed data for this figure. Scale bars represent 50 μm in **a** and 10 μm in **b**–**d**.*

with SOX10 as a general oligodendrocyte lineage marker in long-fixed material (**Fig. 3.2d**, **e**). The antibody to OLIG2 labelled only a subset of PDGFRα+ cells in short-fixed tissue, a fact most likely attributed to failure of the OLIG2 antibody to work reproducibly under this fixation. For this reason, the antibody to OLIG2 was not used in short-fixed material.

3.*2.2 Fate mapping adult oligodendrocyte progenitor cells in the adult CNS*

3.2.2.1 Characterization of PDGFRα-CreER^{T2}/R26-YFP transgenic mouse

In order to follow the fates of PDGFRα+ adult OLPs, a transgenic line was generated that expressed a tamoxifen-inducible form of Cre recombinase (CreER^{T2}) under *Pdgfra* transcriptional control. *In situ* hybridization revealed that *CreER^{T2}* RNA transcripts were expressed in scattered cells throughout the postnatal brain, similar to endogenous *Pdgfra* transcripts (**Fig. 3.3**). In particular, the proportion of cells expressing Cre mRNA in the cortex was equivalent to the proportion of cells expressing PDGFRα mRNA (92% ± 19.9%; **Fig. 3.3a-d**). Double-label *in situ* hybridization showed that there was near complete overlap between *Pdgfra* and *cre* expression in the neocortex (>99% of *cre* expressing cells co-expressed *Pdgfra*; **Fig. 3.3e**). In the corpus callosum, where *in situ* hybridization was less sensitive, >95% of *cre*-expressing cells expressed detectable *Pdgfra* (Rivers *et al*., 2008). Therefore, expression of the Cre transgene appeared faithful to that of endogenous PDGFRα and this transgenic mouse was used to trace the behaviour of OLPs in the adult mouse brain.

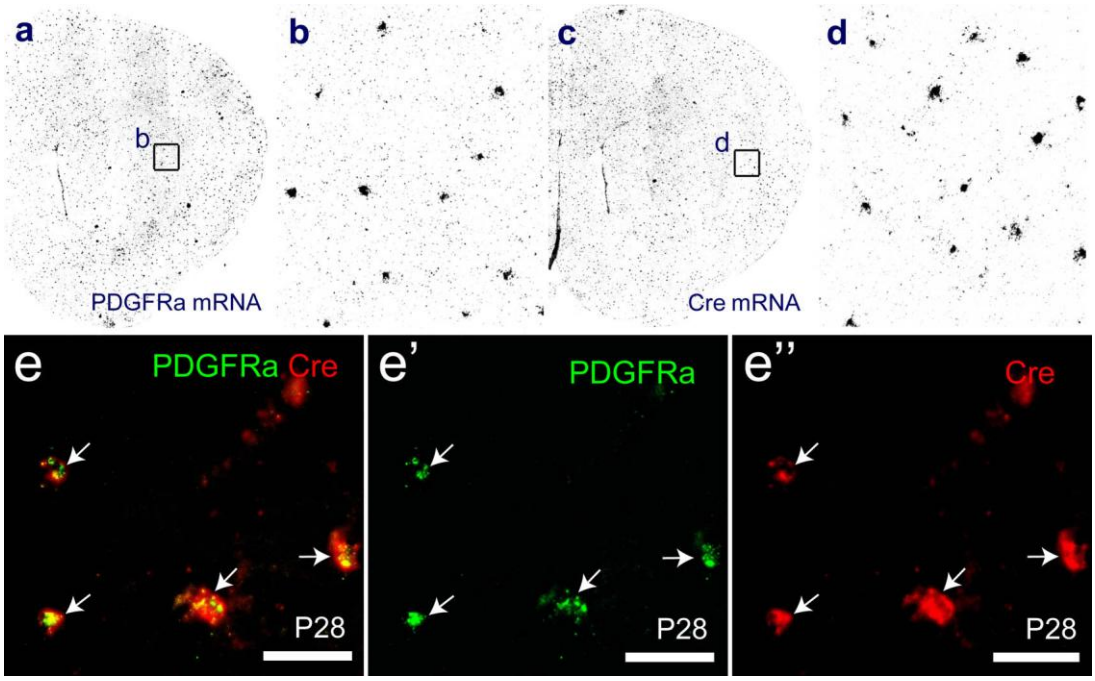

Figure 3.3 *Characterization of PDGFRa-CreER^{T2} transgenic mice. To ensure appropriate expression of the transgene, in situ hybridization was performed to detect PDGFRa (a) and Cre mRNA (c) on P28 brain taken from PDGFRa-CreER^{T2} transgenic mice (b and d are taken from the brain regions, indicated by the small rectangle in a and c respectively. The proportion of PDGFRα+ cells that co-expressed Cre was 92% ± 1.9%. Co-expression of these mRNA transcripts was confirmed by double fluorescent in situ hybridization (e). Arrows indicate the double-labelled cells.*

For these tracing studies, homozygous *PDGFRα-creER^{T2}* mice were crossed to homozygous *Rosa26-YFP* reporter mice to generate double-heterozygous *PDGFRα-creER^{T2}/R26-YFP* offspring (see **2.7.1**). Due to limitations in genotyping that prevent distinction between mice that are homozygous versus heterozygous for the *PDGFRa-CreER^{T2}* BAC transgene, the efficiency of recombination in *PDGFRα:hom/R26-YFP* could not be directly compared with *PDGFRα:het/R26-YFP* mice. However, *PDGFRa-CreER^{T2}/R26-YFP* double heterozygous transgenic mice from the above mating were mated with homozygous *PDGFRα-CreER^{T2}* mice and their offspring were genotyped for expression of the PDGFRα transgene (see **2.2.1**). Of the mice that were positive for R26YFP, it was expected that 50% should be *PDGFRα:het/R26-YFP* and ~50% were *PDGFRα:hom/R26-YFP*. Tamoxifen (TM) was administered to offspring of mixed litters of *PDGFRα:het* and *PDGFRα:hom,* and known *PDGFRα:het/R26-YFP* transgenic mice in young adulthood (P45). Tamoxifen induces nuclear translocation of CreER^{T2} and promotes Cre-mediated recombination, which in turn leads to YFP expression (see **2.7.1.3**). For both groups of mice, brain tissue was collected 7 days post-tamoxifen (P45 +7) and was immunolabelled with antibodies against YFP and *PDGFRa* (**Fig. 3.4a-b**). The percentage of *PDGFRa*+ cells that were YFP+ in the corpus callosum was determined for 5 *PDGFRα:het/hom/R26-YFP* mice and 4 *PDGFRα:het/R26-YFP* mice. For the *PDGFRα:het/R26-YFP* group, ~45% of *PDGFRa*+ cells were observed to express YFP, i.e. 45% recombination (**Fig. 3.4c**). If the efficiency of recombination was increased for homozygous *PDGFRa-CreER^{T2}* mice compared to heterozygotes, we would expect to see an increase in the proportion of PDGFRα+ cells labeled in some mice, which would increase the variability within the group.

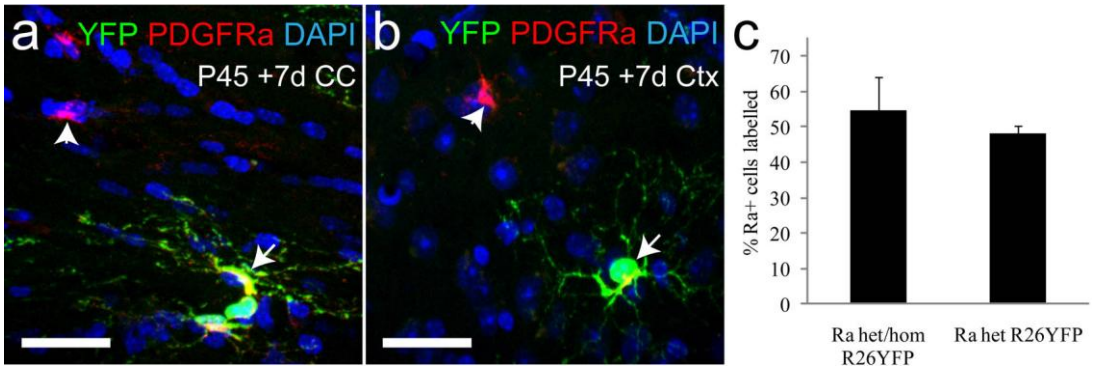

Figure 3.4 *Recombination efficiency in the PDGFRa-CreER^{T2}/R26-YFP transgenic mice. PDGFRa-CreER^{T2}/R26-YFP mice were crossed with homozygous PDGFRa-CreER^{T2} and their offspring were administered TM at P45. Brain sections from P45 +7d mice was examined in the corpus callosum (a) and cortex (b) by double fluorescent immunohistochemistry with antibodies against YFP and PDGFRa. The proportion of PDGFRa+/YFP+ cells in the total PDGFRa+ cell population in the corpus callosum was quantified. ~50% OLPs were YFP-labelled with no statistically significant difference between PDGFRa:het/R26-YFP mice and PDGFRa:het/hom/R26-YFP mice (t test; P=0.19; c). However, both the mean and standard deviation in the hom/het mice were higher that in uniformly het mice, suggesting that generating homozygous PDGFRa-CreER^{T2}/R26-YFP mice might be useful to increase recombination efficiency if required in future studies. White arrows and arrowheads show YFP+/PDGFRα+ and YFP-/PDGFRα+ cells respectively.*

We detected no overall significant change (two-tailed t test; P=0.19). However, within the group the highest level of recombination detected (highest proportion of YFP-labeled OLPs) in an individual mouse was 68%. This experiment suggests that generating *PDGFRα:hom/R26-YFP* mice might be able to increase recombination from ~45% to ~70% for future studies. However, in the studies described in this Thesis I used *PDGFRa-CreER^{T2}/R26-YFP* double heterozygous transgenic mice to keep the breeding strategy simple.

3.2.3 Adult OLPs give rise to myelinating oligodendrocytes in the postnatal brain

In experiments conducted by Leanne Rivers, tamoxifen was administered to adult (P45) *PDGFRα-creER^{T2}/R26-YFP* transgenic mice in order to label and follow the fates of adult-born OLPs. Mice were sacrificed at several time-points post-tamoxifen and tissue sections immunostained to detect PDGFRα and YFP. An accumulation of PDGFRα-/YFP+ cells was observed over time (**Fig. 3.5**). This accumulation was noted to be much faster in the corpus callosum than in the motor cortex (**Fig. 3.5**). These data suggested that PDGFRα+ OLPs were differentiating and turning off PDGFRα expression during the time course of the experiment.

When I administered tamoxifen to more mature *PDGFRa-CreER^{T2}*/R26-YFP mice (P60) and examined brain sections at various time-points thereafter by immunostaining for YFP and PDGFRα (**Fig.3.6a**; **Fig.3.7a**), I also observed a decline in the proportion of YFP+ cells that were PDGFRα-labelled in the corpus callosum with time (**Fig. 3.6c**). This was also detected in the motor cortex (**Fig. 3.7c**). To determine the identity of the differentiated OLPs, I labelled brain sections from P60 *PDGFRa-CreER^{T2}*/R26-YFP mice for YFP and CC1 (**Fig.3.6b**; **Fig.3.7b**).

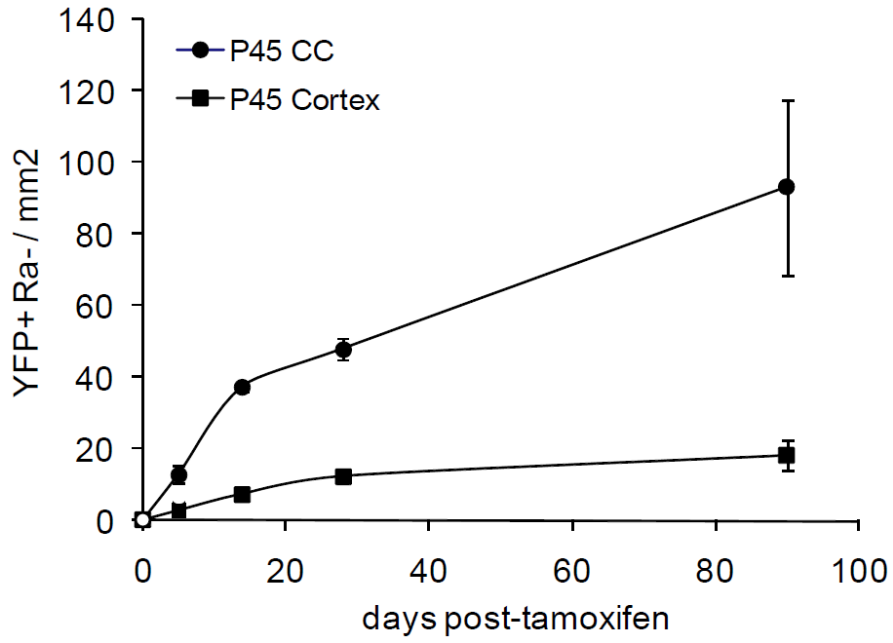

Figure 3.5 *Tracing studies of OLPs in early adulthood. TM was administered to PDGFRa-CreER^{T2}/R26-YFP transgenic mice at P45. The brains were immunolabelled with antibodies against YFP and PDGFRa. The number of differentiated (PDGFRa-negative) YFP+ cells was counted in the corpus callosum and cortex at 5, 14, 28 and 90 days post tamoxifen. The numbers of YFP+/PDGFRa-negative cells increases with time (cells/mm^2 in a 14μm section, n=4) in both brain regions. (Rivers et al., 2008; data from Leanne E Rivers)*

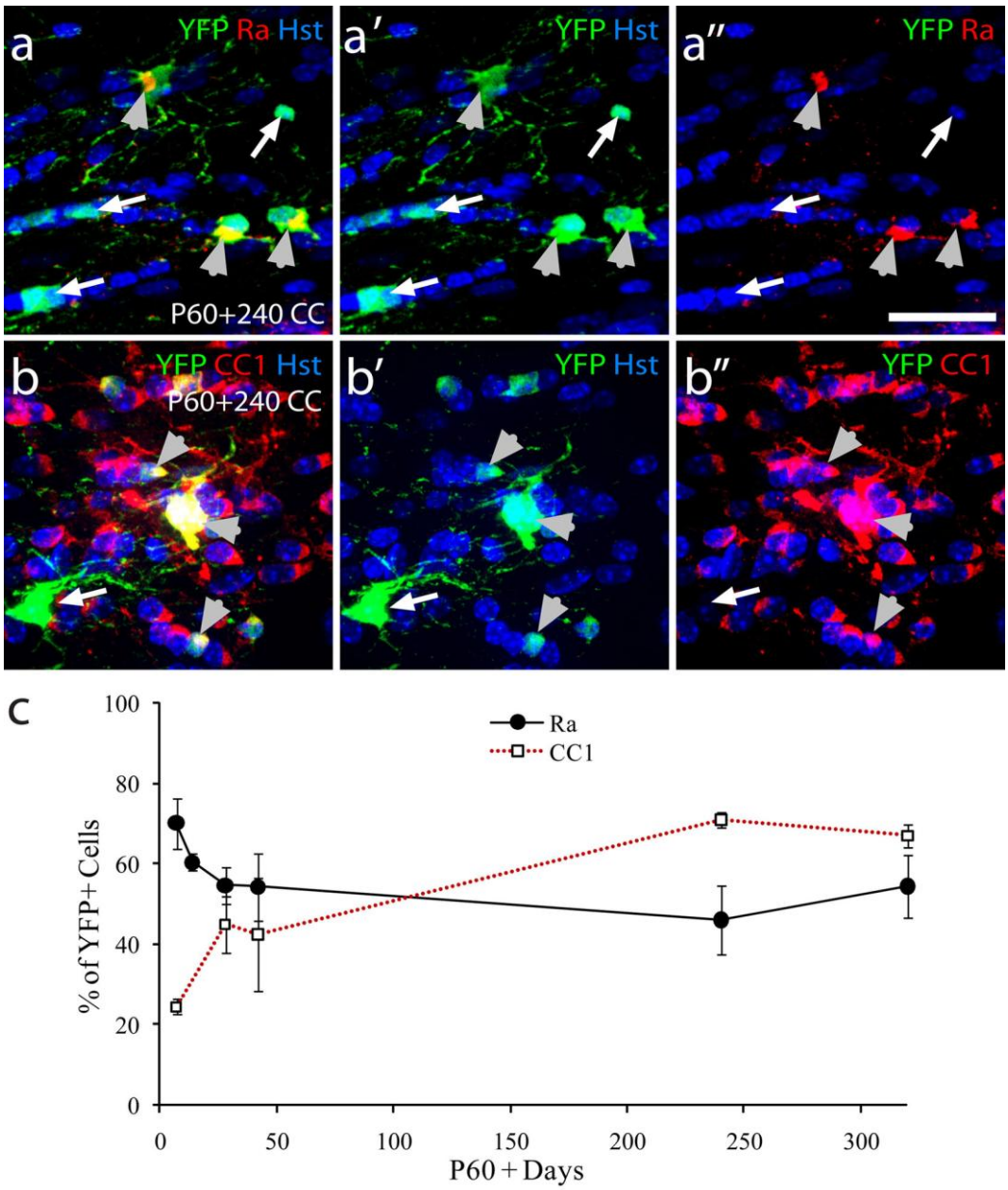

Figure 3.6 *Oligodendrogenesis by adult-born OLPs in the corpus callosum. TM was administered to PDGFRa-CreER^{T2}/R26-YFP transgenic mice at P60. Brain sections were immunolabelled with antibodies against YFP (green) and either PDGFRα (c; red) or CC1 (d; red). White arrowheads show double-positive YFP+/PDGFRα+ or YFP+/CC1+ cells and white arrows single-positive YFP cells. The proportions of OLPs that have differentiated versus the proportion of OLPs that remained at the progenitor stage were plotted as percentages of YFP+/CC1+ and YFP+/PDGFRα+ cells, respectively, from the total number of YFP cells present in the corpus callosum (e).*

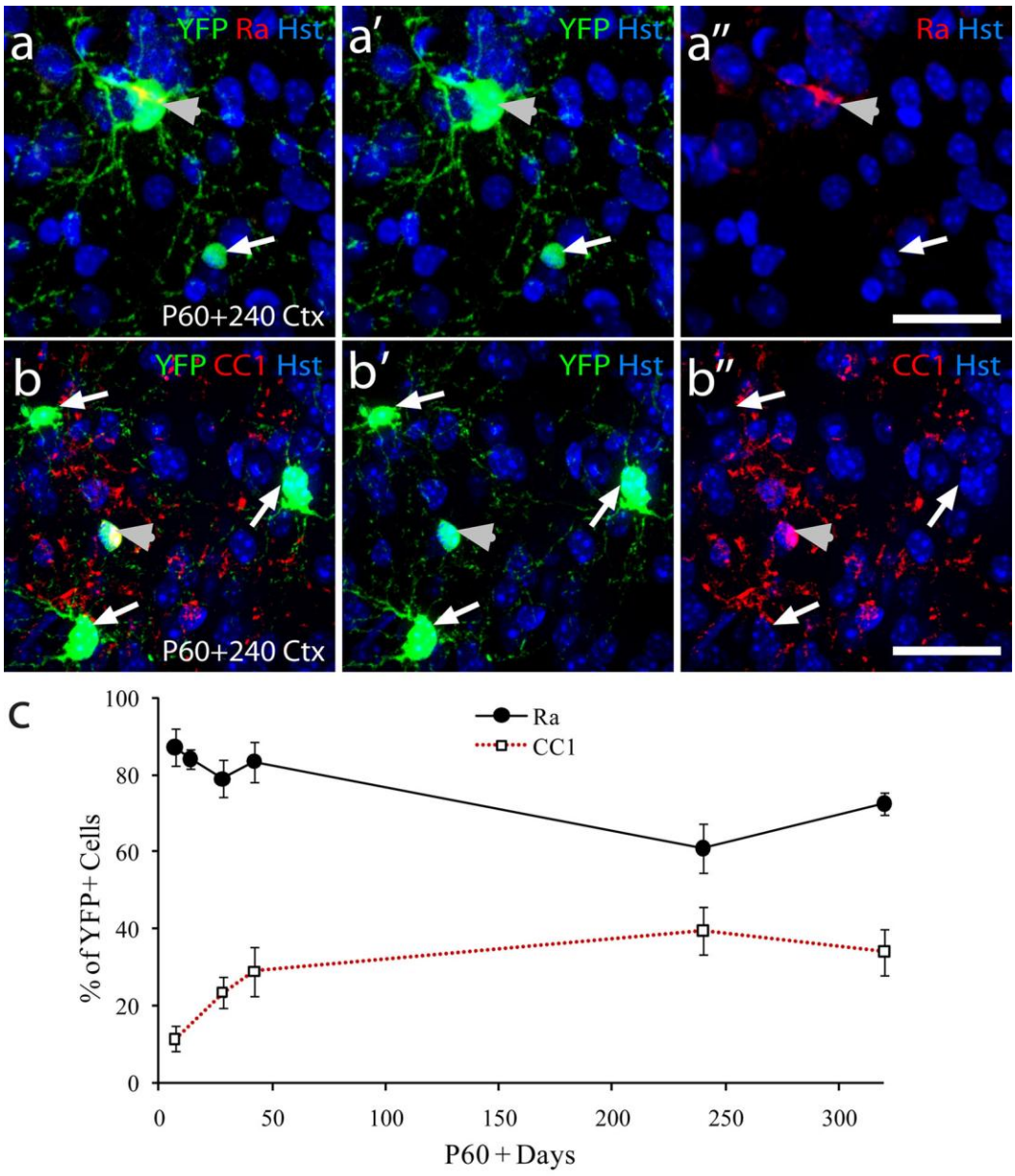

Figure 3.7 *Oligodendrogenesis by adult-born OLPs in the motor cortex. TM was administered to PDGFRa-CreER^{T2}/R26-YFP transgenic mice at P60. Brain sections were stained with YFP (green) and either PDGFRα (c; red) or CC1 (d; red). White arrowheads show double-positive and white arrows single-positive YFP cells. The proportions of differentiated and undifferentiated OLPs were plotted as percentages of YFP+/CC1+ and YFP+/PDGFRα+ cells, respectively, from the total number of YFP cells present in the cortex (e).*

I found that the decline in YFP+ cells co-expressing PDGFRα observed with time, was roughly in line with the increase in YFP+ cells co-expressing CC1 in both the corpus callosum (**Fig. 3.6e**) and the motor cortex (**Fig. 3.7e**). These data support the interpretetion that the YFP+/PDGFRα-negative cells in both the corpus callosum and motor cortex are differentiated oligodendrocytes. Furthermore, Kaylene Young found that YFP+ cells in the corpus callosum and motor cortex co-express OLIG2 but not NeuN or GFAP (Rivers et al., 2008) indicating that OLPs in these regions of the adult brain produce oligodendrocytes but not neurons or astrocytes.

To determine whether the differentiated YFP+ oligodendrocytes produced in the corpus callosum and cortex were myelinating, I performed double immunohistochemistry on tissue from P45 *PDGFRa-CreER^{T2}/R26-YFP* mice sacrificed 210 days post-tamoxifen (P45+210), to label for YFP and either Opalin or Ermin. Opalin is a marker for early myelinating oligodendrocytes and Ermin is a marker for fully mature, myelinating oligodendrocytes (**Fig. 3.1;** Kipper *et al*., 2008; Brockschnieder *et al*., 2006). Numerous YFP+/Opalin+ and YFP+/Ermin+ cells could be identified in both the corpus callosum and the motor cortex (**Fig. 3.8**). In fact, ~50% of YFP+ cells were found to be Opalin+ and ~30% of YFP+ cells were Ermin+ when quantified in the corpus callosum (**Fig. 3.8**). The expression of the more mature oligodendroglial marker, Ermin, by YFP+ cells strongly supports the notion that OLPs in the normal adult brain continue to produce myelinating oligodendrocytes until at least P60.

YFP is a useful tool for the labelling of cells for fate-mapping studies, but, as YFP

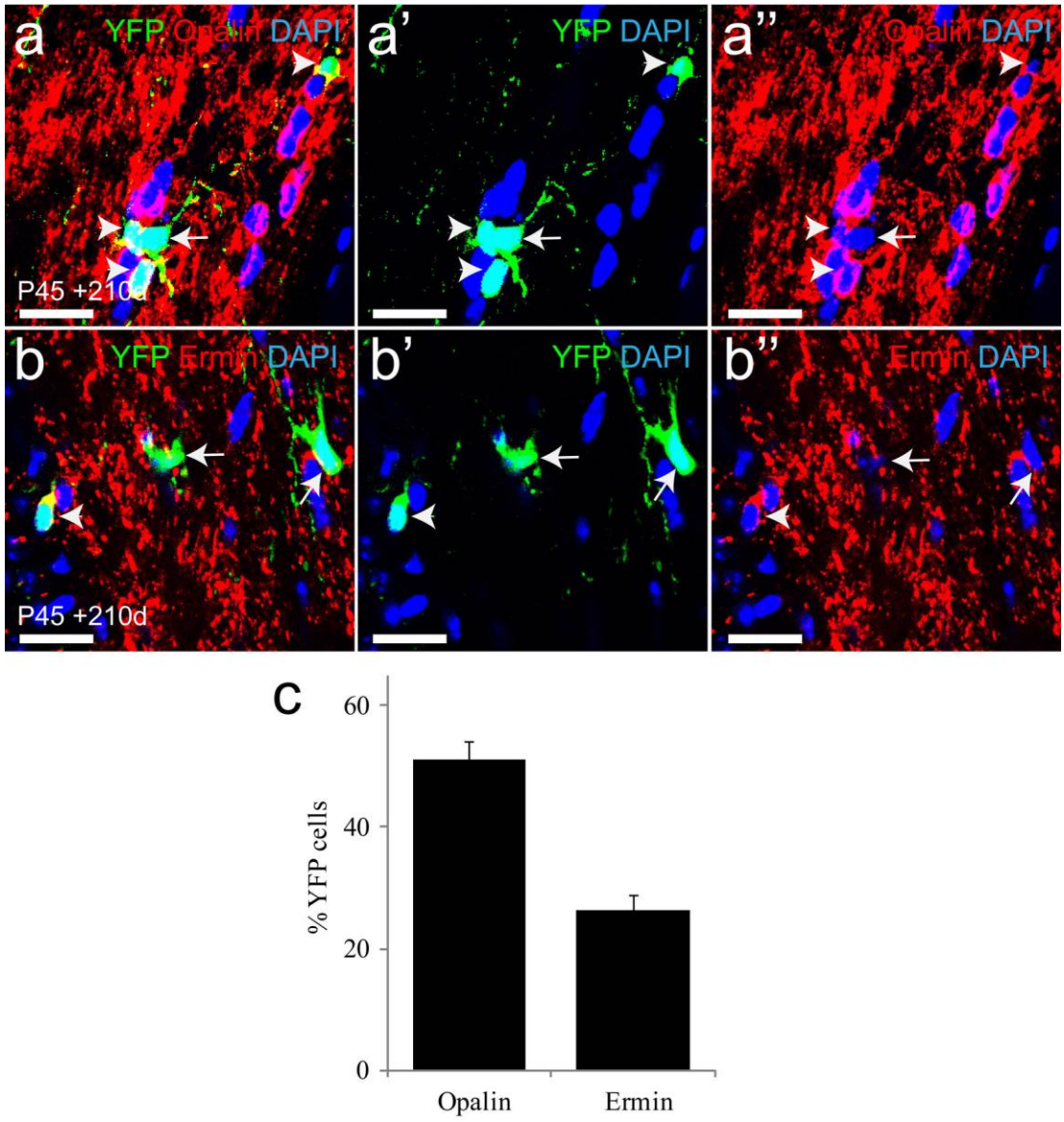

Figure 3.8 *Adult-born OLPs generate myelinating oligodendrocytes in the adult brain. TM was administered to PDGFRa-CreER^{T2}/R26-YFP transgenic mice at P45. The brains were co-stained to detect YFP and either Opalin (a) or Ermin (b) at P255. Within the corpus callosum, the proportion of YFP+ cells that co-expressed Opalin or Ermin was determined against the total number of YFP+ cells present (c). Arrowheads show double-positive YFP+/Opalin+ or YFP+/Ermin+ cells; arrows show YFP+/Opalin- or YFP+/Ermin- cells.*

does not travel into thin cellular processes of oligodendrocytes or to the myelinating sheath, it cannot be used to obtain morphological evidence of myelination.

Therefore, the morphology of adult-born oligodendrocytes was examined by administering tamoxifen to P45 *PDGFRa-CreER^{T2}* transgenic mice crossed with *Tau-mGFP* knock-in reporter mice (see **2.7.1**), in which membrane-targetted GFP (mGFP) is expressed under the transcriptional control of the Tau promoter (Hippenmeyer *et al.*, 2006). Tau is expressed in oligodendrocytes and neurons, but not in OLPs (Richter-Landsberg and Gorath, 1999). Therefore, in *PDGFRa-CreER^{T2}/Tau-mGFP* transgenic mice, tamoxifen administration induces recombination in the OLPs, but GFP is only expressed if the OLP differentiates into an oligodendrocyte and turns on Tau expression. This has two advantages: 1) as the mGFP is membrane targeted it will reveal the full external morphology of oligodendrocytes and 2) the OLPs will remain mGFP-negative, such that, unlike YFP+ cells in the *PDGFRα-CreER^{T2}*/R26-YFP mice, all mGFP+ cells should be differentiated cells.

Sections from P45+150 *PDGFRa-CreER^{T2}/Tau-mGFP* transgenic mice were immunolabelled to detect mGFP expression. By performing conventional (**Fig. 3.9**) and confocal (**Fig. 3.10**) fluorescence microscopy, the morphology of the mGFP+ cells in the corpus callosum, motor cortex, striatum, piriform cortex and external capsule of these mice was examined. The mGFP+ cells in all regions resembled oligodendrocytes. In particular, mGFP+ cells in the white matter had small, circular cell bodies with numerous, dense and extensive processes that run parallel to the

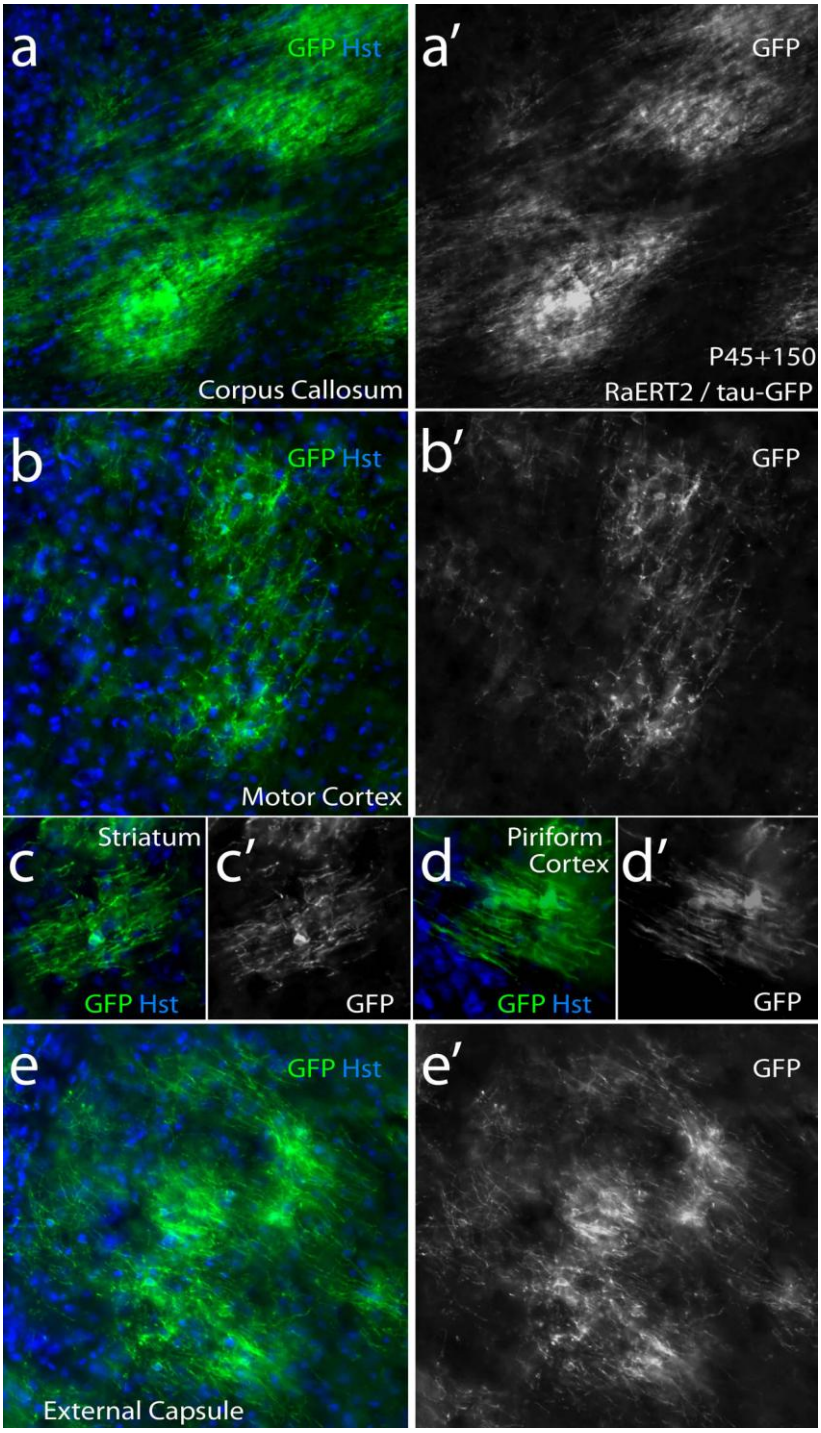

Figure 3.9 *Cells with the morphology of oligodendrocytes are generated from OLPs in the adult CNS. TM was administered to PDGFRa-CreER^{T2}/Tau-mGFP transgenic mice at P45. The brains were stained to detect GFP at P195. The morphology of mGFP+ cells was examined under the conventional microscope in the corpus callosum (a), motor cortex (b), striatum (c), piriform cortex (d) and external capsule (e).*

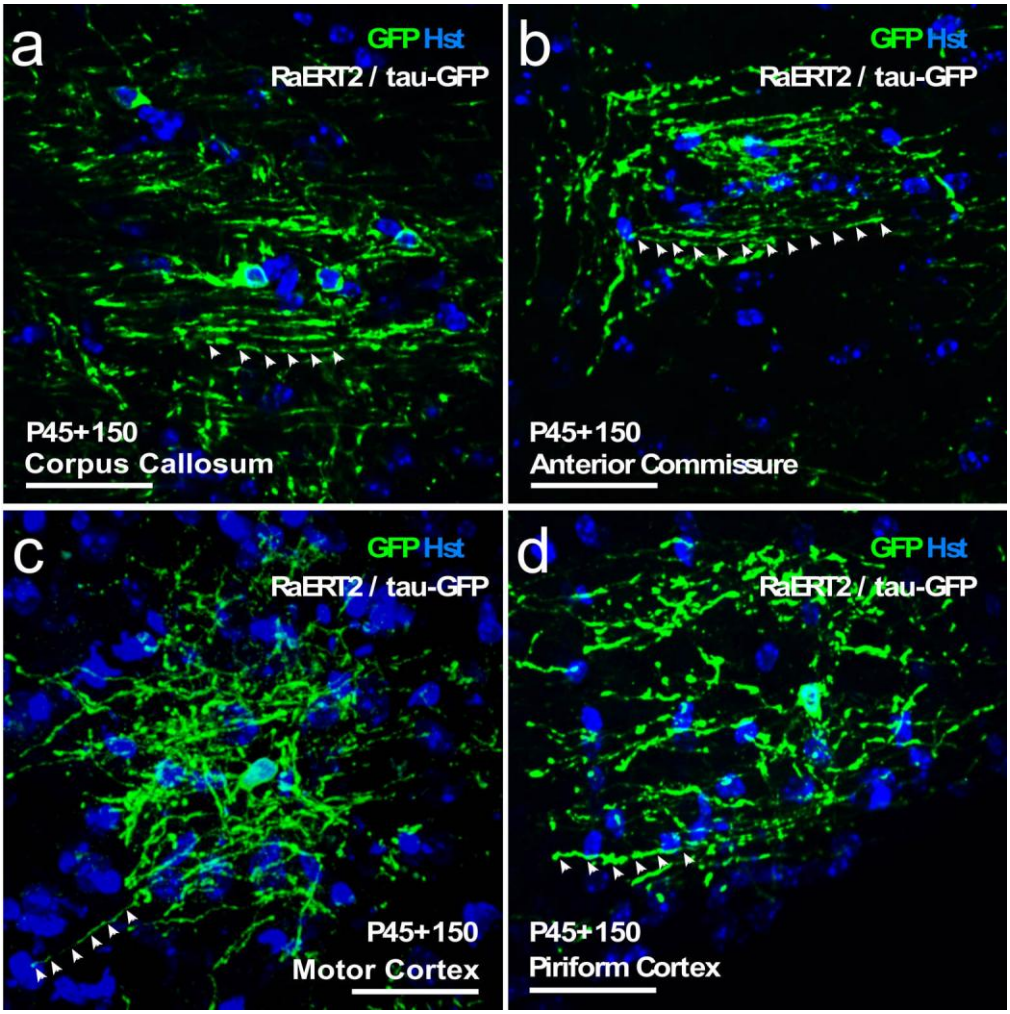

Figure 3.10 *GFP+ cells form thin cytoplasmic processes that resemble oligodendrocytes in the adult mouse brain. Forebrain sections from PDGFRa-CreER^{T2}/Tau-mGFP (P45 T+150d) were prepared and immunolabelled for mGFP. Compressed confocal images were captured to show the many thin cytoplasmic extensions (arrowheads) of the mGFP+ cells in the corpus callosum (a), anterior commisure (b), motor cortex (c) and piriform cortex (d).*

white matter tract (**Fig. 3.9a**). In the grey matter, the cell processes were less dense and less numerous but myelin profiles were still visible (**Fig. 3.9b-e**). By confocal microscopy it was clear that in contrast to the parallel processes of mGFP+ cells in the corpus callosum (**Fig. 3.10a**) the myelinating processes of mGFP+ cells in the cortex were oriented randomly. This is the anticipated morphology of an oligodendrocyte in the cortex, as axons are not closely aligned in grey matter. Higher magnification images clearly show the cellular processes of the mGFP+ cells (**Fig. 3.10**). The identity of the mGFP+ cells in the *PDGFRa-CreER^{T2}/Tau-mGFP* transgenic mice was next confirmed by immunolabelling with the oligodendrocyte progenitor marker NG2 (**Fig. 3.11a**), the oligodendrocyte marker CC1 (**Fig. 3.11b**), the general oligodendroglial-lineage marker OLIG2 (**Fig. 3.11c**) in combination with the astrocyte marker, s100 (**Fig. 3.11c**) and the neuronal marker NeuN (**Fig. 3.11d**). mGFP+ cells were never s100+/OLIG2-, indicating that astrocytes are not labelled in *PDGFRα-CreER^{T2}/R26-YFP* (Rivers *et al*., 2008) or *PDGFRα-CreER^{T2}/Tau-mGFP* transgenic mice (**Fig. 3.11c, e**). As predicted from tracing OLPs previously using the *PDGFRα-CreER^{T2}/R26-YFP* transgenic mice, the mGFP+ cells detected using *Tau-mGFP* reporter mouse were negative for NeuN (**Fig. 3.11d, e**). However, all mGFP+ cells were found to be positive for OLIG2, which reflects the notion that they all belong to the oligodendrocyte lineage (**Fig. 3.11c, e**). Of the mGFP+ cells present in the corpus callosum, a small proportion (~5%) expressed the OLP marker NG2 (**Fig. 3.11a, e**). This proportion was greater in the motor cortex (~35%) (**Fig. 3.11a, e**). The vast majority of mGFP+ cells clearly expressed the oligodendrocyte marker CC1 both in the corpus callosum (~96% of all mGFP+ cells were CC1+) and in the motor cortex (~85% of all mGFP+ cells were CC1+) (**Fig. 3.11b, e**). The apparent overlap

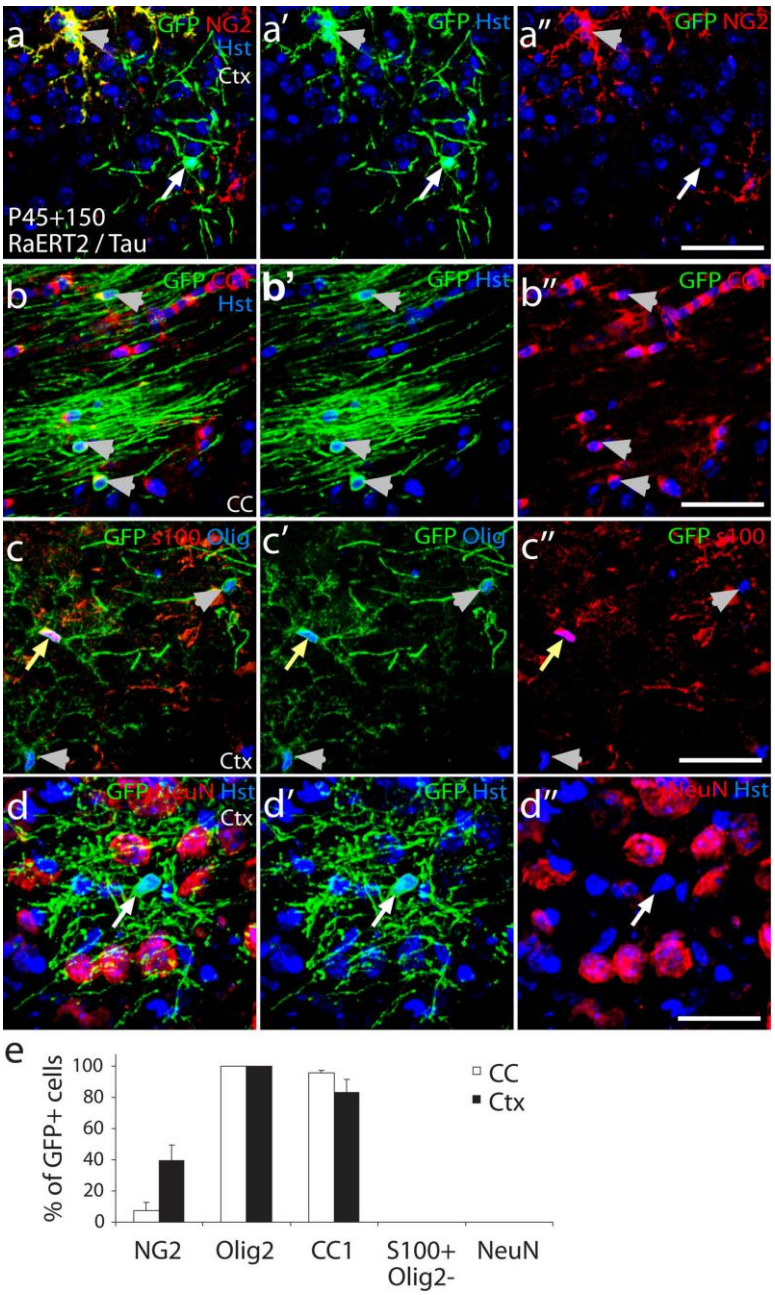

Figure 3.11 *Identity of GFP+ cells in the motor cortex of the PDGFRα-CreER^{T2}/Tau-mGFP transgenic mice. Brain sections from P60 PDGFRα-CreER^{T2}/Tau-mGFP transgenic mice were immunolabelled with antibodies against GFP and NG2 (a), CC1 (b) OLIG2+s100 (c) and NeuN (d). Double positive mGFP+/CC1+ and mGFP+/OLIG2+/s100- cells (white arrowheads) were detected in the corpus callosum and motor cortex. A small number of double positive mGFP+/NG2+ cells were also present in both brain regions. No double positives were detected by staining for GFP and NeuN. White arrows show the single positive mGFP cells. The proportion of mGFP+ cells that co-expressed the aforementioned markers was quantified (e).*

of NG2+ and CC1+ expression by cells in the motor cortex may reflect the differing rate of cell production in the white versus the grey matter and a corresponding slower differentiation rate, with NG2 being downregulated more slowly in the cortex than in the corpus callosum.

In addition to staining for cell body markers of oligodendrocytes, expression of mGFP in what appears to be the myelin internodes of oligodendrocytes labelled in *PDGFRα-CreER^{T2}/Tau-mGFP* transgenic mice allowed, unlike with the *R26YFP*, co-staining for GFP and myelin markers such as MBP. Both in the corpus callosum (**Fig. 3.12b**) and motor cortex (**Fig. 3.12a**) the "bars" of mGFP co-localized with MBP.

Collectively, tracing from *PDGFRα-CreER^{T2}/R26-YFP* and *PDGFRα-CreER^{T2}/Tau-mGFP* transgenic mice has provided strong evidence that adult OLPs are generating a significant number of myelinating oligodendrocytes in both the grey and white matter in adult life. Furthermore, oligodendrocytes are the only cell type being produced by OLPs in the corpus callosum and motor cortex.

These findings raise questions concerning the necessity of adult oligodendrogenesis in such a significant amount under healthy conditions. To determine whether the rate of adult oligodendrogenesis was plastic, we attempted to trigger activity-dependent oligodendrocyte production by voluntary exercise (wheel running), which requires inter-hemispherical communication, and might potentially stimulate oligodendrogenesis in the corpus callosum. For this, *PDGFRα-CreER^{T2}/R26-YFP*

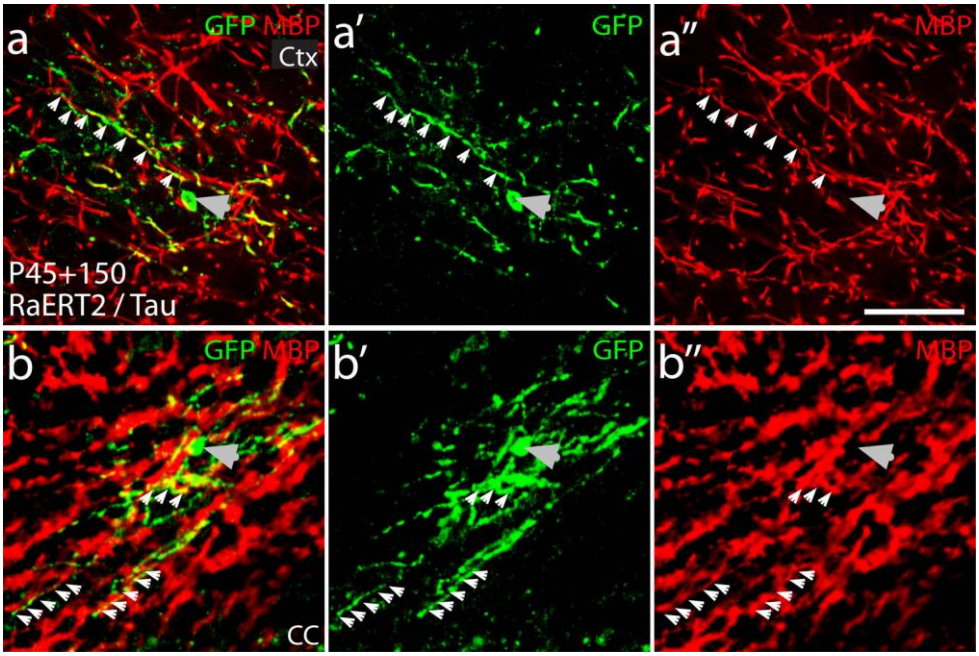

Figure 3.12 m*GFP+ cells in the PDGFRa-CreER^{T2}/Tau-mGFP transgenic mice are myelinating oligodendrocytes. Brain sections from adult (P45+150) PDGFRa-CreER^{T2}/Tau-mGFP were immunolabelled with antibodies against GFP and MBP and single-scan confocal images were taken in the motor cortex (a) and corpus callosum (b). Large arrowheads show the cell bodies of the cells and small arrowheads follow the cytoplasmic extensions.*

transgenic mice were given tamoxifen at P80 and were housed individually either with access to a running wheel for 1 month, or in equivalent housing with a non-functional running wheel. Mice housed in voluntary exercise conditions ran ~7km per day between 6pm and 6am. Brain sections from these mice were then immunolabelled with antibodies against YFP and PDGFRα, and the percentage of YFP+ cells that were PDGFRα- was quantified in the corpus callosum (**Fig. 3.13**). The production of differentiated cells (YFP+/PDGFRα-) was elevated in male running mice when compared to controls (two-tailed t-test; $P<0.002$; n=6 controls, n=10 runners).

Similarly, an elevated production of differentiated cells was noted in female running mice when compared to controls (two-tailed t-test; $P<0.002$; n=6 controls, n=11 runners). Since the data were not noticeably affected by sex, i.e. there was no statistically significant difference between male and female control groups ($P=0.95$) nor between male and female running groups ($P=0.90$), data from the control and running groups of both genders were pooled (two-tailed t-test; $P=0.015\text{x}10^{-5}$; n=12 controls, n=21 runners). ~30% of YFP+ cells had down-regulated PDGFRα in the control group compared to ~40% in the running group suggesting that the rate of adult oligodendrocyte production in the corpus callosum increased as a result of exercise that requires inter-hemispherical communication (**Fig.3.13**). This finding indicates that the behaviour of adult OLPs is dynamic and under environmental control.

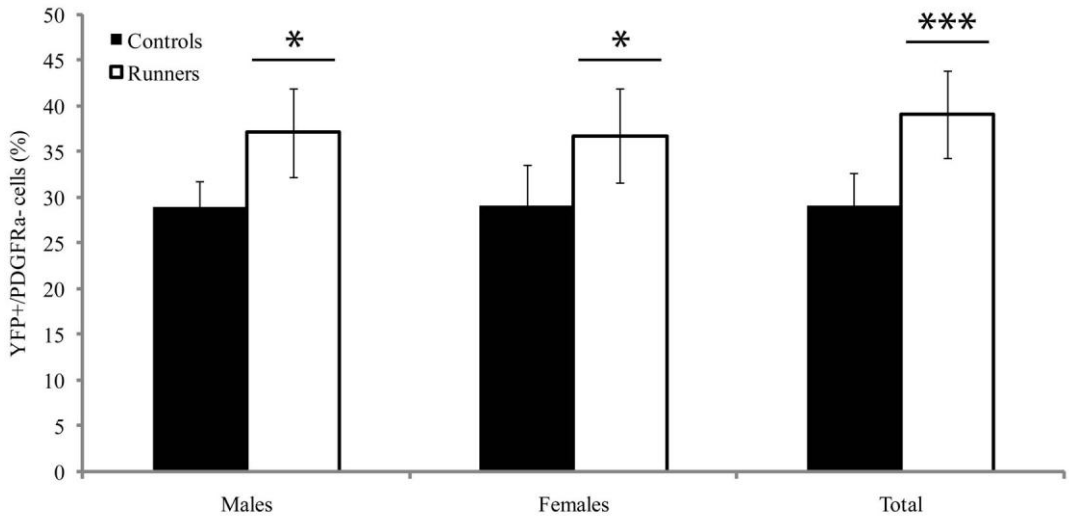

Figure 3.13 *Voluntary exercise increases oligodendrocyte production by adult OLPs. Tamoxifen was administered to P80 PDGFRα-CreER^{T2}/R26-YFP transgenic mice, which were then individually housed either with non-functional running wheel (controls) or with normal running wheels (runners). Oligodendrogenesis by adult OLPs is expressed as the percentage of YFP+/PDGFRα- cells in the total YFP+ cells. Males and females were first plotted separately and were subsequently merged (t-test; *P<0.0002, ***P=0.015x10^{-5}). Data for this figure was contributed by Ian McKenzie and Konstantina Psachoulia.*

3.2.4 Adult OLPs give rise to cortical projection neurons

When examining brain regions, outside of the corpus callosum and motor cortex in tamoxifen-dosed *Pdgfra-creER^{T2}/R26-YFP* mice, it was noted that some of the YFP+ cells in the anterior piriform cortex did not have the typical OLP or oligodendrocyte morphology, but rather resembled neurons, and co-stained for NeuN (**Fig. 3.14a**). These cells were either labelled by direct recombination in the neurons, or were produced by differentiation of PDGFRα+ OLPs. Labelling by direct recombination was unlikely as NeuN+ piriform cortical neurons did not express PDGFRα by protein staining (**Fig. 3.14b**) nor did they express Cre mRNA by double in situ/immunohistochemistry (Rivers *et al*., 2008). When *Pdgfra-creER^{T2}/R26-YFP* transgenic mice were dosed with TM at P45 and YFP+ cells were traced for up to 210d, the number of YFP+/NeuN+ cells in the anterior piriform cortex was found to significantly increase with time (**Fig. 3.14c-d**). ~1.4% of the NeuN+ cells present in layers II and III of the piriform cortex at 8 months (P45 + 210) were generated after P45 (~250 surviving YFP+/NeuN+ neurons found in 18 sections containing an estimated 4×10^4 NeuN+ projection neurons; 250x1/0.45x4x10^4x100, where 0.45 corresponds to the recombination efficiency in the *Pdgfra-creER^{T2}/R26-YFP* transgenic mice). The same experiment was performed using the *Fgfr3-iCreER^{T2}/R26-YFP* transgenic mice to examine the contribution of SVZ stem cells and brain astrocytes to neurogenesis in the piriform cortex. No accumulation of YFP+/NeuN+ cells was noted (**Fig. 3.14c**). Therefore, we are confident that the YFP+ neurons detected derive from differentiating PDGFRα-expressing precursors, most probably OLPs.

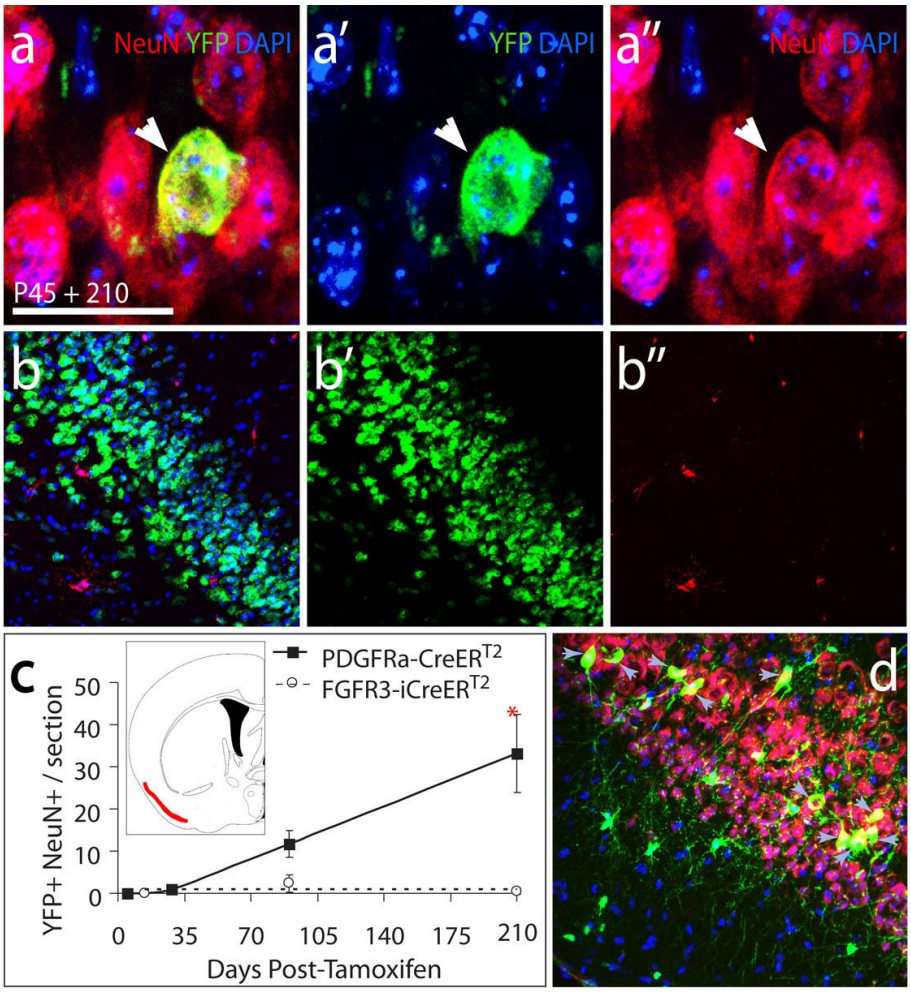

Figure 3.14 *OLPs generate cortical projection neurons in vivo. TM was administered to PDGFRa-CreER^{T2}/R26-YFP transgenic mice at P45. Ventral forebrain sections were prepared and immunolabelled for YFP and neuronal lineage (NeuN; a) OLP (PDGFRα; b) markers at P255. YFP+/NeuN+ cells appeared in the anterior piriform cortex (a). Co-localization of PDGFRα and NeuN was never observed (b) excluding the possibility of expression of PDGFRα in neuron driving the transgene expression. YFP+/NeuN+ cells accumulated over time (c, d) in contrast to Fgfr3-iCreER^{T2}/R26-YFP transgenic mice (YFP labels for all SVZ stem cells and many protoplasmic) (c), supporting the conclusion that adult-born neurons are formed outside the SVZ. Arrowheads point to the YFP+/NeuN+ cells. Leanne E Rivers, Kaylene M Young and Konstantina Psachoulia contributed data for this figure.*

To determine which type(s) of neuron was being produced from OLPs in the piriform cortex of adult mouse brains, brain sections from *PDGFRa-CreER^{T2}/R26-YFP* transgenic mice (P45 T+210) were triple labelled for YFP, NeuN and a variety of interneuron markers; calbindin (Cb), calretinin (Crt), neuropeptide-Y (NPY), parvalbumin (Pv) nitric oxide synthase (nNOS), tyrosine hydroxylase (TH), somatostatin (SST) and reelin (**Fig. 3.15**). No triple positive cells were found among an average of about 120 YFP+/NeuN+ cells counted for each interneuronal marker. Therefore, it is extremely unlikely that these cells are cortical interneurons (**Fig. 3.15g**). In addition, for brain sections stained with tyrosine hydroxylase and somatostatin, no cells were detected that stained for these markers in layer II of the anterior piriform cortex.

Therefore, we examined the morphology of OLP-derived YFP+ neurons in the piriform cortex in more detail. High magnification images revealed that YFP+ cells appeared to be of two morphological types, reminiscent of the two types of projection neurons known to reside in layer II of the anterior piriform cortex: semilunar and superficial pyramidal (**Fig. 3.16**). As YFP does not penetrate fine processes, we again switched to analysing tissue from *Pdgfra-CreER^{T2}/Tau-mGFP* (P45 +150d). As we previously observed using the *Pdgfra-CreER^{T2}/R26-YFP* transgenic mice, a considerable number of neurons were found in the piriform cortex of the *Pdgfra-CreER^{T2}/Tau-mGFP* mice. The mGFP+ neurons detected had their cell bodies in layer II, but their dendritic arbors projected to the pial surface, which is the location of the lateral olfactory tract. This is consistent with the notion that the neurons derived from adult OLPs are projection neurons, as projection neurons of the

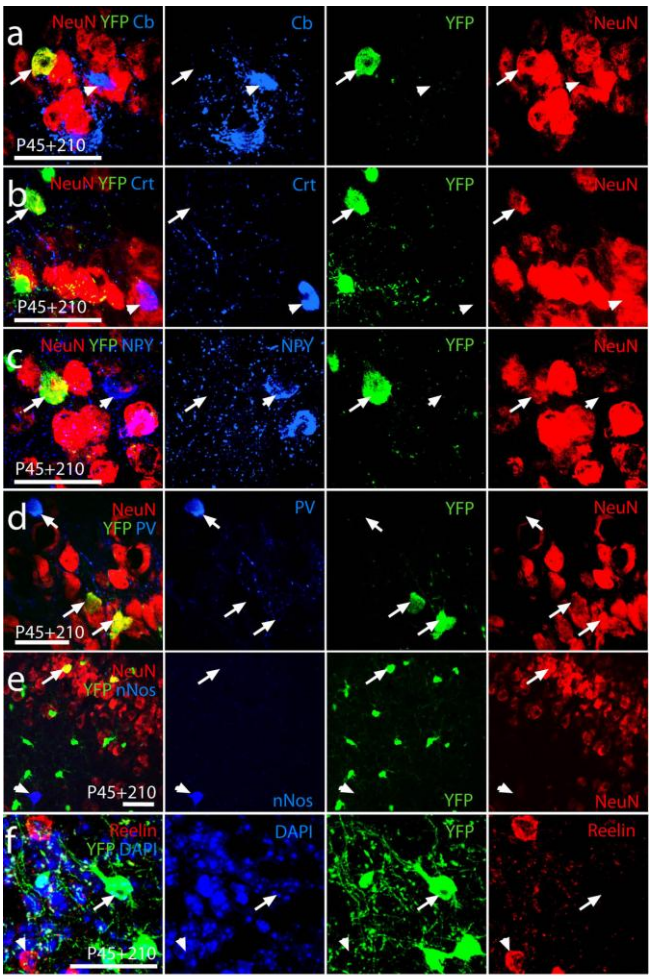

g

Interneuron Marker	P45 + 210 days PDGFRα-CreERT₂	YFP+ NeuN+ cells in the PC that are interneuron +	YFP+ cells in the PC that are interneuron +
Calbindin (Cb)	n = 3	0 / 125	0 / 500
Calretinin (Crt)	n = 3	0 / 166	0 / 500
Neuropeptide Y (NPY)	n = 3	0 / 172	0 / 500
Parvalbumin (PV)	n = 3	0 / 129	0 / 500
Neuronal Nitric Oxide Synthase (nNOS)	n = 3	0 / 92	0 / 500
Reelin	n = 3	0 / 85	0 / 500

Figure 3.15 *Adult-born piriform neurons do not express interneuron markers. Images in a-d show layer 2 of the piriform cortex immunolabelled for YFP, NeuN and one of the interneuron markers (arrowheads) Calbindin (Cb), Calretinin (Crt), Neuropeptide-Y (NPY) or Parvalbumin (Pv). YFP+/NeuN+ neurons are indicated by arrows. No immunolabelled interneurons were YFP+. Two other interneuron markers, Tyrosine Hydroxylase (TH) and Somatostatin (SST) were also tested but no immuno-positive interneurons were detected, either YFP+ve or YFP–ve, in this part of the piriform cortex. YFP+ neurons (NeuN+ or Sox10-) did not label for Nitric Oxide Synthase (nNOS) (e) or Reelin (f). Numbers of cells scored are tabulated in g.*

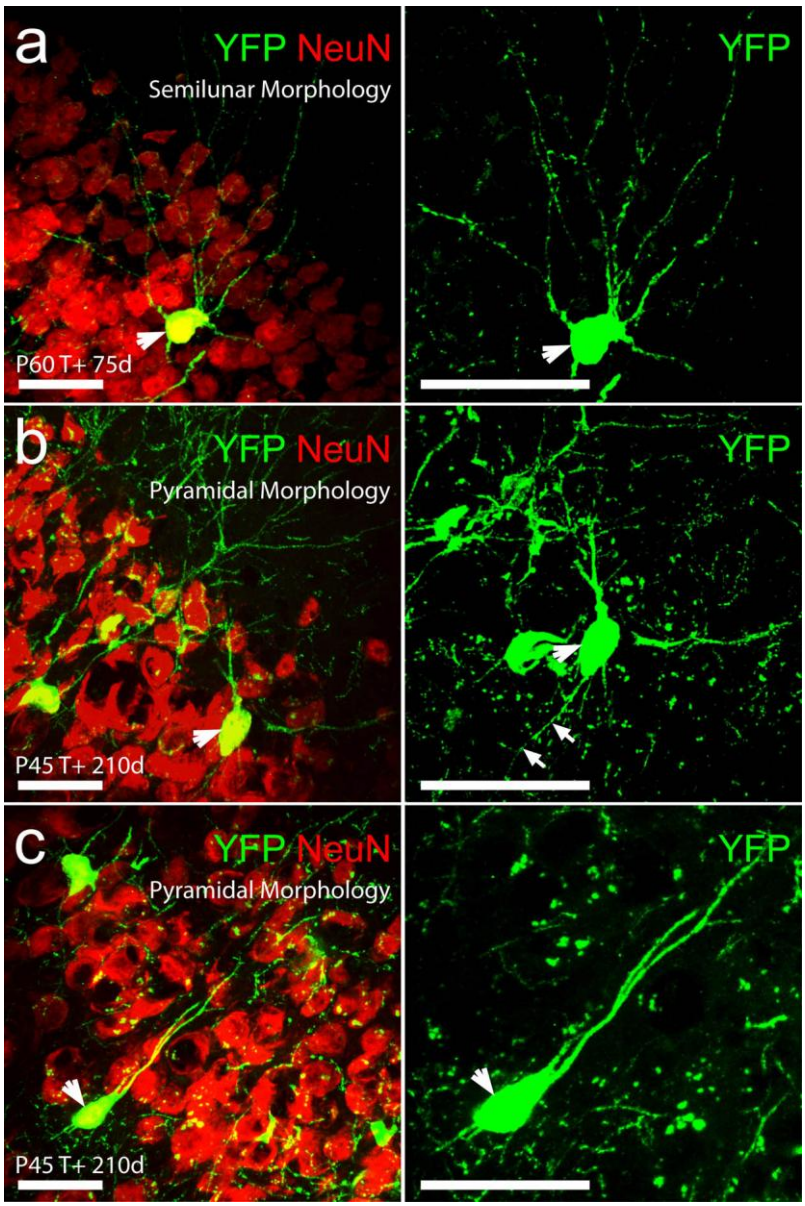

Figure 3.16 *Morphologies of YFP-labeled neurons in the piriform cortex. TM administration to PDGFRa-CreER^{T2}/R26-YFP transgenic mice at P45 or P60 and immunostaining of brain section to detect YFP and NeuN 75 or 210 days post-TM, revealed two types of principal neurons; semilunar neurons and superficial pyramidal (**a**–**c**). Semilunar neurons are often located more superficially than superficial pyramidal neurons (layer 2a and 2b, respectively). From morphology and their positions in layer 2, YFP+/NeuN+ neurons observed are considered to correspond to semilunar (**a**) and superficial pyramidal (**b**,**c**) neurons. Scale bars represent 30 µm.*

piriform (olfactory) cortex receive input from the olfactory bulb along the lateral olfactory tract (**Fig. 3.17**). To be completely confident that these new neurons were indeed projection neurons, it would have been ideal to trace their axonal projections. However, due to the significant number of mGFP-labelled oligodendrocytes with highly complex morphology that were present in layer III of the piriform cortex, it was not possible to trace the mGFP+ neuronal axons.

Collectively, these data indicate that OLPs in the adult piriform cortex do not produce interneurons, but produce projection neurons at a steady rate throughout adult life. To examine whether these neurons were newly-born, i.e. produced from a recent cell division, *Pdgfra-CreER^{T2}/R26-YFP* transgenic mice were tamoxifen-dosed and given BrdU into their drinking water for a period of 100 days. BrdU is taken up by cells as they divide (see **2.7.2**), and brain sections from these mice were subsequently stained with antibodies against YFP, NeuN and BrdU (**Fig. 3.18**). It was not possible to find a single BrdU+/NeuN+/YFP+ cell. Therefore, we conclude that these neurons are most likely formed by direct trans-differentiation of PDGFRα+ cells, i.e. without an intervening cell division.

3.3 Discussion

Adult OLPs have been implicated in the generation of new myelinating oligodendrocytes in adulthood under demyelinating conditions, due either to mechanical injury or chemically-induced acute experimental demyelination (Gensert *et al.*, 1997; Watanabe *et al.*, 2002). However, the extent to which OLPs add new myelinating oligodendrocytes to the healthy adult CNS has not previously been

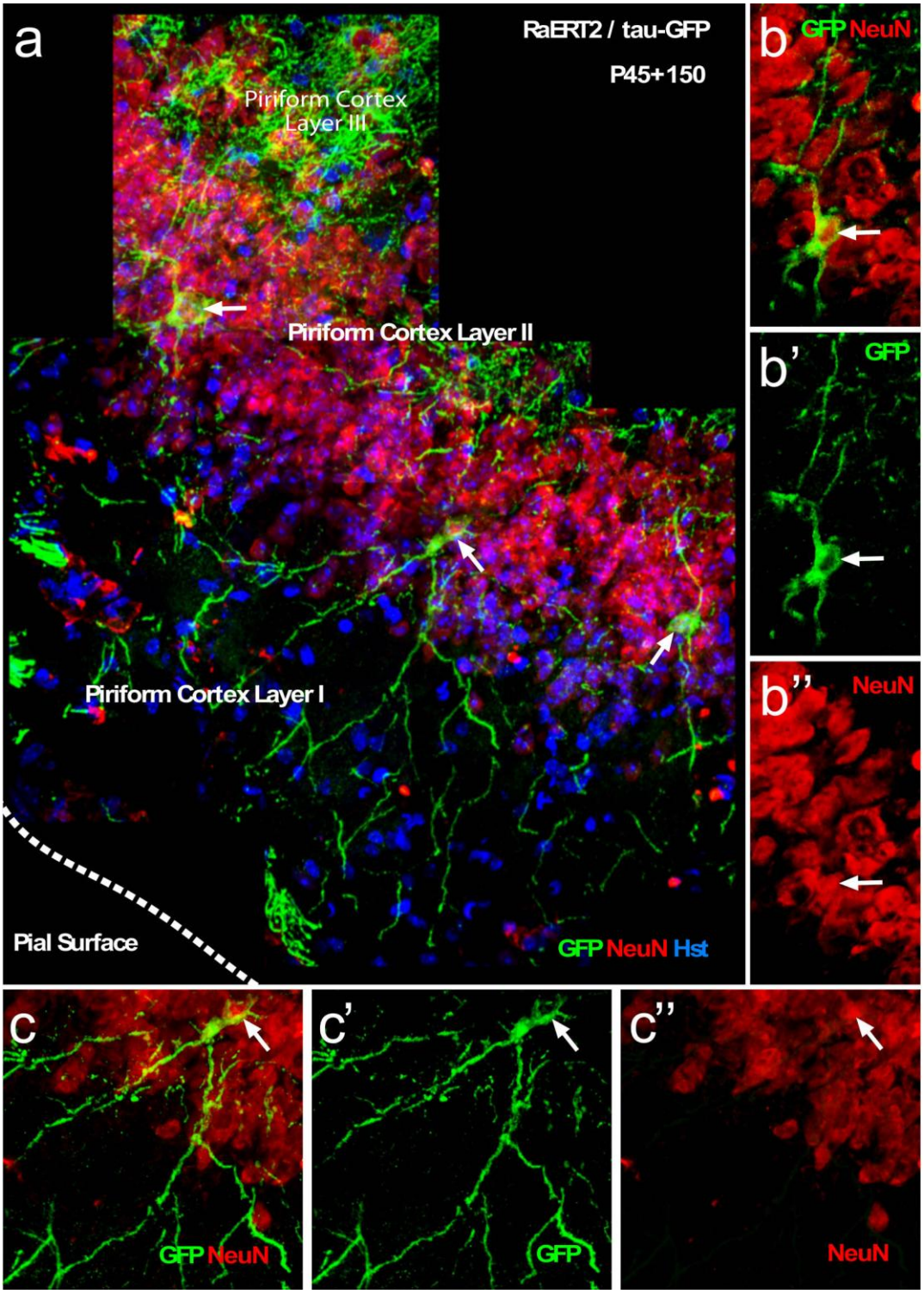

Figure 3.17 *GFP+ neurons in the CNS of PDGFRa-CreER^{T2}/Tau-GFP. Forebrain sections from P45 T+150d mice were prepared and immunolabelled for GFP and NeuN. Compressed (a) and single-scan (b-c) confocal images were captured to show the neuronal morphology, orientation and extent of the GFP+ neuronal processes.*

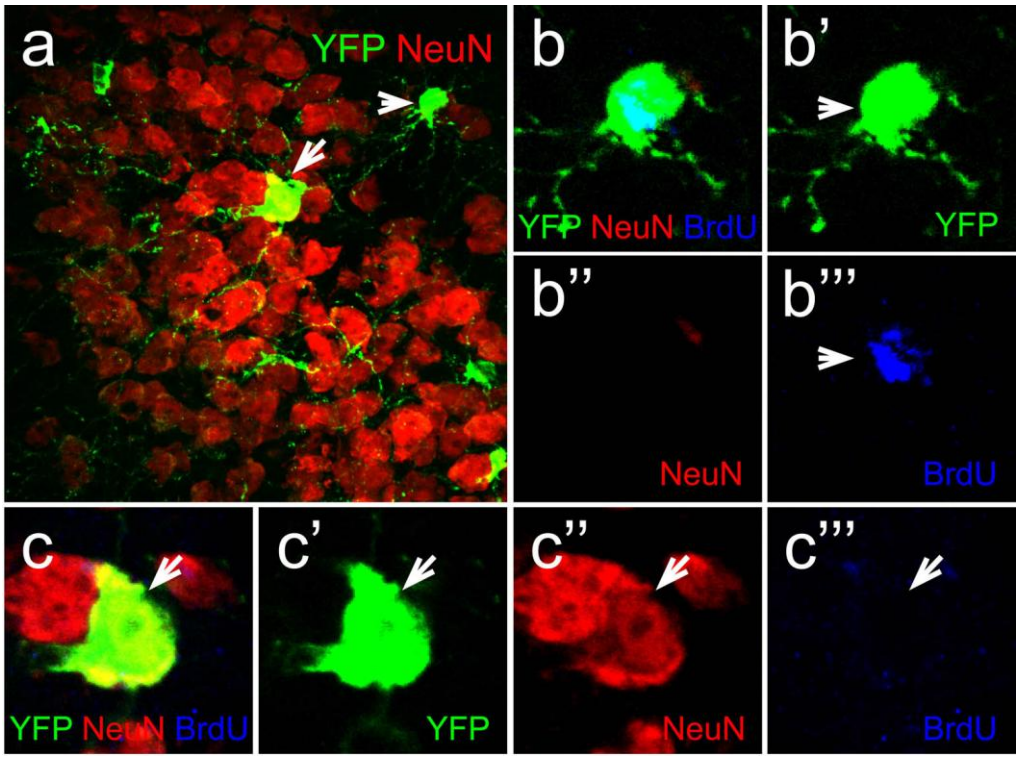

Figure 3.18 *YFP+/NeuN+ cells are not labelled with BrdU. In order to determine whether YFP+ neurons arise from the dividing OLP population, BrdU was administered to PDGFRa-CreER^{T2}/R26-YFP transgenic mice at P45 for a period of 100 days. No YFP+/NeuN+/BrdU+ cell was found in the anterior piriform cortex across three 30µm brain sections from 3 mice examined.*

investigated. This has been clearly addressed here using *PDGFRa-CreER^{T2}/R26-YFP* transgenic mice to label and trace OLPs in the adult brain. We show that PDGFRα+ cells generate new myelin-forming oligodendrocytes in the adult corpus callosum. The importance of this finding is two-fold: firstly, it indicates that adult OLPs in the white and grey matter generate progeny that persist in the brain for at least one year after birth, a remarkable amount of time considering the average lifespan of mice (~2 years in captivity). Secondly, when taken alongside our P45 tracing data which indicated that all YFP+ cells were oligodendrocyte lineage cells (SOX10+/OLIG2+; Rivers *et al.*, 2008), these data suggest that OLPs exclusively produce oligodendrocytes in the corpus callosum and motor cortex of the normal adult brain. That the new cells are truly myelinating oligodendrocytes was further confirmed using *PDGFRa-creER^{T2}/Tau-mGFP* transgenic mice. While OLPs were not mGFP labelled in this reporter mouse, all neurons and oligodendrocytes generated from OLPs were clearly labelled by the membrane targeted mGFP, which highlighted the myelin internodes of the adult born oligodendrocytes. Many new differentiated cells (PDGFRα- and NG2-negative) were also produced in the motor cortical grey matter of the *PDGFRa-CreER^{T2}/R26-YFP* transgenic mice. An independent study using *Olig2-CreER^{T2}* transgenic mice (in which transgene activity in adulthood marked NG2 cells but not differentiated oligodendrocytes) came to similar conclusions (Dimou *et al.*, 2008).

There were prominent differences when comparing adult oligodendrogenesis in the white versus grey matter: 1) the rate of oligodendrocyte production was less in the grey versus white matter and 2) the morphology of the adult-born oligodendrocytes

in white matter was that of classical myelinating oligodendrocytes with parallel processes, whereas those that formed in the motor cortex had processes resembling myelin internodes, but these were fewer in number and they were randomly oriented with respect to the cell body.

Similarity between oligodendrocytes, in white and grey matter, lies with their expression of the oligodendrocyte protein CC1 and the myelin protein MBP, which in turn means that adult OLPs are capable of generating myelinating oligodendrocytes under normal conditions in both grey and white matter. Nevertheless, the fact that in the *PDGFRa-CreER^{T2}/Tau-mGFP* mouse there were significantly more mGFP+ cells that expressed NG2 in the motor cortex than in the corpus callosum might imply that, in the grey matter, OLPs differentiate more slowly allowing overlap between NG2, Tau and possibly CC1 expression. These data are consistent with those from the *PDGFRa-CreER^{T2}/R26-YFP* transgenic mice, where there was an overlap between YFP+ cells that expressed PDGFRα and YFP+ cells that expressed CC1.

We report that a substantial number of oligodendrocytes are added to the adult brain. The function of adult oligodendrogenesis however is still not understood, yet, it could be serving two roles in the adult CNS: 1) new oligodendrocytes might replace oligodendrocytes that die through normal wear-and-tear and 2) OLPs might generate new, additional oligodendrocytes in the mature brain. The functional necessity of oligodendrocyte addition is still unclear. However, evidence for activity-dependent changes in white matter volume in humans suggests that it may be necessary for

motor learning, adding to the notion of cellular plasticity for the adult brain (Bengtsson *et al*., 2005). It is interesting to note that the corpus callosum is a mixture of both myelinated and unmyelinated axons. Even in P240 mice, ~70% of corpus callosal axons remain unmyelinated (Sturrock *et al*., 1980). Therefore, OLPs might differentiate into oligodendrocytes that myelinate previously naked axons. This would represent a new form of neural plasticity. As myelination speeds up axonal conduction, it could therefore enhance/alter the functional significance of neuronal circuits. The running wheel experiment is consistent with this concept, as it demonstrates that oligodendrogenesis can be increased in the corpus callosum of the adult brain as a result of exercise that involves inter-hemispherical communication. However, this experiment does not determine how running is altering oligodendrogenesis. It is known that running increases neurogenesis in the brain by increasing neurotrophin release (Wolf *et al*., 2006). As oligodendrocyte lineage cells can also respond to neurotrophins and other growth factors (reviewed in Du and Dreyfus, 2002), these might be responsible for the 20% increase in oligodendrocyte production observed. Further experiments would be required to determine what physiological changes are induced by exercise and how they promote oligodendrogenesis.

It is important to note that no astrocyte production by OLPs was observed in adulthood. In contrast, Zhu *et al.* (2008) showed a small population of protoplasmic astrocytes in the ventro-lateral forebrain of *Ng2-Cre/CAGG-Z/EG* double- transgenic mice (Zhu *et al*., 2008). As this experiment collectively traced the fate of OLPs over the lifetime, it is likely that the GFP+ astrocytes cells identified in adulthood were

generated embryonically or early in postnatal development as was reported by Guo *et al*. (2009) using the *PLP-CreER*^{T2} transgenic mouse to trace the developmental behaviour of OLPs. Similar to our findings, fate mapping adult OLPs using *Olig2-iCreER*^{T2}*/CAGG-Z/EG* transgenic mice detected no production of astrocytes by adult OLPs under normal conditions (Dimou *et al.,* 2008).

In addition to oligodendrogenesis, we found constitutive neurogenesis from OLPs in part of the normal adult brain. In the anterior piriform cortex of the *PDGFRa-creER*^{T2}*/R26-YFP* mice, YFP+ neurons emerged a few weeks after tamoxifen administration and accumulated with time. mGFP+ neurons were also detected in the piriform cortex of *PDGFRa-creER*^{T2}*/Tau-mGFP* transgenic mice. These neurons did not express any of the investigated interneuron markers (calbindin, calretinin, neuropeptide-Y, parvalbumin, somatostatin, reelin or tyrosine hydroxylase). Consistent with this, their morphology resembled that of projection neurons, having large cell bodies in layer II and long dendritic arbors directed towards the pial surface, where piriform cortical projection neurons are known to make synaptic connections with axons of the (unmyelinated) lateral olfactory tract (Haberly *et al*., 2001; Suzuki *et al.,* 2006).

The fact that there was no co-localization of the proteins PDGFRα and NeuN by cells within the piriform cortex, strongly suggests that the YFP+ neurons were not labelled in the piriform cortex directly by the expression of PDGFRα. It does not, however, rule out the possibility of ectopic expression of the *PDGFRa-creER*^{T2}*/R26-YFP* transgene by some neurons in this region. However, if piriform cortical neurons did

express the transgene, then YFP+ neurons would be expected to appear soon after tamoxifen treatment, not to accumulate slowly over several months, as observed. Another possibility is that YFP+ neurons might be formed by the fusion of unlabeled neurons with YFP+ non-neuronal cells, but this is also less probable as YFP+ neurons start to appear a few weeks after tamoxifen treatment. Moreover, the fact that YFP is expressed in a particular subset of neurons in the piriform cortex, would imply that the putative fusion event must be highly cell-specific. This still is highly unlikely, especially since YFP+ projection neurons were not observed in *Fgfr3-iCreER^{T2}/Rosa26-YFP* mice, despite the fact that many YFP+ protoplasmic astrocytes were present as potential fusion partners. The simplest scenario is that the YFP+ neurons are formed by differentiation of local, PDGFRα+ OLPs and this explanation has been given further credibility by recent fate mapping studies using other transgenic mice that label OLPs. For example, Guo *et al*. (2010) recently used *Plp-CreER^{T2}/R26-YFP* transgenic mice to label and fate map adult OLPs (Guo *et al*., 2010). Approximately 3 weeks post-tamoxifen treatment, they observed EYFP+ neurons primarily in layer II of the piriform cortex with pyramidal and to a lesser extent semilunar morphology (Guo *et al.,* 2010). These neurons expressed the vesicular glutamate transporter 1 (vGLUT1) and glutaminase, showing that they were glutamatergic pyramidal neurons (Guo *et al*., 2010). Additionally, while Dimou *et al*. (2008) published that they observed no neurogenesis in *Olig2-Cre/CAGG-GFP* transgenic mice, subsequent examination of *Olig2-CreER^{T2}/R26-YFP* transgenic mice revealed neuron production in the piriform cortex, comparable with our own (M. Götz, unpublished communication). Therefore, OLPs in the adult

brain have been labelled using three different transgenes and shown to produce piriform cortical projection neurons in each case.

The fact that no YFP+/NeuN+/BrdU+ cells were detected in animals given BrdU for a 100 days period suggests that YFP+ neurons are derived by the direct differentiation of post-mitotic OLPs into neurons. *In vitro* studies have proven the ability of OLPs from perinatal optic nerve to generate neurons and astrocytes in addition to oligodendrocytes (Kondo *et al*. 2000). Another study has shown that SVZ cells that express a *CNP-GFP* transgene, co-express NG2 and generate olfactory bulb interneurons and hippocampal and striatal neurons *in vitro* and *in vivo* (Aguirre *et al*., 2004). In addition, there have been several reports of adult neurogenesis outside of the olfactory bulb and hippocampus, both in rodents (Tamura *et al*., 2007; Dayer *et al*., 2005; Kokoeva *et al*., 2005; Shapiro *et al.*, 2007) and primates (Gould *et al*., 1999; Zhao *et al*. 2003), indicating that typical neurogenic regions are not the sole source of neurons in the brain.

The scale of neurogenesis observed in the present study was small, when compared to the overall population of projection neurons. The physiological importance of this adult neurogenesis is unclear, however, it is particularly intriguing in light of the known plasticity of the olfactory bulb, which provides the main input to this region of the piriform cortex. Moreover, small numbers of neurons, even single neurons, are capable of producing a considerable behavioural effect (Houweling and Brecht, 2008; Huber *et al*., 2008). At present, we have been unable to investigate whether these YFP+ neurons manage to extend their axons to their neuronal targets and form

active connections. Unfortunately, this process, as well as electrophysiological phenotyping of these neurons, has not been possible using the *Pdgfra-creER^{T2}/Tau-mGFP* mouse due to the large number of GFP-labelled oligodendrocytic processes, which mask the relatively small number of neurons. Electrophysiological experiments could only be carried out by generating a neuron specific reporter mouse line, such as *NSEΔSTOPΔYFP*, where expression after recombination would be driven by NSE (Neuron Specific Enolase).

It has been reported that defined cortical neurons can be regenerated by endogenous precursors after experimental ablation and the replacement neurons can extend long-range axons toward their original targets (Magavi *et al.*, 2000). Therefore, it could be possible that OLPs, like those present in the piriform cortex, are responsible for generating those replacement neurons. If this notion is correct, it might mean that local OLPs could be a potentially useful resource for neuronal replacement during neurodegenerative disease.

Chapter 4

‘Cell Cycle Dynamics of OLPs in the Postnatal Mouse Brain’

4.1 Introduction

In addition to their on-going role in adult oligodendrogenesis in the healthy mouse brain (**Chapter 3**), OLPs are thought to be crucial for remyelination following demyelinating injury or disease. For example, during cytotoxin-induced focal demyelination and subsequent re-myelination of the mouse spinal cord, the dynamic behaviour of OLPs in and around the lesion suggests that they are the source of the remyelinating oligodendrocytes (Keirstead *et al.*, 1998; Watanabe *et al.*, 2002; Dawson *et al.*, 2003). The efficiency of remyelination following experimental demyelination is observed to decrease with ageing, which might be attributed to an age-related decline in the regenerative properties of OLPs (Sim *et al.*, 2002), while the factors that cause these age-related changes are unknown they could result from changes in the ability of OLPs to proliferate and generate new oligodendrocytes as the brain matures and ages.

There is strong evidence that myelin production is compromized in aged mice (Shields *et al.*, 2000). Oligodendrocyte and OLP cell intrinsic changes are likely to play a role in this process. Alterations at the level of micro-RNA have not been investigated, but recent studies implicate age related changes in epigenetic control (Shen *et al.*, 2008; Shen *et al.*, 2008b). Histone deacetylase (HDAC) enzymes are generally inhibited in OLPs present in the developing and adult CNS (Marin-Husstege *et al.*, 2002; Shen *et al*., 2005; Liu *et al.*, 2007) and therefore histones in OLPs tend to be acetylated and associated with open, active chromatin. This is in contrast to the histones of myelinating oligodendrocytes which tend to be deacetylated and associated with compact chromatin. The significance of the different HDAC levels in OLP differentiation is reflected by the increased expression of HDAC1 by OLPs in the corpus callosum of young adult mice, following cuprizone exposure. HDAC1 binds to the promoters of anti-myelination genes, reducing their expression and promoting oligodendroglial differentiation in order to induce remyelination. These modifications were not observed in OLPs of equivalently treated aged mice (Shen *et al.*, 2008), which had correspondingly impaired re-myelination (Shen *et al*., 2008). These data suggest an impaired ability of OLPs to differentiate in the aged brain, but say nothing of their proliferative capacity.

Work by van Heyningen *et al*. (2001) has shown that at E13 all OLPs are mitotically active, however their cell division rate slows as their numbers increase in late embryogenesis (van Heyningen *et al.*, 2001). For example, E17 OLPs cycle more slowly (Tc ~78h) than E13 OLPs (Tc ~12h) *in vivo* (van Heyningen *et al.*, 2001). A

similar trend has been noted when perinatal and adult OLPs were compared *in vitro*. An increase in the cell cycle time from ~38 hours to 60-65 hours was observed for cultured OLPs taken from optic nerves of P3 and P21 rats respectively (Wren *et al.*, 1992). A lengthening of OLP cell cycle time as the demands of developmental oligodendrogenesis subside is hardly surprising. But, how and why the behaviour of NG2 cells alters beyond development with normal ageing is a very important question that must be addressed in order to know whether OLPs in the aged brain can act as a reservoir of new cells for neural repair. In this chapter, changes to the cell cycle kinetics of OLPs and their rate of oligodendrocyte production will be examined throughout postnatal life.

4.2 Results

4.2.1 Dividing and non-dividing OLP sub-populations in the P60 brain

OLPs are the major dividing cell population in the adult rat CNS. However, neither the proportion of cells in cycle (growth fraction) nor their cell division times have been determined to date. To gain a more detailed understanding of the *in vivo* cell cycle dynamics of adult OLPs, cumulative BrdU-labelling experiments were carried out using two different methods of administration. BrdU was administered to young adult mice in their drinking water continuously for up to 21 days (see **2.7.2**), starting at P60. Alternatively, cumulative BrdU administration was achieved by the subcutaneous implantation of mini osmotic pumps that continuously release BrdU. Coronal forebrain sections were analyzed after various BrdU-labelling periods by immunohistochemistry for BrdU and PDGFRα (see **2.8.5**; **Fig. 4.1a-d)**. The

proportion of PDGFRα+ OLPs that had incorporated BrdU was counted in defined regions of the corpus callosum and medial cortex in confocal micrographs (see **2.9**). For each time point and labelling method, the proportion of OLPs (PDGFRα+ cells) that incorporated BrdU was calculated in the corpus callosum and the motor cortex (**Fig. 4.1e-f**). These data were plotted as BrdU labelling index versus labelling period in order to compare the rate of labelling of proliferating OLPs by each methodology (see **2.9.3**). Both BrdU delivery methods produced similar results, that is, a similar rate of BrdU incorporation and similar proportion of labelled cells (**Fig. 4.1**). Therefore, the data were combined for analysis.

In the corpus callosum, the labelling index (% of BrdU+ OLPs) increased with time for 7–10 days, but then reached a plateau at ~55% (**Fig. 4.1c**). The plateau indicates the point at which all dividing cells within the population have been labelled and therefore these data suggest that only ~half of the PDGFRα+ cells are actively engaged in the cell cycle. These data were also used to calculate the cell cycle time (Tc; see **2.9.3**), which indicated that the dividing cell population had a Tc of approximately one week. In the cortex, the labelling index increased steadily over the labelling period (**Fig. 4,1f**). At 21 days, nearly 40% of PDGFRα+ cells in the cortex had incorporated BrdU. If the labelling index continues to increase at the same rate until all cortical OLPs are labelled, then that would imply that the whole population divides with an average cycle of ~50 days. However, with the data available, it can only be concluded that 40% or more of cortical adult OLPs are dividing with an average cell cycle time of at least 21 days.

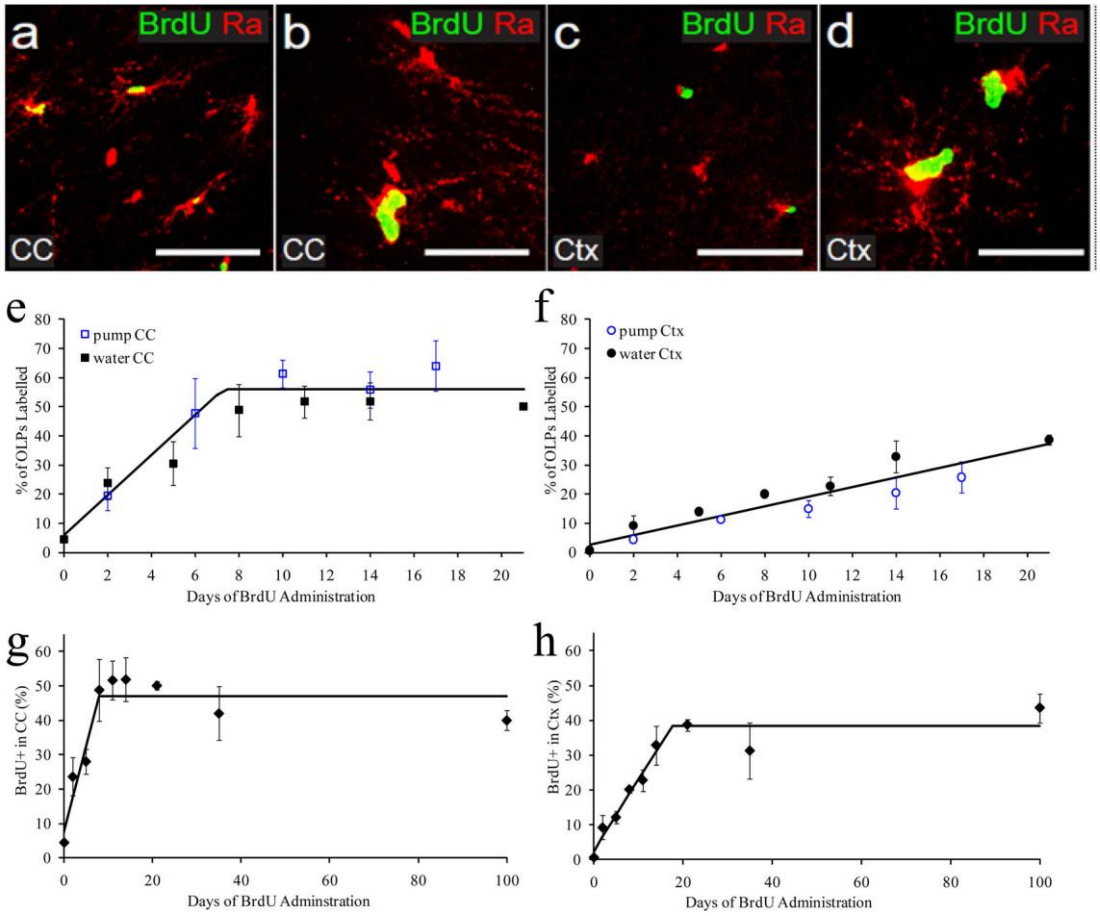

Figure 4.1 *Cumulative BrdU labelling of adult OLPs in vivo. BrdU was administered to young adult (P60) mice for up to 21 consecutive days via osmotic mini-pumps (Rivers et al. 2008) or by including BrdU in the drinking water for up to 21 d. Double immunolabelled brain sections for BrdU and PDGFRA revealed double-positive (replicating) OLPs in both corpus callosum (a-b) and cerebral cortex (d-e). Both routes of BrdU delivery gave comparable data. In corpus callosum (c), the BrdU labelling index increased to ~55% in 7–10 d, but did not increase further. In the cortex (f), the labelling index increased linearly for 21 d until ~40% of OLPs were BrdU+. The cumulative BrdU experiment was extended by BrdU in the drinking water administration for up to 100d. Data were graphed as the percentage of BrdU+ OLPs in the total OLP population in the corpus callosum (g) and motor cortex (h). At each time point, the labelling index was determined from cell counts (means ± s.d.) on at least three sections from each of three animals. The 2-h time point is from a single intra-peritoneal injection of BrdU.*

To determine the Tc and GF for OLPs in the motor cortex, it was necessary to extend the period of BrdU labelling. As BrdU administration via the drinking water or mini osmotic pump produced similar labelling of OLPs, BrdU was subsequently administered to the mice via the drinking water, so that the mice did not have to undergo surgery to replace mini-pumps every 10-11 days. BrdU in the drinking water was administered for up to 100 days. Coronal brain sections were double-immunolabelled for PDGFRα and BrdU to visualize OLPs that had undergone DNA replication during the labelling period.

For the corpus callosum, an accumulation of PDGFRα+/BrdU+ cells with time was detected until ~8 days, when a plateau was reached (**Fig. 4.1g**). Once the ~45% plateau was reached, it remained stable for the remaining 92 days of BrdU administration. This was true for the cortex as well (**Fig. 4.1h**). Although the labelling plateau was reached later in the cortex (~21 days) it was reached when ~40% of OLPs had incorporated BrdU and then remained stable for the remainder of the 100 day labelling period. These data were used to calculate the Tc according to the formula given in **2.9.3,** and indicate that OLPs in the brain white matter proliferate more rapidly (Tc ~9 days; **Fig. 4.7**) than their counterparts in the grey matter (Tc ~18 days; **Fig. 4.7**). Furthermore, there appear to be 2 sub-populations of OLPs in both regions of the postnatal mouse brain that can be distinguished depending on their proliferative behaviour, that is, mitotically active versus inactive.

4.2.2 Mitotic status of OLPs is unrelated to their developmental site of origin

It is known that adult OLPs in the forebrain derive embryonically from both the cortical and striatal VZs (Kessaris *et al*., 2006). Since ~50% of SOX10+ cells in

adulthood come from each of the two embryonic VZ regions (Kessaris *et al*., 2006), and ~50% of OLPs are actively engaged in the cell cycle (see above), this suggests the possibility that there might be a connection between the developmental origin of OLPs in the forebrain and their cycling behaviour in adulthood. To examine this possibility, P60 forebrain sections from *Gsh2-iCre/R26-YFP* and *Emx1-iCre/R26-YFP* transgenic mice were first immunolabelled for PDGFRα and GFP (**Fig. 4.2a, b**) to identify OLPs that had originated from stem cells in the embryonic LGE or cortex respectively. PDGFRα+ cells that had originated from each region were intermingled in both the corpus callosum and cortex and were found to be present in similar proportions (~40% from each) (**Fig. 4.2a-e**). In both corpus callosum and cortex there was a modest fraction of PDGFRα+ cells (10-20%) that appeared not to be derived from either ventral or dorsal forebrain.

Having confirmed the embryonic origins of OLPs in the adult cortex and corpus callosum, I administered BrdU to P60 *Gsh2-iCre/R26GFP* and *Emx1-iCre/R26GFP* transgenic mice via their drinking water for 6 or 35 days, and then immunolabelled brain sections for GFP, PDGFRα and BrdU. Triple-labelled cells were counted in the corpus callosum and cortex and expressed as a percentage of the total number of (GFP+, PDGFRα+) cells in the same region (**Fig. 4.3a-d**). The fraction of (GFP+, PDGFRα+) cells that incorporated BrdU was similar in both *Gsh2-iCre/R26GFP* and *Emx1-iCre/R26GFP* animals and each was representative of the PDGFRα+ cell population as a whole (**Fig 4.3a-d**). It can therefore be concluded that the developmental origin has no influence on the proliferative behaviour of NG2 cells.

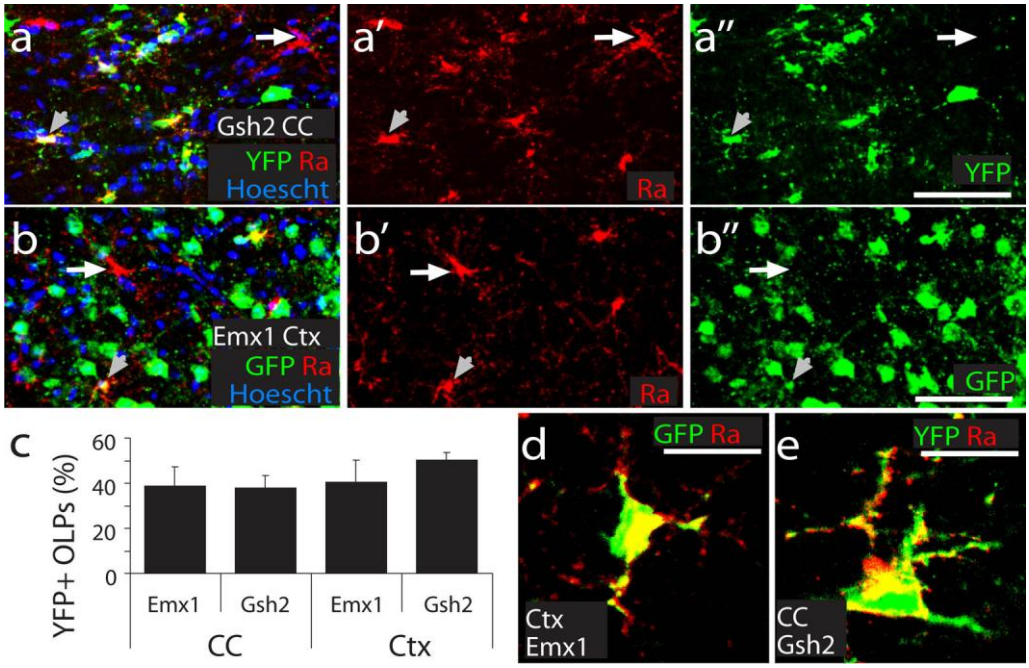

Figure 4.2 *OLPs derived from both the dorsal and ventral VZ contribute equally to the population of NG2 cells. By crossing Gsh2-iCre and Emx1-iCre transgenic mice with Cre-sensitive R26GFP reporter mice we were able to trace GFP+ (green), PDGFRα+ (red) OLPs that originated from the embryonic LGE/MGE and cortical VZ, respectively* ***(a, b)****. **(c)** Numbers of GFP+, PDGFRα+ OLPs in the corpus callosum or cortex (3 sections from each of 6 mice) was expressed as a percentage of all PDGFRα+ OLPs in the same region. Gsh2- and Emx1-derived OLPs were found in approximately equal numbers in both corpus callosum and cortex* ***(d, e)****. Grey arrowheads indicate (GFP+, PDGFRα+) double-positive cells* ***(a, b)****. White arrows indicate a PDGFRα+ single-positive cell* ***(a, b)****. CC, corpus callosum; Ctx cortex. Scale bars:* ***a-b****, 40 µm;* ***d-e****, 10 µm.*

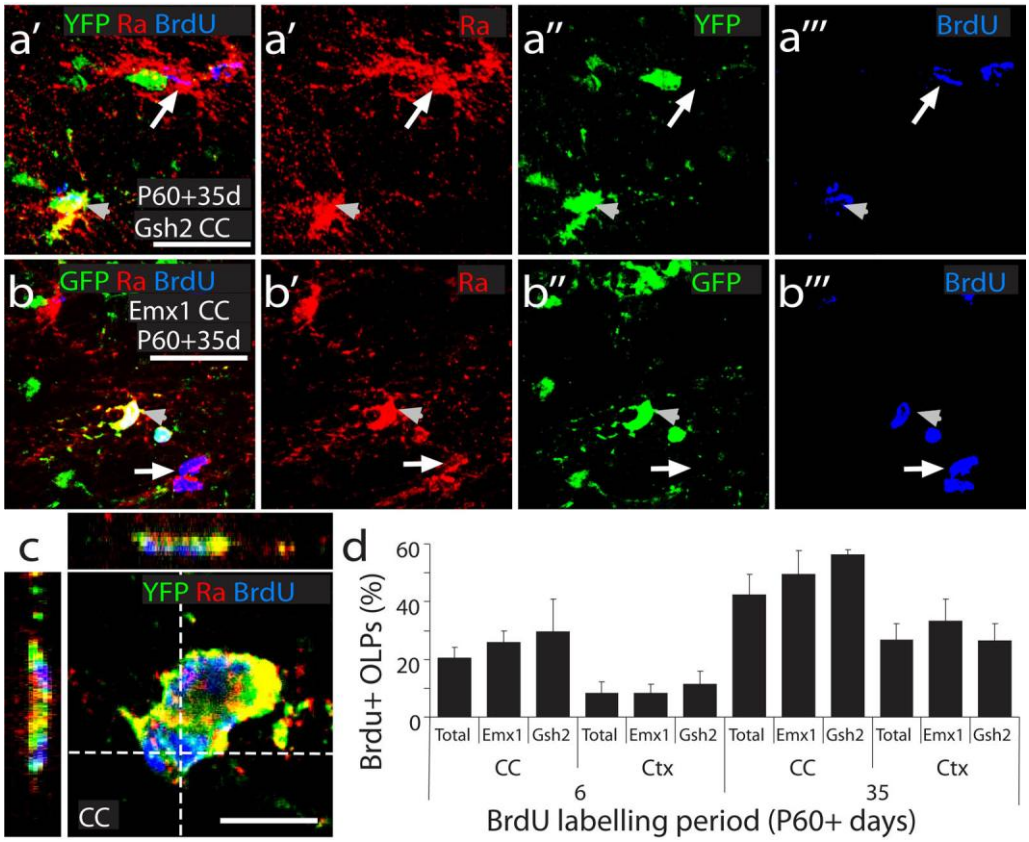

Figure 4.3 *OLPs derived from both the dorsal and ventral VZ contribute to both the cycling and non-cycling populations of NG2 cells. To determine whether both Gsh2- and Emx1-derived adult OLPs were cycling, BrdU was administered via the drinking water for 6 or 35 days starting on P60 and brain sections were triple immuno-labelled for BrdU (blue), PDGFRα (red) and GFP (green) (**a, b**). GFP+/PDGFRα+ OLPs were scored as BrdU-positive or –negative by examining confocal images with orthogonal projections (**c**); numbers of OLPs in corpus callosum and cortex were expressed as a percentage of all OLPs in the same area. Both Gsh2- and Emx1- derived NG2 cells contributed equally to the cycling and non-cycling sub-populations. Grey arrowheads indicate (BrdU+/GFP+/PDGFRα+) triple-positive (**a, b**) cells. White arrows indicate (GFP+/PDGFRα+) double-positive (**a, b**) cell. CC, corpus callosum; Ctx cortex. Scale bars: **a-b**, 17 µm; **c**, 6 µm.*

4.2.3 The OLP cell cycle slows dramatically with age

As mentioned previously, van Heyningen *et al*. (2001) reported that 100% of OLPs in the spinal cord proliferate at E13. As we report that only ~half of OLPs are dividing in the adult brain, there presumably is a switch in OLP cycling behaviour that occurs sometime after E13 and before P60. To determine the age at which this switch occurs, I performed cumulative BrdU-labelling experiments on P6 mice. As P6 mice are too small for mini pump implantation and BrdU does not pass from the mother's drinking water through the milk to her pups (data not shown), BrdU was administered to wild type mice by injecting them subcutaneously every 3.5 hours for up to 3 days. Brain sections were immunolabelled to detect PDGFRα and BrdU and immuno-positive cells were quantified (**Fig. 4.4**). We found that the labelling index plateaued in the corpus callosum and cortex after ~55% of OLPs had incorporated BrdU+. This is slightly higher than the GF of OLPs present at P60, perhaps indicating that some non-dividing OLPs are still being generated and OLPs are sub-divided into two populations (mitotic and non-mitotic) within the first postnatal week.

Using the cumulative BrdU labelling data, the cell cycle time was calculated for OLPs at P6 using the method previously outlined (see **2.9.3**). Interestingly, Tc was found to be much more rapid at P6 (CC: 1.7 days ± 0.2; Ctx: 2 days ± 0.2) than at P60 (CC: 9 days ± 0.2; Ctx: 18 days ± 3), demonstrating that Tc is slowing with age even during the early postnatal period (**Fig. 4.7a**).

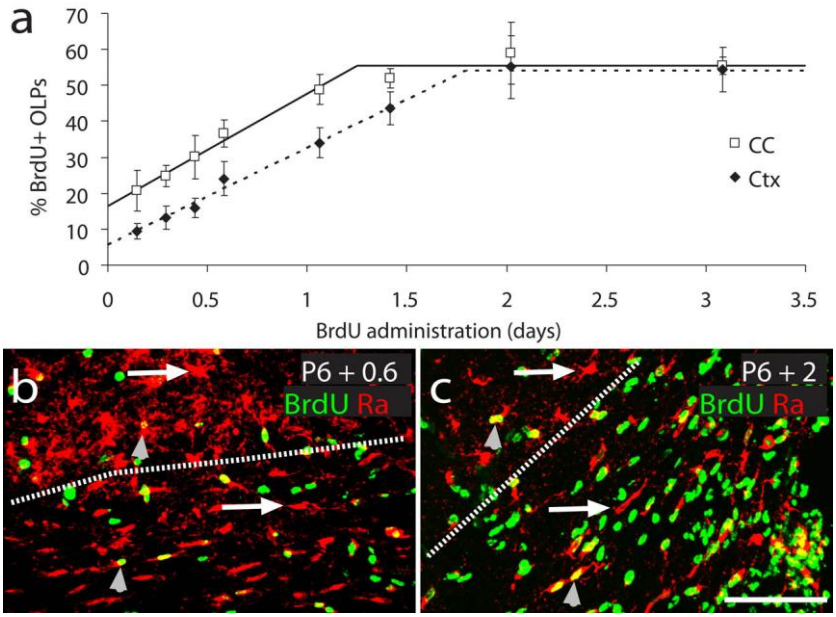

Figure 4.4 *Post-mitotic OLPs are born before the end of the first postnatal week. BrdU was administered by sequential subcutaneous injections at P6. (**a**) At various times after the start of BrdU administration, BrdU+, PDGFRα+ OLPs were counted in the corpus callosum and cortex and the number of dividing OLPs expressed as a percentage of the total number of OLPs. BrdU+ (green), PDGFRα+ (red) OLPs could be detected readily in the grey and white matter after all BrdU labelling periods examined (**b-c**). Grey arrowheads indicate cycling, BrdU+ OLPs and white arrowheads non-cycling OLPs. The white dashed line indicates the border between the corpus callosum (CC) and cortex (Ctx). Scale bars: **a-b**, 60 µm*

To further examine the effect of ageing on the cell cycle kinetics of OLPs, coronal brain sections of P6 and P60 mice were stained with Ki67 (**Fig. 4.5**). The Ki67 monoclonal antibody identifies a nuclear antigen that is expressed during the late G1, S, M and G2 phases of the cell cycle while its expression diminishes quickly after mitosis (Siitonen et al. 1993; Gasparini et al. 1994; Pena et al. 1998). It was found that ~29% of PDGFRα/NG2 cells in the P6 mouse corpus callosum were Ki67+ (154 double +ve PDGFRα+/Ki67+ cells out of 535 PDGFRα+ cells), compared to only ~15% at P60 (31 PDGFRα+/Ki67+ cells out of 206 PDGFRα+ cells). In the P6 cortex, 7% of PDGFRα+ cells were Ki67+ (41 double +ve PDGFRα+/Ki67+ cells out of 589 of total PDGFRα+), while only 4% of the total PDGFRα+ cells were also stained with Ki67 in the P60 cortex (10 double +ve PDGFRα+/Ki67+ cells out of 242 of total PDGFRα+). Thus, the Ki67 labelling index does not match the growth fraction estimated by cumulative BrdU labelling (~50% at both ages) but it does decline in parallel with the increase in the length of the cell cycle.

Having observed that the Tc of OLPs lengthens between P6 and P60, I further determined the Tc of OLPs in the brain of mice at various postnatal ages to see whether Tc is influenced by ageing. For this, BrdU was administered to wild type mice via their drinking water for up to 100 days starting from P240 (eight months) and P540 (eighteen months) and brain sections were immunostained to detect PDGFRα and BrdU (**Fig 4.6b-d, f-h**). In the corpus callosum, T_C increased from <2 days at P6 to ~70 days at P240 and older (**Fig. 4.7**). In the cortex, T_C increased steadily from ~2 days at P6 to >100 days at P540 (**Fig. 4.7**). It was not possible to determine T_C in the P540 cortex with confidence because the GF is not known; even

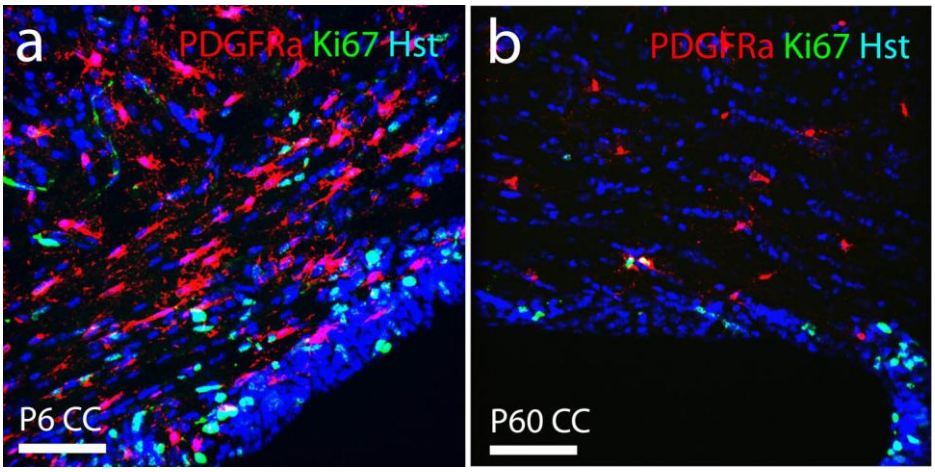

Figure 4.5 *Ki67 staining showed increase in the length of Ng2 cell cycle with age. Brain sections of P6* ***(a)*** *and P60* ***(b)*** *mice were stained with antibodies against Ki67 (green), PDGFRα (red) and DAPI (blue). Arrows and arrowheads indicate Ki67+/PDGFRα+ and Ki67-PDGFRα+ cells respectively in the corpus callosum of these mice.*

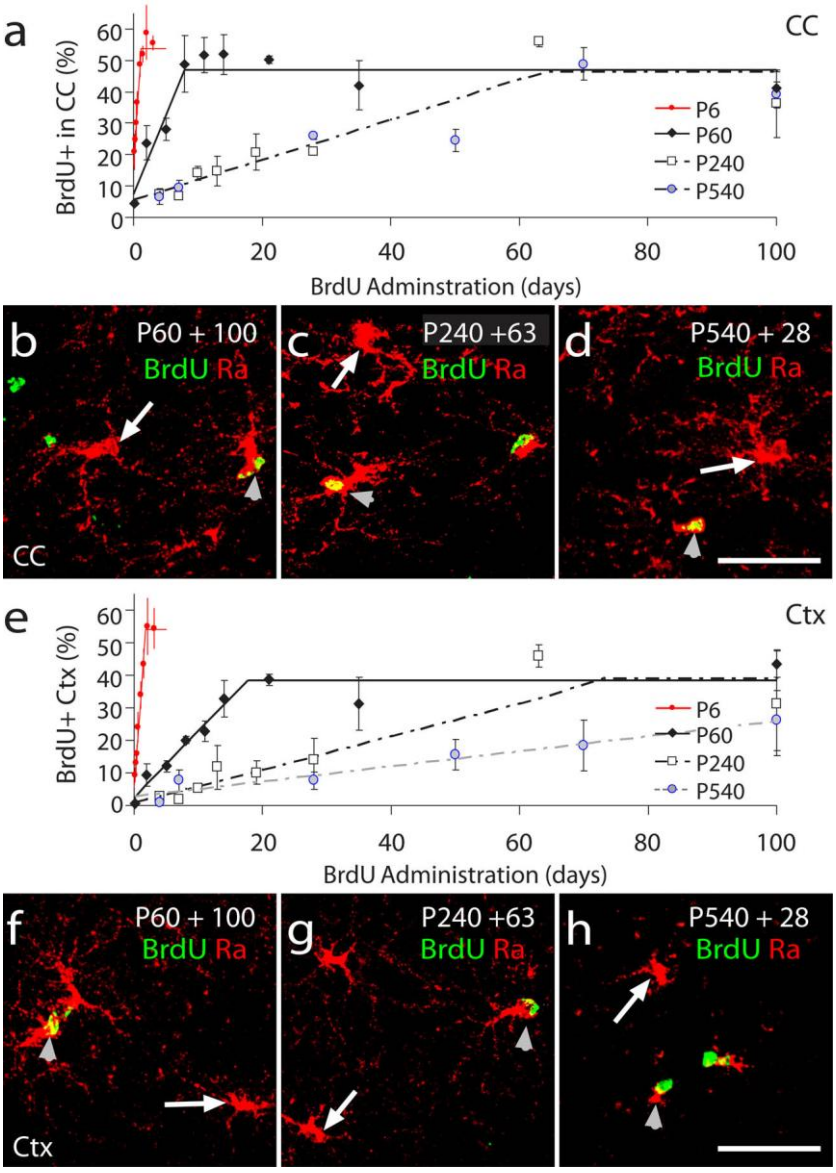

Figure 4.6 *OLPs continue to proliferate throughout postnatal life in the corpus callosum and cortex. BrdU was administered to mice via their drinking water for up to 100 days starting on P6 (P4-P7), P60 (2 months), P240 (8 months) or P540 (18 months). At various times after the start of BrdU administration, the number of BrdU+, PDGFRα+ OLPs was counted in the corpus callosum (**a**) and cerebral cortex (**e**) and expressed as a percentage of the total number of PDGFRα+ OLPs. BrdU+ (green), PDGFRα+ (red) OLPs could be detected readily in the grey (**b-d**) and white (**f-h**) matter at all ages. The point at which a plateau is reached indicates the fraction of the OLP population that is actively cycling. Grey arrowheads indicate BrdU+, cycling OLPs and white arrowheads indicate non-cycling OLPs. CC, corpus callosum; Ctx, cortex. Scale bars: **b-d** and **f-h**, 20 µm*

at P540 +100 days of BrdU labelling the labelling index still appeared to be on the increase (**Fig. 4.6e**). If I assume that GF = ~0.4 at P540, as it is at P240, then T_C (P540) ≅ 170 days. It is likely that most of the increase in T_C observed with age results from an increase in the amount of time cells remain resting in early G1, that is, when Ki67 is not expressed.

When we investigated a possible relationship between postnatal age and cell cycle length for cortical OLPs, it was found to be linear (**Fig. 4.7b**). With every extra day after birth, the cell cycle increases by around one third of a day. This relationship allows the estimation of T_C for any given postnatal age. In the corpus callosum there is no simple relationship between age and T_C (**Fig. 4.7b**). In contrast to the cortex, it seems that in the corpus callosum T_C reaches its maximum around P240 and does not increase significantly after that.

Despite the considerable increase in T_C with age, the GF was relatively invariant (**Fig. 4.6a, e; Fig 4.7a**). In the corpus callosum, GF was not significantly different from 50% at any age. In the cortex, the growth fraction fell from ~54% at P6 to ~40% at P60 and older. These data imply that in both the white and grey matter of the postnatal forebrain only around half of all NG2 cells are actively engaged in the cell cycle at any age, the other half being post-mitotic. Furthermore, these separate dividing and non-dividing populations are already present in the brain shortly after birth at P6.

a

		Postnatal Age (days)			
		6	60	240	540
CC	GF	0.54 ± 0.02	0.47 ± 0.02	0.46 ± 0.06	0.45 ± 0.03
	m	0.31 ± 0.02	0.05 ± 0.01	0.006 ± 0.001	0.006 ± 0.001
	Tc	1.7 ± 0.2	9 ± 2	72 ± 21	75 ± 18
Ctx	GF	0.55 ± 0.03	0.38 ± 0.02	0.39 ± 0.03	-
	m	0.27 ± 0.01	0.021 ± 0.002	0.0051 ± 0.001	0.0023 ± 0.0005
	Tc	2 ± 0.2	18 ± 3	76 ± 28	170 ± 54

b

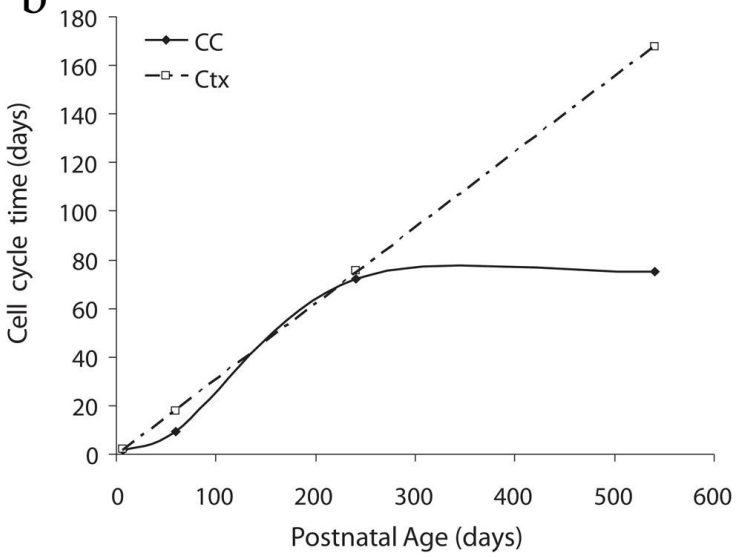

Figure 4.7 *The OLP cell cycle slows down during postnatal life. BrdU was administered to mice via their drinking water starting on P6, P60, P240 or P540 and the fraction (percentage) of OLPs that was BrdU+ was plotted versus the BrdU labelling period.* ***(****a) GF, m and* T_C *for OLPs in the corpus callosum and cortex at the ages examined.* ***(b)*** *There was a linear relationship between age and cell cycle length of OLPs in the cortex (Ctx) at all ages. In the corpus callosum (CC) cell cycle time reached a plateau after ~P240.*

4.2.4 EdU incorporation by OLPs in vitro

In contrast to these findings, research conducted by Carlos Parras' laboratory indicated that over half of the OLPs present in the adult mouse cortex underwent cell division (unpublished communication). After trialling a variety of antigen retrieval methods for BrdU detection, to verify our data we decided to adapt an alternative method for labelling proliferating OLPs. EdU is another thymidine analogue, which like BrdU, is incorporated into the DNA of cells as they undergo cell division. However, EdU detection does not require DNA denaturation or antigen retrieval for detection (see **2.8.6**). As EdU has been previously used for labelling dividing cells in vitro, we first determined whether it could be used to label dividing OLPs in culture. Therefore, OLPs were isolated from the cortex of P15 mice as described in **2.8.1**. These culture conditions select for cells of the oligodendroglial lineage, as confirmed by co-staining of these cultures to detect OLIG2 and NeuN (**Fig.4.8a**). ~99% of cells were OLIG2+, while no cell was found to be NeuN+. When EdU was added into the medium of P15 mouse cortical OLP cultures for 18 hours (**2.7.3**) and the cells were fixed and co-stained to detect EdU and the OLP marker NG2 (**2.8**), ~99% of cells in the culture were NG2-positive and around half of these cells were also EdU-positive (**Fig. 4.8b, c**). These data indicate that EdU can be incorporated by OLPs, and therefore used to identify proliferating OLPs.

4.2.5 EdU incorporation by OLPs in vivo

EdU can be administered as a single intraperitoneal injection in order to acutely label cells that are proliferating *in vivo* (Chehrehasa *et al*., 2009; **Fig. 4.9f**). However for the cumulative labelling of proliferating OLPs *in vivo* it was necessary to first determine whether EdU could be detected after administration through the drinking

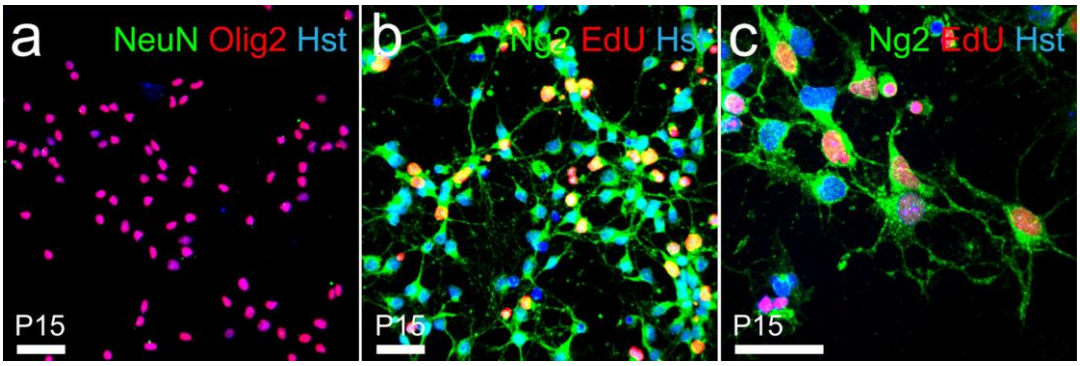

Figure 4.8 *EdU incorporation by OLPs in vitro. P15 cortical cultured cells were stained for NeuN (green) and OLIG2 (red) to establish their identity (a). EdU was next added to the cultured cells and left for 18 hours. Cultured cells were immunolabelled for NG2 (green) and EdU (red) and imaged at 20x (b) and 40x magnification (c).*

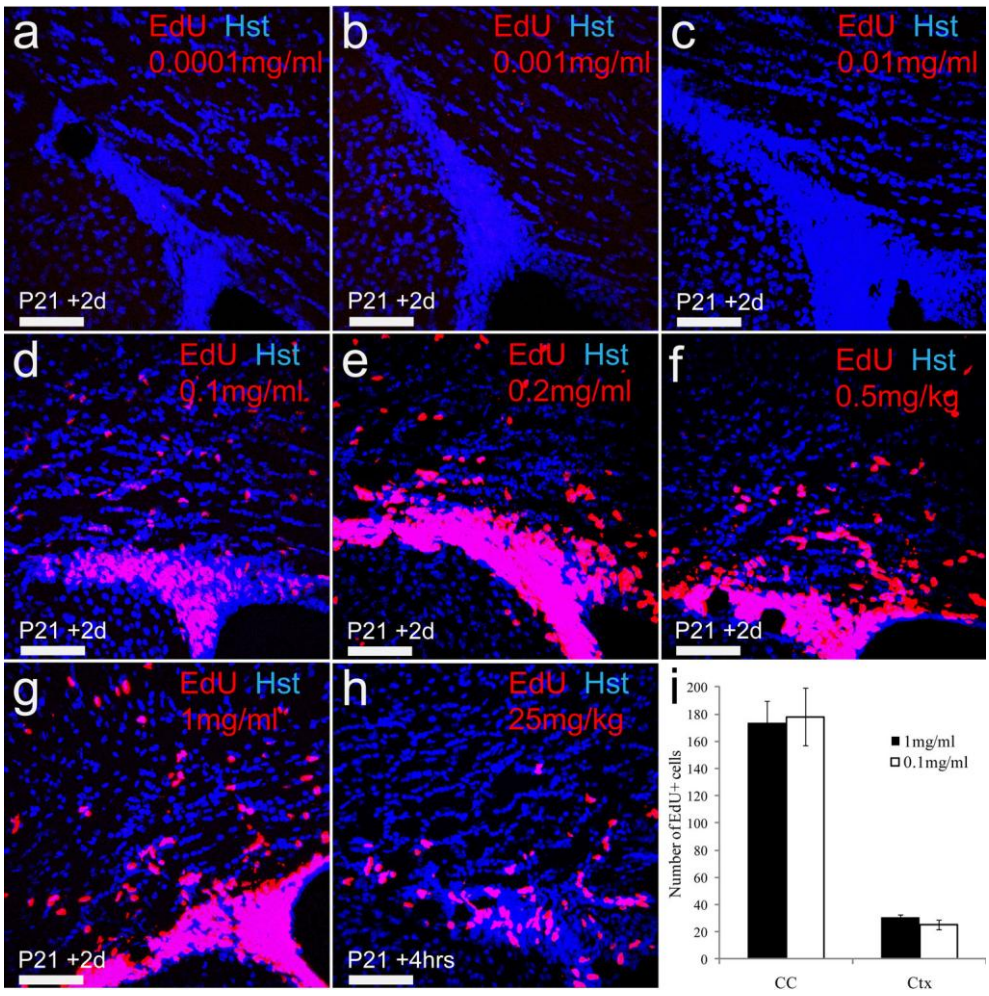

Figure 4.9 *Cumulative EdU labelling in vivo. EdU was administered to mice via their drinking water at P21 for up to 2 days. Different EdU concentrations were tested in order to determine optimal EdU labelling (a-g). A single subcutaneous injection of 25mg/kg body weight acted as a positive control for the EdU staining (h). Dividing cells had incorporated EdU (red) and were then counterstained with DAPI (blue). The absolute number of EdU+ cells in 3 non-overlapping regions in the corpus callosum were counted in mice dosed with 0.1 and 1mg/ml EdU for 48hrs (i).*

water, whether there was toxicity associated with long-term EdU administration and if so, decide upon the optimum EdU concentration to use for these experiments. Therefore, P21 mice were exposed to different EdU concentrations in their drinking water for a 48hr period and brain sections processed to detect EdU as described in **2.8.6**. To screen for detectable *in vivo* labelling of proliferating cells, the SVZ, which contains a population of rapidly proliferating progenitor cells, was first imaged for EdU incorporation. Concentrations of 0.001mg/ml and 0.01mg/ml EdU produced no detectable labelling of the SVZ (**Fig. 4.9a, b**). However at concentrations of 0.1mg/ml EdU and above, EdU-positive cells could be readily detected (**Fig. 4.9c**). Doses of 0.2mg/ml, 0.5mg/ml and 1mg/ml produced significantly brighter cell labelling (**Fig. 4.9e, f, g**). The number of dividing EdU+ cells labelled by each dosing regime was quantified, within a fixed corpus callosal area. This did not vary significantly from 0.1mg/ml to 1mg/ml EdU administration (**Fig. 4.9i**). These data suggested that any dose between 0.1mg/ml and 1mg/ml of EdU in the drinking water of mice could label proliferating cells in the brain, including those of the corpus callosum.

When 1mg/ml EdU was maintained in the drinking water of n=3 mice from P21, by 13 days we observed evidence of toxicity: n=1 mouse lethal, n=2 mice exhibited hunched posture and were therefore euthanized. Similarly when 1mg/ml EdU was maintained in the drinking water of mice from P60 it was also found to be toxic by 13 days; n=1 mouse lethal, n=2 mice exhibited hunched posture and were therefore euthanized, n=6 mice appeared normal and were therefore perfusion fixed at 14 and 21 days for histological analysis. No such side effects were observed by

administering a dose of 0.2mg/ml EdU to P21 and P60 mice, even when it was provided for 50 days (n=3 of each). Doses longer than 50 days were not tested.

Brain sections from P60 mice that received either 0.2mg/ml or 1mg/ml of EdU were processed to detect EdU and PDGFRα (see **2.8**) in order to determine the proportion of OLPs labelled in each instance. EdU incorporation by OLPs in the motor cortex increased linearly with time with an EdU dose of 0.2mg/ml, as we would expect from our BrdU studies. EdU incorporation by OLPs did not exceed ~20% in mice that received a dose of 1mg/ml EdU, even when it was administered for 21 days (**Fig. 4.10**). As ~40% of OLPs become labelled by 0.8mg/ml of BrdU and 0.2mg/ml of EdU in an equivalent time frame, these data indicate that even mice that do not present visible symptoms of toxicity were still experiencing toxic side effects of EdU labelling at a concentration of 1mg/ml (**Fig. 4.10**). Therefore, since 0.2mg/ml EdU was found to provide very bright, clear labelling of proliferating cells, including OLPs in the corpus callosum (**Figure 4.9e**) and cortex (**Fig. 4.10**), without detectable toxicity, this concentration was used for further cumulative labelling experiments, described below.

4.2.6 Proliferative behaviour of OLPs in adolescent (P21) and young adult (P60) mice as determined by cumulative EdU administration

EdU was administered into the drinking water (0.2mg/ml) of P21 mice for various periods of time for up to 50 days. After each labelling period, the proportion of proliferating OLPs was determined in the corpus callosum and motor cortex, as well as the piriform cortex.

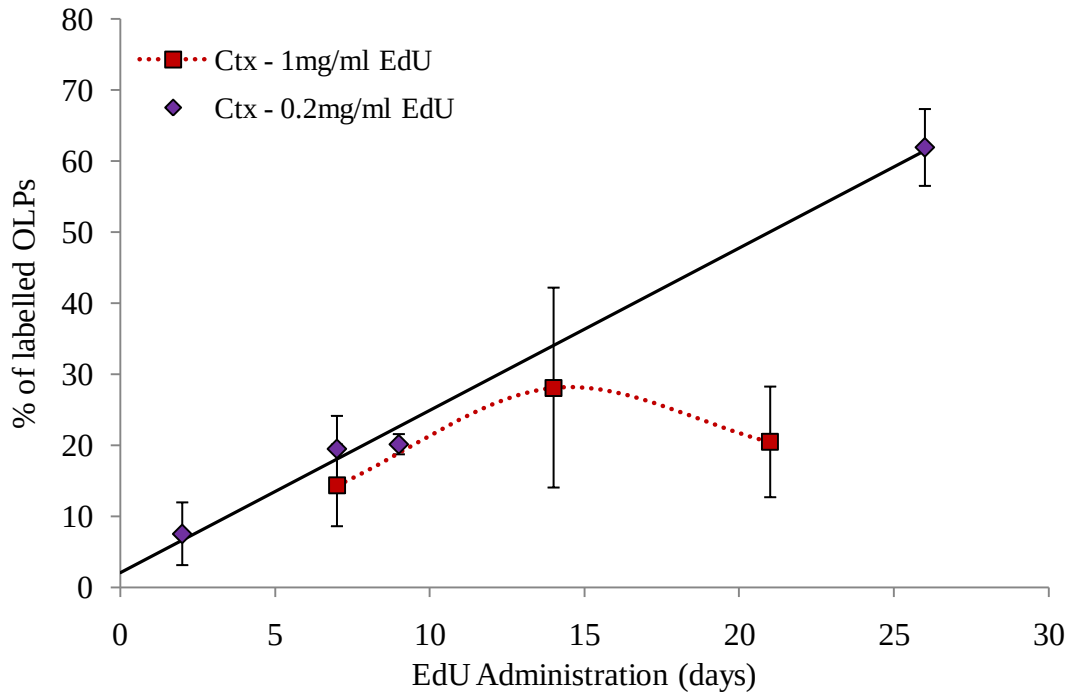

Figure 4.10 *Toxic effects of cumulative EdU labelling in vivo. EdU was administered to P60 mice via their drinking water at a concentration of 1mg/ml and 0.2mg/ml for up to 21 days. Toxicity of high EdU concentration in vivo is shown by the decreased proportion of EdU+ OLPs after 21 days of EdU administration in the motor cortex.*

EdU+ OLPs had already accumulated in significant quantities in the corpus callosum within 2 days after EdU administration (**Fig. 4.11a**). The proportion of EdU+ OLPs in the corpus callosum increased rapidly (at a rate of ~18% per day; **Fig. 4.11; 4.13**) and reached a plateau by 3 days at ~75%. The growth fraction of dividing OLPs remained unaltered for the rest of the labelling period (**Fig. 4.11b, c, j**). Even after 50 days of continuous EdU administration, EdU-/PDGFRα+ cells were visible in the CC (**Fig. 4.11c**). These data confirm that both a proliferating and a non-proliferating population of OLPs exist and that the BrdU labelling/detection method under-estimated the size of the proliferating population.

In the motor cortex and piriform cortex, EdU+ OLPs were detected soon after EdU administration commenced, but their rate of accumulation was significantly less (~5% and ~6% per day respectively; **Fig. 4.13a**) than in the corpus callosum (**Fig. 4.11d, g**), but similar to the corpus callosum, a plateau in EdU labelling of PDGFRα+ cortical OLPs was reached at ~75% (**Fig. 4.11f, i, j**). In the motor cortex, a plateau was reached after ~2 weeks, while in the piriform cortex it took ~20 days (**Fig. 4.11j**). These data support our previous findings using cumulative BrdU labelling that OLPs in the white matter proliferate more rapidly than those in grey matter. However, they also suggest that the previous methodology underestimated the GF of the OLP population.

Cumulative EdU-labelling of OLPs was also carried out in mice aged P60 and the proportion of proliferating OLPs was examined for the three aforementioned brain regions. The proportion of EdU-labelled PDGFRα+ cells detected increased more rapidly with time in the corpus callosum than the motor or piriform cortex (**Fig. 4.12;**

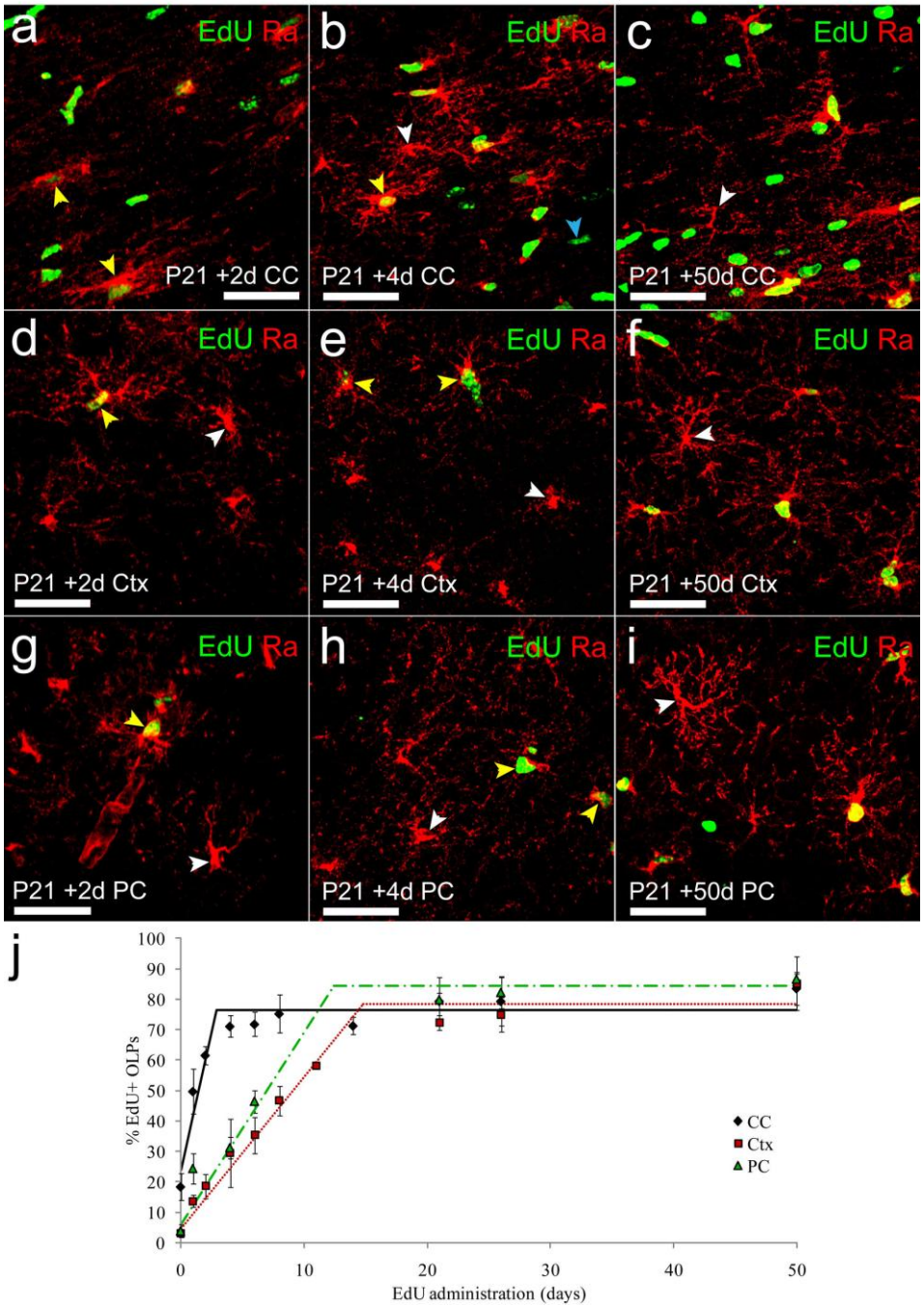

Figure 4.11 *OLP proliferation at P21: Dividing OLPs were labelled by continuous EdU administration to P21 mice for 50 days. At various times after commencing EdU administration, the number of EdU+ (green), PDGFRA+ (red) adult OLPs was counted in the corpus callosum (a-c) and medial (primarily motor) cortex (d-f) and piriform cortex (g-i). Yellow, white and blue arrowheads show EdU+/PDGFRα+, EdU-/PDGFRα+ and EdU+/PDGFRα- cells respectively. The number of EdU+ OLPs at various days of EdU administration was expressed as a percentage of the total number of PDGFRA+ OLPs (j). The point at which a plateau is reached indicates the fraction of the OLP population that is actively cycling (growth fraction).*

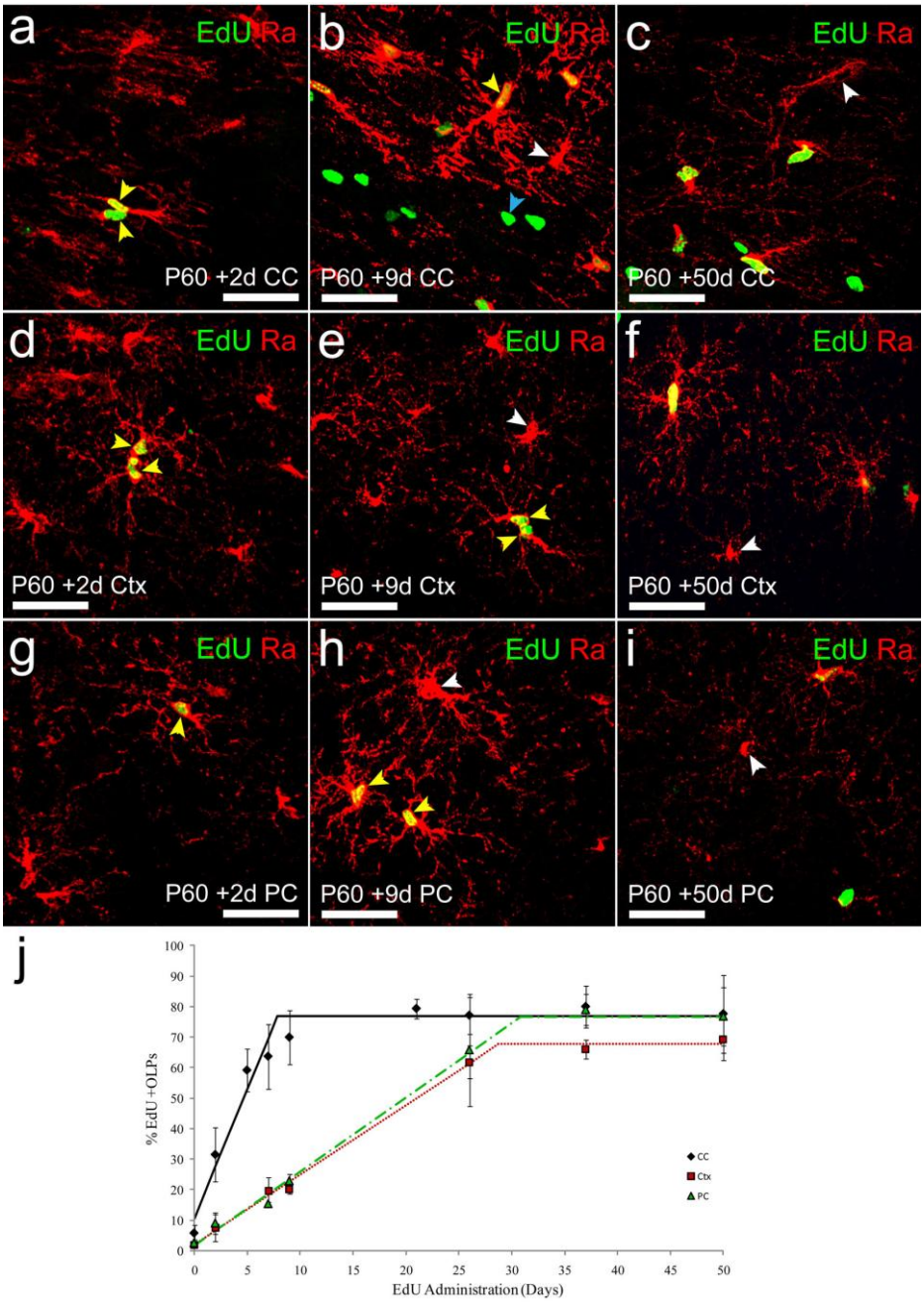

Figure 4.12 *OLP proliferation at P60: Dividing OLPs were labelled by continuous EdU administration to P60 mice for 50 days. The number of EdU+ (green), PDGFRA+ (red) adult OLPs was counted after various points of EdU administration in the corpus callosum (a-c) and medial (primarily motor) cortex (d-f) and piriform cortex (g-i). Yellow, white and blue arrowheads show EdU+/PDGFRα+, EdU-/PDGFRα+ and EdU+/PDGFRα- cells respectively. The number of EdU+ OLPs at various days of EdU administration was expressed as a percentage of the total number of PDGFRA+ adult OLPs (j). The point at which a plateau is reached indicates the fraction of the OLP population that is actively cycling (growth fraction).*

Fig. 4.13a). By 50 days of EdU, ~75% of PDGFRα+ cells was EdU labelled in all three regions examined, consistent with data obtained from P21 mice (**Fig. 4.12c, f, i**). In all regions, OLPs were found to be proliferating more slowly at P60 when compared to their counterparts at P21 (**Fig. 4.13a**). For example, EdU labelling at P21 OLPs in the corpus callosum have a Tc of ~4 days, while at P60 OLPs in the same region have a Tc of ~8 days. These data are consistent with our previous observations using BrdU that the cell cycle time of OLPs declines progressively with postnatal age (**Fig. 4.7**).

A direct comparison was made between P60 cumulative labelling experiments with BrdU and EdU (**Fig. 4.13b, c**). While the GF determined by each methodology was significantly different, the rate of accumulation of labelled OLPs was consistent for BrdU and EdU within the corpus callosum (**Fig. 4.13b**) and the motor cortex (**Fig. 4.13c**). Therefore, the effect of underestimating GF using BrdU is the underestimation of the cell cycle time Tc. Assuming that GF remains roughly constant at ~75% (rather than to ~50% as estimated earlier), this implies that Tc could be re-calculated more accurately at all ages. For example, at P240 OLPs in the corpus callosum are likely to be cycling every 125 days (=75/0.6) instead of every ~72 days (**Fig. 4.7**). Similarly, in the motor cortex of P240 mice, OLPs divide every ~147 days (=75/0.51) instead of every ~76 days (**Fig. 4.7**).

a

P21	CC	m	18.0 ± 0.9
		GF	76.5 ± 1.7
		Tc	4.3 ± 0.9
		S	1.3 ± 0.6
	Ctx	m	4.8 ± 0.3
		GF	78.2 ± 3.7
		Tc	16.4 ± 1.8
		S	1.6 ± 0.4
	PC	m	6.0 ± 1.6
		GF	84.4 ± 2.0
		Tc	14.1 ± 4.4
		S	1.6 ± 1.5
P60	CC	m	8.4 ± 1.4
		GF	76.8 ± 7.9
		Tc	9.15 ± 1.8
		S	1.3 ± 1.0
	Ctx	m	2.3 ± 0.1
		GF	67.6 ± 5.0
		Tc	29.6 ± 2.0
		S	0.9 ± 0.5
	PC	m	2.4 ± 1.6
		GF	76.5 ± 6.9
		Tc	31.6 ± 2.8
		S	0.7 ± 0.7

b

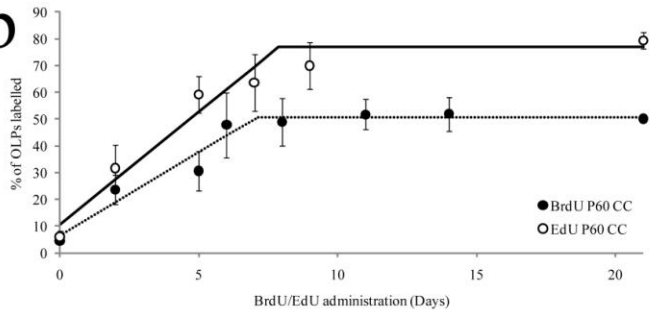

c

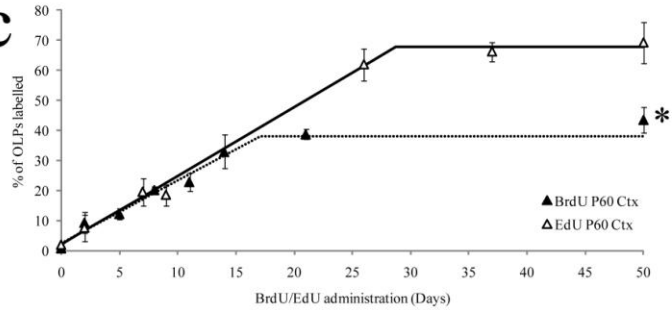

Figure 4.13 *OLP cell cycle slows with ageing irrespective of the GF determined by BrdU vs EdU administration. (a) EdU was administered to P21 and P60 mice via their drinking water for up to 50 days. m, GF, Tc and S was calculated for OLPs in the corpus callosum, motor cortex and piriform cortex. A direct comparison of the rate of accumulation of BrdU and EdU labelled OLPs in the corpus callosum (b) and motor cortex (c) of P60 mice. *To allow comparison with 50 day EdU data on a truncated scale, BrdU data plotted at 50 days was actually acquired from mice that had received BrdU for 100 days.*

4.2.7 Oligodendrocyte production declines in parallel with the lengthening of the OLP cell cycle

We previously showed that many new myelinating oligodendrocytes are formed in the corpus callosum during young adulthood (Rivers *et al.*, 2008). In that study we treated *Pdgfra-CreER^{T2}/R26YFP* mice with tamoxifen at P45 (Rivers *et al.*, 2008) and P60 (Chapter 3) and followed the subsequent differentiation of labelled NG2 cells (YFP+/PDGFRA+) into oligodendrocytes (YFP+/SOX10+/PDGFRA-negative) over the following months. By this means we found that ~29% of the myelin-forming oligodendrocytes present at P240 were formed after P45 (Rivers *et al.*, 2008). As OLPs continue to proliferate, albeit more slowly, in the aged brain, we asked whether oligodendrocyte production continues after P240. Tamoxifen was administered to P240 *Pdgfra-CreER^{T2}/R26YFP* mice and the subsequent appearance of differentiated YFP+ progeny was followed for up to 100 days post-tamoxifen (P240+100). It was first determined that ~48% of all PDGFRA+ cells became YFP-labelled following tamoxifen administration (**Fig. 4.14a-c**) – very similar to the fraction that became labelled after tamoxifen administration at P45 (Rivers *et al.*, 2008). No difference was detected in the proportion of YFP-labelled cells in the corpus callosum versus the cortex (**Fig. 4.14**). Maximal YFP-labelling of OLPs was achieved by 10 days after the first dose of tamoxifen (6 days after the final dose) (**Fig. 4.14a**). We previously found that maximal labelling in P45 mice took ~8 days (Rivers *et al.*, 2008), which might indicate that tamoxifen is metabolized to the biologically active form (4-hydroxy tamoxifen) more rapidly in younger mice or that accumulation of YFP takes longer in older cells. Nevertheless, at early times (10 days) post-tamoxifen the great majority of YFP-labelled cells in both white and grey

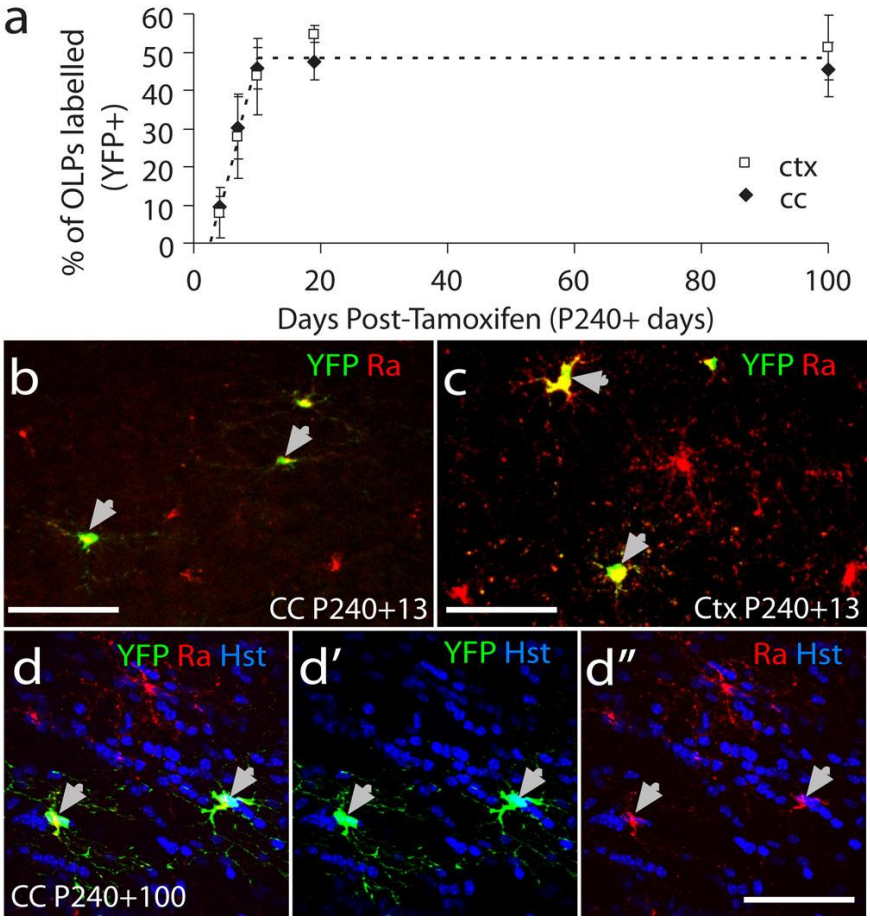

Figure 4.14 *YFP is expressed by PDGFRα+ cells in the Pdgfra-CreER^{T2} / R26YFP transgenic mice at P240. To trace the fate of OLPs in the mature brain, tamoxifen was administered to Pdgfra-CreER^{T2} / R26YFP mice starting on P240.* ***(a)*** *The proportion of PDGFRA+ OLPs that became YFP-labelled is plotted against time post-tamoxifen. Within ~10 days post-tamoxifen ~45% of PDGFRA+ (red) cells in the corpus callosum* ***(b)*** *and cortex* ***(c)*** *become stably labelled with YFP (green).*

matter were also PDGFRα+, as predicted (**Fig. 4.14b, c**). The great majority of YFP+ cells continued to co-label for PDGFRα at all time points examined post-tamoxifen (**Fig. 4.15a**). However, there was a slow but steady accumulation of YFP+/PDGFRα-negative cells in the grey and white matter so that by P240+100 approximately 18% of YFP+ cells in both corpus callosum and cortex were PDGFRA-negative, presumably differentiated cells (**Fig. 4.15b-d**). The YFP+/PDGFRA-negative cells in the corpus callosum had the appearance of oligodendrocytes (**Fig. 4.15c**) and they co-immunolabelled for CNPase, a marker of differentiated oligodendrocytes (**Fig. 4.15e**). This confirmed that new oligodendrocytes continue to be generated from NG2 cells even after eight months of age.

4.3 Discussion

The cell cycle dynamics of NG2 cells and their contribution to cell genesis in the postnatal forebrain were studied and the following conclusions were reached. Firstly, the cell cycle time in both white and grey matter increases dramatically from ~2 days to >70 days between ~P6 to P240. Secondly, oligodendrocyte differentiation continues throughout adulthood but declines in parallel with the rate of precursor cell division. Thirdly, there are two distinct populations of OLPs; apart from the mitotically active population there is a separate population that never undergoes cell division. And lastly, the subdivision into dividing and non-dividing NG2 cell populations is not related to their developmental origins in the ventral or dorsal telencephalon.

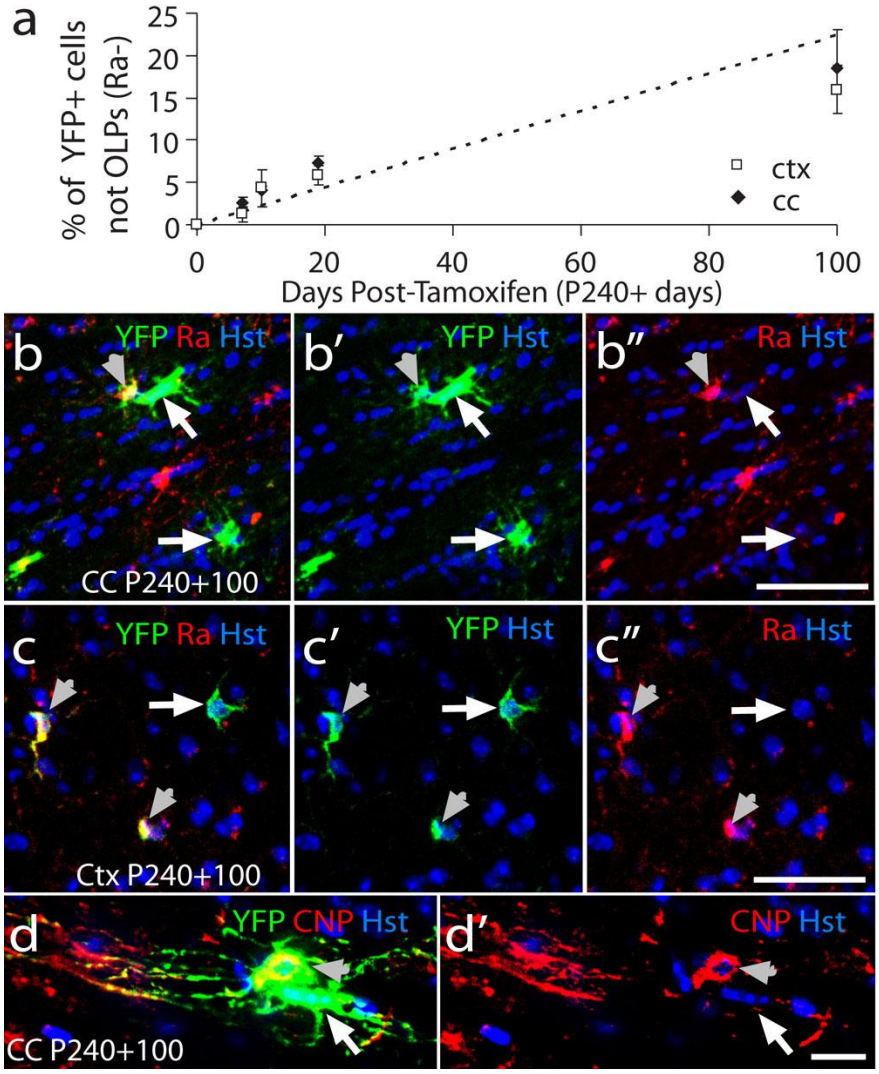

Figure 4.15 *OLPs continue to produce oligodendrocytes after 8 months of age. The proportion of YFP+ cells that were PDGFRA-negative increased slowly with time (**b**). YFP+, PDGFRA-negative cells with the morphology of differentiating oligodendrocytes were generated in both the corpus callosum (**c**) and cortex (**d**). Grey arrowhead indicates a YFP+, PDGFRA+ NG2 cells, white arrow indicates a YFP+, PDGFRA-negative oligodendrocyte. CC, corpus callosum; Ctx, cortex. Scale bars: **b-d**, 35 µm; **f-g**, 30 µm.*

We have demonstrated that the cell cycle duration for OLPs in the postnatal mouse brain lengthens with ageing. It is likely that most of the increase in T_C observed with age results from an increase in the amount of time cells remain resting in early G1, as even when Tc was significantly different, often S phase was unchanged. For example, at P21 Tc was much shorter for white matter OLPs than grey matter OLPs, however, both had an S phase of ~1.3 days (**Fig. 4.13a**). These data are supported by a recent study, analysing human surgical specimens derived from healthy adult human brain (mean, 50 years old) which has provided evidence that, at any one time, a substantial fraction of cycling adult human OLPs is in the early G1 phase of the cycle (Geha *et al.*, 2010). This study exploited the fact that the cell cycle-related antigen Ki67 is detectable in cells from late G1 through to M-phase but not in early G1, whereas the mini-chromosome maintenance protein-2 (Mcm-2) is expressed at all stages of the cycle. Geha *et al.* (2010) found that cycling cells identified by either Ki67 or Mcm-2 in the cortical grey or white matter all co-expressed NG2 and OLIG2. However, Mcm-2+ cells outnumbered Ki67+ cells ~3-fold, consistent with a long cell cycle and an extended G1. In my own studies, only 29% of PDGFRα+ cells co-labelled with Ki67 (less than the ~75% that could be labelled by EdU), which also suggests that many of the cycling PDGFRα+ cells were in early G1.

Taking into consideration previous reports that all embryonic OLPs are proliferating and our data that indicate that ~75% of OLPs proliferate in adulthood while 25% remain quiescent, it is understood that there should be a switch in the OLP cycling behaviour that occurs sometime between E13 and P60. Work by Kukley *et al.* (2008) combined BrdU labelling and PCNA immunohistochemistry and placed the

growth fraction of OLPs in P7 mice at ~50% (Kukley *et al*, 2008). In contrast to our initial BrdU study that shows the GF of OLPs in the P6 brain to be ~55%, EdU studies carried out by Kaylene Young in the Richardson laboratory indicate that >90% of OLPs can be labelled by EdU injections between P4 and P9 (unpublished). Thus, it seems likely that the mitotically quiescent population of OLPs forms during the first ~2 weeks of postnatal life.

Mitotically active cells can be labelled *in vivo* and *in vitro* using a variety of methods. Though different in their application, BrdU, EdU, Ki67 and PCNA are the most commonly used methods. PCNA expression increases in late G1, peaks in S phase and remains high during G2 and M phase (Bravo *et al*., 1987). Due to its long half life, some non-degraded protein still remains in cells that have recently left the cell cycle (Bravo *et al*., 1987). The two patterns of immunostaining for PCNA described to date reflect this; nuclei of cells in the S phase of the cell cycle are stained strongly while nuclei of cells in other cell cycles phases are stained weakly. Another marker used to identify cells that are mitotically active is Ki67. Ki67 distinguishes highly proliferative cells (G1, S and G2 phases) from cells in remission (Bacus *et al*., 1989; Gaglia *et al*., 1993). Due to its short half life which is approximately 1 h, it is rarely detectable in resting cells (G0), a fact that can provide a reliable means of evaluating growth fraction (Gerdes *et al*., 1984; Gerdes *et al*., 1991; du *et al*., 1991). Overestimation of the growth fraction is more likely with PCNA than with Ki67 analysis, due to the involvement of PCNA in DNA repair (Bravo and McDonald-Bravo 1987; Toschi and Bravo 1988) and to its presence in

early G0 due to its relatively long half-life of 8-20 h (Scott *et al.*, 1991; Bruno and Darzynkiewicz 1992).

Staining for BrdU required an antigen retrieval protocol to allow the anti-BrdU antibody access to the DNA strand (**2.8.5**). There are several BrdU treatment protocols available that differ in terms of the acid concentration used, ranging from 2M to 6M HCl, and the duration and the temperature of the acid treatment. For my study, BrdU+ cells were scored as positive only when the fluorescence signal clearly delineated the whole nucleus (though not necessarily uniformly). This however might exclude cells that had just entered S phase during the BrdU labelling period, or exited from S→G2 early during BrdU exposure. Therefore, my criteria for scoring BrdU positive cells might have tended to under-estimate GF. This seems all the more likely since repeating the cumulative label experiments with EdU rather than BrdU gave consistently higher GFs (~75% rather than ~50%). The signal intensity and signal-to-noise with EdU was higher than with BrdU, rendering the labelling procedure less prone to false negatives. I, therefore, put more faith in the higher EdU estimates of GF.

Although the growth fraction estimates increased, the main conclusions of my cumulative labelling experiments remained. Firstly, there are two distinct populations of OLPs in the adult mouse brain, one that is mitotically active and one that is not (75% : 25% respectively). Secondly, there is significant slowing of the OLP cell cycle with postnatal age. Thirdly, the OLP cell cycle length can differ between brain regions e.g. grey versus white matter.

The discovery of two different categories of NG2 cells and the demonstration that the mitotically active cells function as oligodendrocyte precursors raises the question of what is the function of the non-dividing NG2 cells? Two categories of NG2 cells in the P7 cerebellar white matter have been identified on the basis of their electrical properties; one class expresses voltage-gated sodium and potassium channels and can fire action potentials in response to a depolarizing stimulus whereas the other class does not express voltage-gated channels and displays a linear voltage-current relationship (Karadottir *et al.*, 2008). These two types of OLPs were also identified in the corpus callosum (Karadottir *et al.*, 2008). These two electrophysiological subtypes of OLPs are present in approximately equal proportions. It has been reported that mitotically active NG2 cells form morphological synapses with axons and maintain those synapses during and after mitosis (Kukley *et al.*, 2008; Ge *et al.*, 2009), suggesting that the electrically active sub-class of Karadottir *et al*. (2008) might correspond to our dividing sub-population. This hypothesis is now being directly investigated and the electrically active and dividing OLPs do appear to correlate (Clarke *et al*., manuscript in preparation).

It is possible that during perinatal development all newly-generated OLPs attach to unmyelinated axons, some of which fire action potentials and deliver a mitogenic signal to the associated OLP. These OLPs consequently divide, renewing themselves and producing myelinating oligodendrocytes. The other OLPs are associated with axons that never fire, or do not fire above a sufficient threshold, so these cells are destined to remain mitotically inactive (**Fig. 4.16**). They might also lose their expression of voltage-gated ion channels, rendering them electrically passive. It is

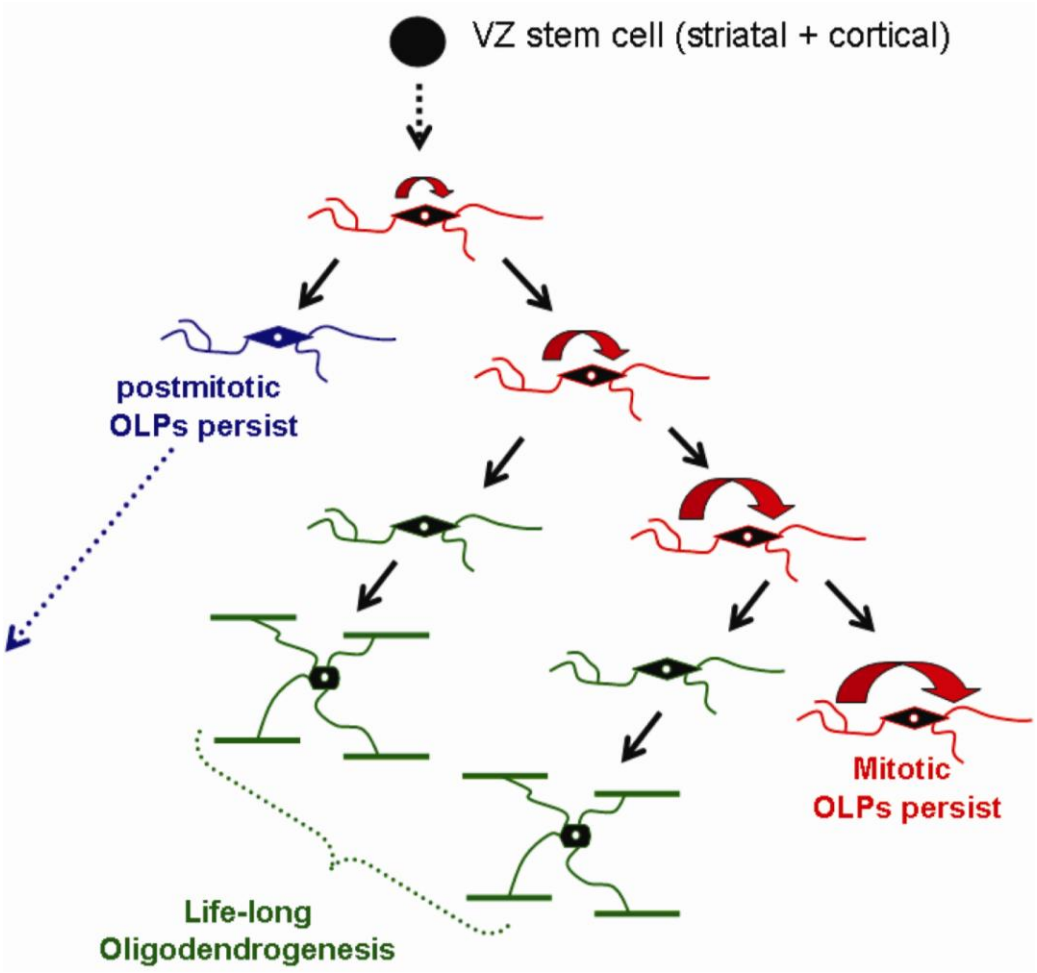

Figure 4.16 *The birth and behaviour of OLPs. From the data presented here, we conclude that forebrain OLPs are initially derived from embryonic VZ stem cells located in both the dorsal (cortical) and ventral (LGE/MGE) telencephalon. Their embryonic origin does not have any bearing on their mitotic activity as adult OLPs. A population of post-mitotic OLPs, comprising approximately half of all OLPs, is born some time before the end of the first postnatal week and persists throughout life. The function of these cells is unknown. The other half of the OLP population remains in cycle throughout life, although their cell cycle length increases with age (e.g. from ~2 days at P4-7, to ~70 days at 8 months and >150 days at 18 months in the cortex). One major function of the proliferating OLPs is to generate new oligodendrocytes throughout life. However, the rate of oligodendrogenesis progressively slows with age, roughly in parallel with the slowing cell cycle. (Figure drawn by Kaylene M. Young)*

possible that they contribute in some other way to the neuronal circuitry – for example they might perform some essential homeostatic function at nodes of Ranvier or at neuron-neuron synapses (Butt *et al.*, 2002).

Are the non-dividing cells permanently post-mitotic, or can they ever re-enter the cell cycle? It seems very likely that they never divide under normal conditions because, once the labelling plateau was reached, there was no sign of any further increase even after a very long labelling period. For example, at P60 the EdU labelling index in the corpus callosum reached 75% after ~8 days (~20 days in cortex) but did not increase further than that even after 50 days of continuous EdU exposure (until P110). Kukley *et al*. (2008) also demonstrates a major functional sub-division in the NG2+/PDGFRα+ OLP population, suggesting heterogeneity based on the mitotic activity of OLPs. By immunolabelling for the proliferating cell nuclear antigen (PCNA), Kukley *et al*. (2008) show that the growth fraction of P7-P12 mouse hippocampal OLPs is also close to 50% (Kukley *et al.*, 2008). Moreover, Keirstead *et al.* (1998) found that ~50% of OLPs in the adult rat spinal cord were resistant to killing by X-irradiation, suggesting that they were dividing very slowly or not at all.

OLPs have been suggested to fall into two (or more) categories on the basis of a range of criteria. These include: 1) cell morphology, in white matter there are bipolar and multipolar NG2+ cells (Lytle *et al*., 2009); 2) their immunohistochemical profile, a small proportion of NG2+/PDGFRα+ cells have been demonstrated to co-express markers such as s100beta (Rivers *et al*., 2008; Lytle *et al*., 2009) and nestin (Lytle *et al*., 2009); 3) their electrophysiological properties, white and grey matter oligodendrocyte progenitor cells have been reported to differ in their K+ and Na+

channel expression profiles (Chittajallu *et al*., 2004); 4) their embryonic origins, with all major forebrain regions containing OLPs derived from the embryonic cortical and striatal VZs (Kessaris *et al*., 2006); 5) proliferative status (Kukley *et al*., 2008; Rivers *et al*., 2008; Psachoulia *et al*., 2009; this Thesis). Both proliferative activity and embryonic origin split the OLP population in two. It is evident from my studies that the dividing and non-dividing OLPs do not correspond directly to ventrally- or dorsally-derived OLPs in the forebrain at least. It will be interesting and important to discover how the different OLP populations arise and what their functional specializations are, if any.

Whether the non-dividing NG2 cells are intrinsically incapable of division or else are segregated into a different environmental compartment than their dividing counterparts is another question. This might be answered by culturing dissociated cells in saturating concentrations of mitogens (e.g. PDGF), which would be expected to override environmental regulation. PDGF is a potent mitogenic stimulant for OLPs (Richardson *et al*., 1988; Pringle *et al*., 1989; Wolswijk *et al*., 1991; Noble et al, 1998) and increasing the supply of PDGF *in vivo* (van Heyningen *et al*., 2001) and *in vitro* (van Heyningen *et al*., 2001; Wolswijk *et al*., 1991; Wolswijk and Noble, 1992; Baron *et al*., 2002) can increase the proliferation rate and reduce cell cycle length. For example, Van Heyningen *et al*. (2001) previously showed that the cell cycle time of OLPs in the embryonic mouse spinal cord increases from ~30 hours to 70-100 hours between E13 and E17, but that both E13 and E17 cells can accelerate their cycle to ~20 hours when cultured in medium containing saturating PDGF-AA. This demonstrated that slowing of the OLP cell cycle during late embryogenesis

results from a change in their mitogenic environment, not a shift in the intrinsic properties of the cells (van Heyningen *et al.*, 2001). Similarly, in the presence of PDGF adult OLPs take ~60hrs to divide (Wolswijk *et al.*, 1991). This cell cycle time can be reduced to ~30hrs, more similar to embryonic OLPs, by co-stimulating with FGF2 (Wolswijk and Noble, 1992). FGF2 is a mitogen for neural stem cells, as well as OLPs, and these cells have also been reported to senesce in ageing (Jin *et al.*, 2003; Kuhn *et al.*, 1996; Tropepe *et al.*, 1997; Fiore *et al.*, 2002; Maslov *et al.*, 2004). *In vivo* neural stem cells in the aged brain are able to respond to intraventricularly administered EGF and bFGF by increasing their proliferation and exhibiting up to a 450% increase in BrdU incorporation (Jin *et al.*, 2003). This suggests that proliferative cells in the CNS, including OLPs, maybe slowing down with ageing, due to limitations or changes in the availability of mitogens. This could imply that exogenous administration of mitogens might be able to rescue the diminished proliferative properties of these cells.

It is likely that PDGF acts in concert with other mitogenic factors including electrical stimulation; there is evidence that proliferation of OLPs in the perinatal rat optic nerve depends on the electrical activity of retinal ganglion cell axons, one effect of which might be to stimulate release of PDGF from astrocytes within the nerve (Barres and Raff, 1993). The fact that NG2 cells receive synaptic input from axons, together with previous evidence that the neurotransmitter glutamate can inhibit proliferation and differentiation of OLPs in culture suggests that neurotransmitter release at axon-glial synapses might directly or indirectly influence the OLP cycle and the myelination program.

The dividing population of OLPs in white matter tracts generates new myelinating oligodendrocytes. Since the number of OLPs stays relatively constant during the first year (Rivers *et al.*, 2008), it follows that half of the daughters of cell divisions must either differentiate or die. For example, at P45 the cell cycle time in the corpus callosum is ~7.3 days (extrapolating from the data in **Fig. 4.7** and **4.13**), so it will take ~14.5 days (two cell cycles) for the OLPs that are dividing to generate a number of differentiated cells equal to the starting population of OLPs. Put another way, the fraction of YFP+ cells that is differentiated (therefore PDGFRα-negative) 14.5 days after administering tamoxifen to P45 *Pdgfra-CreER^{T2}/R26YFP* mice is predicted to be 50%. At 14 days post-tamoxifen the predicted fraction is ~49% [(14/14.5) ÷ {1+(14/14.5)}]. It was found experimentally that 45% of YFP+ cells were PDGFRα-negative at P45+14 days post-tamoxifen, which is close to expectation, so it appears that there is rather little death of newly differentiated cells in the 14 days after P45 (**Fig. 4.17**).

By applying a similar calculation for P240 ($T_C \approx 125$ days), it is predicted that at 100 days post-tamoxifen ~40% of YFP+ cells should be PDGFRα-negative. The observed value in this case was only 18%, suggesting that less than half of the differentiated progeny of OLPs survive long-term between P240 and P340. Nevertheless, the rate of oligodendrocyte production in the corpus callosum depends on the rate of OLP cell division. The cell cycle slows down ~10-fold between P45 and P240 and the rate of oligodendrocyte production slows ~20-fold in the same period (**Fig. 4.17**). A similar relationship between cell cycle and oligodendrogenesis applies to the cortex, although both cell division and production of YFP+/PDGFRα-

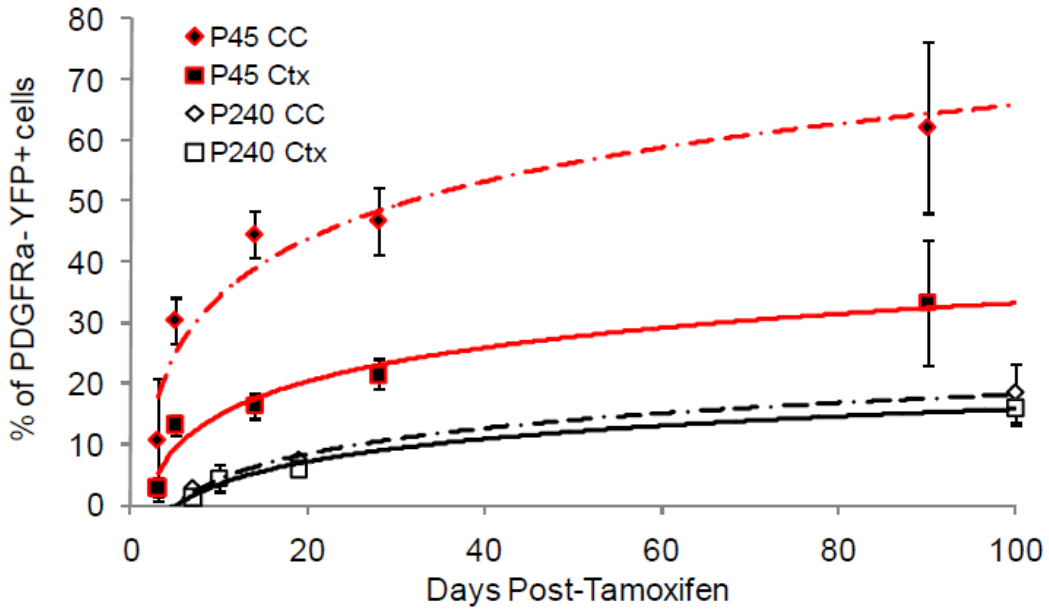

Figure 4.17 *OL production declines in parallel with increasing NG2 glia cell cycle. Tamoxifen was administered to Pdgfra-CreERT2/R26YFP transgenic mice at P45 (L. E. Rivers) and P240 (K. Psachoulia). Brain sections were examined at various time-points post-tamoxifen administration. By plotting the proportion of YFP+ cells that no longer express PDGFRα, it was possible to compare oligodendrocyte production in the CC and Ctx in young and middle-aged mice. (P45 data adapted from Rivers et al., 2008).*

negative cells are slower in the cortex than in the corpus callosum at most ages. It is important to note, however, that although oligodendroglial production at P45 is slower in the cortex than in the corpus callosum, this difference is diminished by P240, when the rate of oligodendrocyte production becomes similar for the two brain regions (**Fig. 4.17**). This comes into agreement with cell cycle length when looking at the same brain regions from mice of similar ages. At P60, the cell cycle length of NG2 cells in the corpus callosum is 3-times faster compared to the cortex, while at P240 the cell cycle is the same for both brain regions. These comparisons further raise confidence in the reliability of my data. My present estimates of cell cycle time (~73 days) in older (8 month old) mice are also compatible with long term retroviral tracing experiments that indicate an oligodendroglial cell doubling time in the 3-8 month old rat cortex of around three months (Levison *et al.*, 1999). An age-related increase in the cell cycle of OLPs in the mouse spinal cord was also noted by Lasiene *et al.* (2009). These authors also observed that the OLP cell cycle started to speed up again in aged mice (21 months of age) but I did not observe this phenomenon in the forebrain of 18 month old animals.

The age-related reduction in the proliferative rate of OLPs and the corresponding reduction in the rate of production of new oligodendrocytes could play an important role in the ageing process. For example, it is becoming clear that white matter volume starts to decline in humans after the fourth decade of life and that this white matter loss correlates with general deterioration of cognitive and motor ability. A recent study on rhesus monkeys came to similar conclusions (Bowley *et al.*, 2010). Even though there is evidence of remyelination in the aged brain and spinal cord

(Lasiene *et al*., 2009; Bowley *et al*., 2010), it could be that myelinating oligodendrocytes have a finite lifetime and, beyond this, the rate of new oligodendrocyte production cannot keep pace with accelerating oligodendrocyte loss. If so, finding ways to maintain NG2 cells in a more proliferation-competent state or promote the survival of newly formed oligodendrocytes might help maintain white matter integrity and slow down age-related mental decline.

Chapter 5

‘The regulation and function of life-long oligodendrogenesis’

5.1 Introduction

In Chapters 3 and 4 I presented data showing that adult OLPs proliferate and differentiate to form myelinating oligodendrocytes throughout life. This observation raises questions about the function of this ongoing oligodendrogenesis. It has been reported that only 28% of corpus callosal axons are myelinated in mice, even by eight months of age (Sturrock, 1980). This suggests that capacity remains for further myelination of axons across the lifespan. Therefore, new adult born oligodendrocytes may be myelinating previously un-myelinated axons. If this were true, it could represent an added and previously unexpected level of neural plasticity, perhaps with a role in some form(s) of learning and memory.

In Chapter 3 I demonstrated that voluntary exercise, on a running wheel, increases oligodendrocyte production in the corpus callosum of adult mice. It is interesting to speculate that these oligodendrocytes may be myelinating naked callosal axons

involved in the acquisition of this new motor task. The idea of activity dependent myelination is supported by reports that extensive piano practise during childhood can cause long-term changes to the structure of white matter tracts, including parts of the corpus callosum (Bengtsson *et al.*, 2005). Another study that used diffusion tensor imaging to look at professional musicians who started their musical training before or after the age of 7 years found enlarged anterior callosa in the early onset group compared to the late onset and control group, suggesting that white matter might be more receptive to the influence of sensorimotor training at younger age (Imfeld *et al*., 2009). However, changes in the white matter architecture of adults have also been reported. Scholz *et al*. (2009) showed (using diffusion tensor imaging) that juggling training resulted in a significant increase in white matter density in the right posterior intraparietal sulcus (Scholz *et al.*, 2009). The differences observed between controls and jugglers correlated with the time of training rather than the training outcome, i.e. juggling proficiency (Scholz *et al*., 2009).

In addition to changes in white matter, juggling induced detectable changes in the grey matter density in the medial occipital and parietal lobe cortical regions (Scholz *et al*., 2009). However, these changes were not detected using T1-weighted MRI scans (Driemeyer *et al*., 2008), which may not be surprising given that diffusion tensor imaging is a more sensitive method for the detection of non-volume related changes, such as synaptic and dendritic changes.

Supporting these human MRI studies, when adult Japanese macaques were trained to use tools and monitored by MRI and voxel-based morphometry, white matter changes were observed in the cerebellar white matter beneath lobule 5 in both hemispheres (Quallo *et al*., 2009). In relation to this, it is important to find out whether the cerebellar output axons are myelinated, as in the optic nerve, or not, as in the corpus callosum. This could impact on how to interpret the cerebellar white matter changes. Grey matter changes were also recorded in the right superior temporal sulcus, the intraparietal sulcus and the anterior intraparietal area (Quallo *et al*., 2009). These two regions that showed significant volume changes, correspond to the areas of the human brain that fMRI studies indicate become activated by tool use (Quallo *et al*., 2009).

These changes in brain architecture with training do not appear to be limited to the young. It is known that cognitive ability and white matter volume increase in parallel until the fourth decade of life, when they start to decline (Bartzokis *et al.*, 2001; Mabbott *et al.*, 2006; Hasan *et al.*, 2008; Ullen *et al.*, 2008; Bartzokis *et al*., 2008; Zahr *et al.*, 2009). However, there is evidence supporting the existence of some brain plasticity in old age. When a group of elderly (~60 years old) volunteers was trained in juggling, their performance was poorer than that of young adults (~20 years old), trained for a similar period. However, the structural changes observed (using T1-weighted MRI and VBM) were similar with the addition of grey matter changes in the hippocampus and the nucleus accumbens (Boyke *et al*., 2008). These data suggest that age does not preclude structural plasticity, but might reduce it.

There are now many MRI, VBM and diffusion imaging correlations between activity and white matter changes, but it has not been clearly demonstrated whether these white matter changes correspond to altered myelination or oligodendrogenesis. Furthermore, the necessity of this plasticity and the function of adult oligodendrogenesis have not yet been addressed. To begin answering these questions requires a different experimental approach in an animal model. To this end, we have embarked on a line of experimentation in mice that necessitates the generation of certain genetically manipulated mice. One such line of transgenic mice should allow the labelling and conditional ablation of adult-born mature myelinating oligodendrocytes. For this, it was necessary to identify a gene that could be used to restrict expression of transgenes to mature myelinating oligodendrocytes. Potential candidates included MAG, MBP, PLP and Opalin but these genes were excluded as they were either expressed by Schwann cells in the peripheral nervous system (PNS) or were expressed too early in the oligodendroglial cell maturation process (Dubois-Dalcq *et al*., 1986; Kippert *et al*., 2008; Fulton *et al*., 2009).

Ermin is a gene that was identified as being exclusively expressed by postnatal oligodendrocytes in the mouse and rat brain and spinal cord (Brockschnieder *et al*., 2006; Zhang *et al*., 2005). *Ermin* consists of 3 exons spanning a region of 7.7 kb on mouse chromosome 2 (**Fig. 5.1, 5.3**). The amino acid sequence of Ermin has some similarity to the ERM (erzin, radixin, moesin) proteins, which are widely distributed membrane-associated proteins that regulate the structure and function of specific domains of the cell cortex, and Ermin is therefore regarded as a distant member of this protein family (Bretscher *et al*., 2002; Ramesh *et al*., 2004).

Within oligodendrocytes, the Ermin protein is found in the cell bodies, processes and along the myelinating fibres (Brockschnieder *et al*., 2006). Ermin is found in the abaxonal, cytoplasmic pocket of the myelin sheath and around the internodes but is undetectable in compact myelin. It is involved in cytoskeletal rearrangements, supporting a role for F-actin in regulating the dynamic morphology of oligodendrocytes during myelination (Brockschnieder *et al*., 2006). The role of Ermin is to regulate cytoskeletal changes at the end of the wrapping and/or compaction phases of myelin assembly, as well as to maintain and stabilize the myelin sheath in the adult (Brockschnieder *et al*., 2006). As such, ermin is expressed along white matter tracks in the brain and spinal cord, including the corpus callosum, medulla and cerebellum (Brockschnieder *et al*., 2006). In mice, ermin expression is completely absent for the first postnatal week. Its expression emerges around P8 and increases dramatically until P14 (Brockschnieder *et al*., 2006), a period when oligodendrocytes are actively myelinating axons in the CNS (Jordan *et al*., 1989). Ermin expression is always confined to MBP-expressing oligodendrocytes and is not present in myelinating Schwann cells of the PNS (Brockschnieder *et al*., 2006). In summary, Ermin is a protein that is restricted to myelinating oligodendrocytes of the CNS, making the *ermin* promoter an excellent candidate for targeting the expression of a transgene that will allow the labelling and conditional ablation of mature myelinating oligodendrocytes.

This chapter describes the generation and characterization of the *ErminΔdsred·STOPΔDTR·Ires·Venus* BAC transgenic mouse, which will be used to investigate the generation and function of adult oligodendrogenesis.

5.2 Results

5.2.1 Selecting BAC clones

Three bacterial artifical chromosomes (BACs) that contained the *Ermin* gene were selected from the published mouse genomic database (www.ensemble.org; **Fig. 5.1**). The BAC clones chosen covered a large region of DNA flanking the gene, to ensure the greatest likelihood of having all of the regulatory elements that control the faithful expression of e*rmin*, which will ultimately control the appropriate expression of the transgene.

To ensure the BAC clones obtained contained the expected DNA sequence, the DNA was amplified, extracted, digested with the restriction enzymes PacI or PmeI (sites internal to the genomic region contained in the BAC) and analysed by PFGE as described in **2.3.2**. All of the clones analysed produced the expected pattern of DNA fragments (data not shown). RP23-384J16 covered the largest genomic region compared to RP23-260D20 and RP23-370M17. Therefore, RP23-384J16 (hereafter referred to as the Ermin BAC) was selected and used in all subsequent work for the generation of the *ErminΔdsred·STOPΔDTR·Ires·Venus* transgenic mouse.

Ermin BAC DNA (circular) was electroporated into EL250 cells. Of the bacterial colonies that formed, ~12 were selected and grown as mini-prep cultures as described in **2.1.1**. DNA was purified from each mini-culture and again digested with either PacI or PmeI. Incorporation of the correct Ermin BAC DNA into the EL250 bacteria cells was confirmed by PFGE (**Fig. 5.2**).

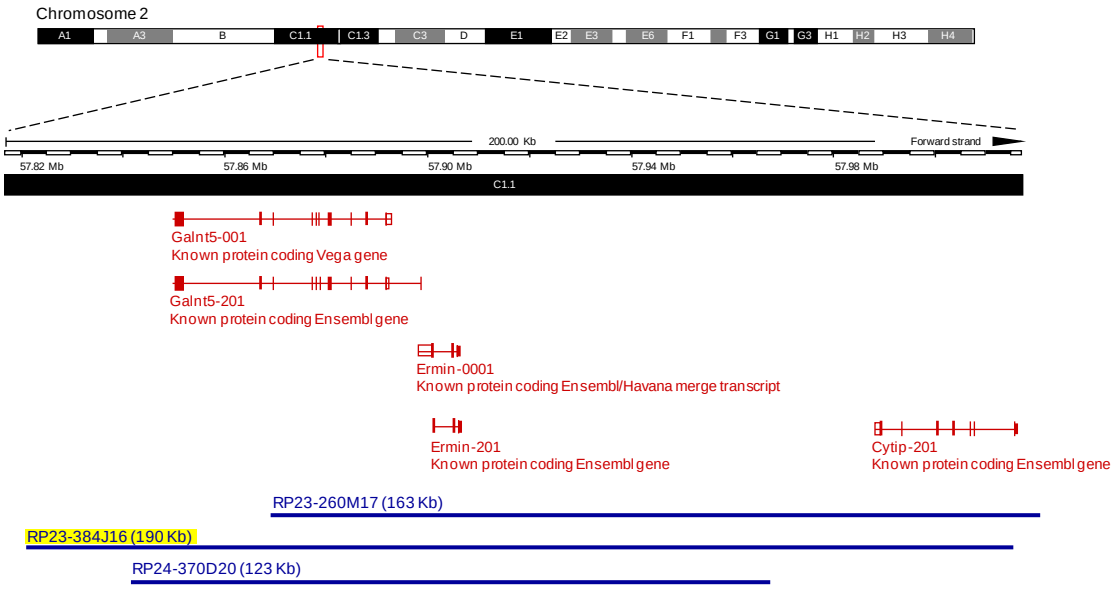

Figure 5.1 *(a) Schematic of mouse chromosome 2 with a higher magnification of the region containing the ermin gene (adapted from: http://www.ensembl.org). The three BACs initially selected are shown in blue. The yellow-highlighted BAC was ultimately selected to generate the ErminΔdsredSTOPΔDTRIresVENUS transgenic mouse.*

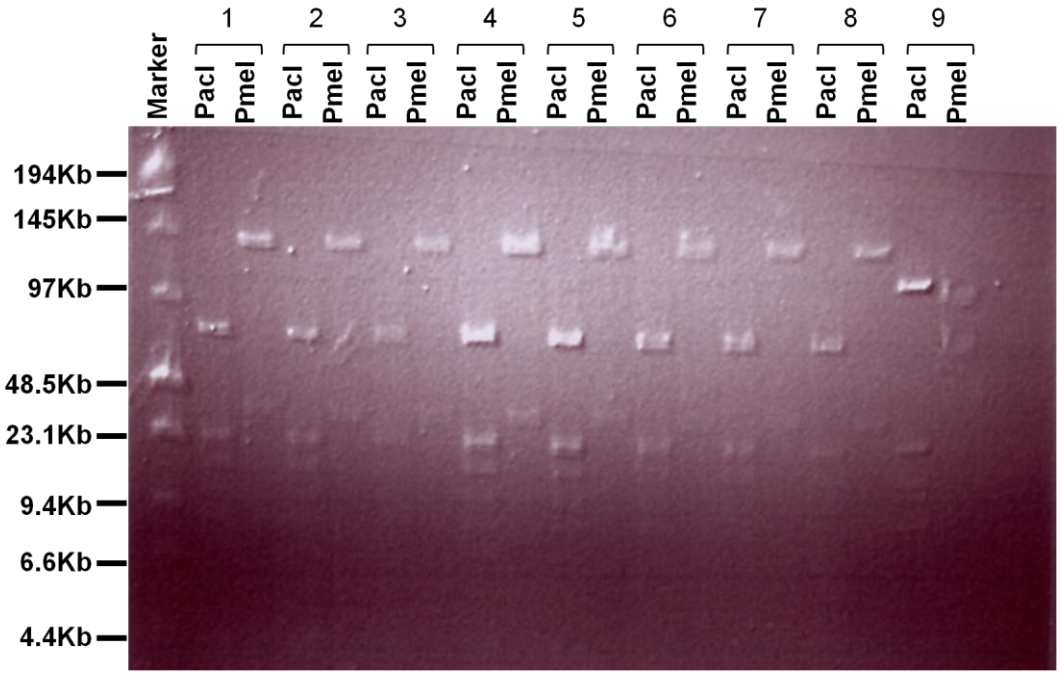

Figure 5.2 *PFGE analysis of BAC DNA digested with PacI and PmeI. BAC DNA was obtained from clones grown following electroporation of the Ermin BAC DNA into EL250 cells. Clones 1-8 represent bacteria that underwent correct transformation, while clone 9 did not.*

Digesting the BAC DNA with PacI should yield fragments of 83,279, 19,028, 16,071, 11,836, 10,362, 9,471, 7,531, 4,530, 3,994, 2,686 and 2,206 base pairs. By comparison, digesting with PmeI should produce DNA fragments of 121,554, 40,859 and 8,581 base pairs. DNA obtained from clones 1-8 produced the expected digest pattern. Clone 4 was selected for further work.

5.2.2 Construction of the targeting vector

Manipulation of the *ermin* coding sequence through homologous recombination in bacteria required the generation of a targeting vector. The targeting vector was designed by Ian McKenzie to contain 5 major elements: the fluorescent protein DsRed and a stop sequence (this will stop the transcription of the sequences located downstream) located between two loxp sites, the human form of the diphtheria toxin receptor (Saito *et al*., 2001), the fluorescent protein Venus (Nagai *et al*., 2002) and the 5' and 3' sequences that are homologous to the ermin gene (**Fig. 5.3**).

The first fluorescent protein, DsRed, is a recently cloned 28-kDa fluorescent protein responsible for the red colouration around the oral disk of a coral of the Discosoma genus (Matz *et al*., 1999). It has a high extinction coefficient and quantum yield, plus excellent resistance to pH extremes and photobleaching (Baird *et al*., 2000). However, DsRed has major drawbacks, such as strong oligomerization and slow maturation (Baird *et al*., 2000). The second fluorescent protein, Venus, is an improved version of YFP (Nagai *et al*., 2002). It contains a novel mutation, F46L, which at 37°C greatly accelerates oxidation of the chromophore, the rate-limiting step of maturation. As a result of other mutations, F64L/M153T/V163A/S175G,

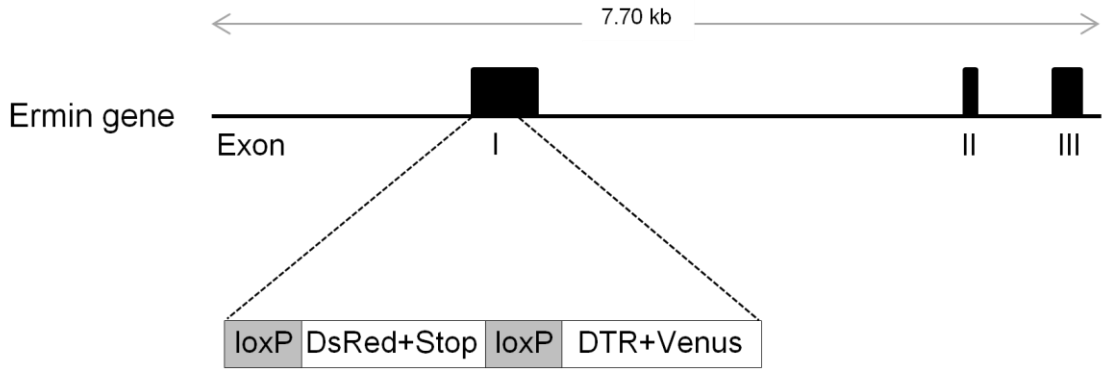

Figure 5.3 *Schematic depicting the position at the beginning of exon I in the ermin gene where the targeting vector will be inserted following homologous recombination.*

Venus folds well and is relatively tolerant of exposure to acidosis and Cl– (Nagai *et al*., 2002). DsRed and Venus should therefore allow robust fluorescent labeling of targeted cells. However, the DsRed and stop sequences are located between 2 loxP sites (**Fig. 5.3**), and the loxP sites must be recombined and the intermediate sequence removed in order for Venus (and the DTR) expression to be turned on. Therefore the two fluorescent proteins will never be co-expressed by the same cell.

Expression of the human form of DTR selectively renders the targeted cells susceptible to death by controlled administration of diphtheria toxin (DT) (Cha *et al*., 2003; Buch *et al*., 2005; Chen *et al*., 2005). Mice are naturally resistant to the effects of DT as their endogenous DTR contains a mutation that renders it incapable of internalizing the toxin (Saito *et al*., 2001). In order to ensure that DsRed (and following recombination), DTR and Venus are only ever expressed by mature myelinating oligodendrocytes, the targeting vector was inserted into the chosen BAC by homologous recombination, directing insertion to exon 1 of the *Ermin* gene due to the presence of the flanking 5' and 3' homologies and deleting the endogenous ATG and most of the coding region of exon 1 (**Fig. 5.4**). The 5' untranslated region (UTR) was left largely untouched, as was intron 1 in the event that regulatory elements are present within these regions (**Fig. 5.4**).

The targeting vector was generated by a series of cloning and ligation steps (**2.5.1.2** and **2.5.1.3**; **Fig. 5.4**). The first step resulted in DsRed, a nuclear localization signal (NLS) and the STOP sequence being ligated between the two loxP sequences (**Fig. 5.4a**). Initially, *DsRed2* was amplified by PCR from pIRES-DsRed2 (Clontech),

adding *XbaI* and *XhoI* to the 5' and 3' flanks respectively (forward primer, 5'-TCT AGA TAA TAT TGG CCA CAA CCA TGG CCT CC-3'; reverse primer, 5'-CTC GAG CCC CAG GAA CAG GTG GTG GCG GC-3'). This PCR product was isolated and cloned directly into pCRII-TOPO® and sequenced as described in **2.1.3** and **2.3.4** respectively. DNA from bacteria containing the vector was isolated and digested with XbaI and XhoI to excise the Dsred sequence. The NLS was annealed from complementary oligonucleotides by gradual cooling from 95ºC for 1 hour: NLStop (5'-TCG AGC CTA AGA AGA AAC GGA AGG TTG AAG ATC CTT AGC TGC A-3') and NLSbot (GCT AAG GAT CTT CAA CCT TCC GTT TCT TCT TAG GC-3'), leaving an XhoI 5'-overhang and a PstI 3'-overhang. *3xPolyA* (3 consecutive polyadenylation sequences) was excised from the *Sox10GFPDTA* construct (Kessaris *et al*., 2006) by digesting with PstI and SpeI. The vector containing the two required loxP sites (*pLoxP2)* was opened by digesting with XbaI and SpeI. The 4 purified DNA fragments were ligated together to produce *ΔDsRed2·nls-STOPΔ* (**Fig 5.4a**).

The second step added the *DTR·IRES-Venus* to the end of the *ΔDsRed2-NLS-STOPΔ*. The *pblueIRES·Venus* vector was opened by digesting with BamHI and NotI. DTR was excised from *DTR-TOPO* by digesting with BamHI and MfeI (compatible sticky ends with EcoRI). *ΔDsRed2·nls-STOPΔ* was excised by digesting with NotI and EcoRI (**Fig 5.4b**).

The third step added another *STOP* sequence and a Kanamycin resistance cassette to the construct. *ΔDsRed2·nls-STOPΔDTR·IRES·Venus*, was opened by digesting the 3'

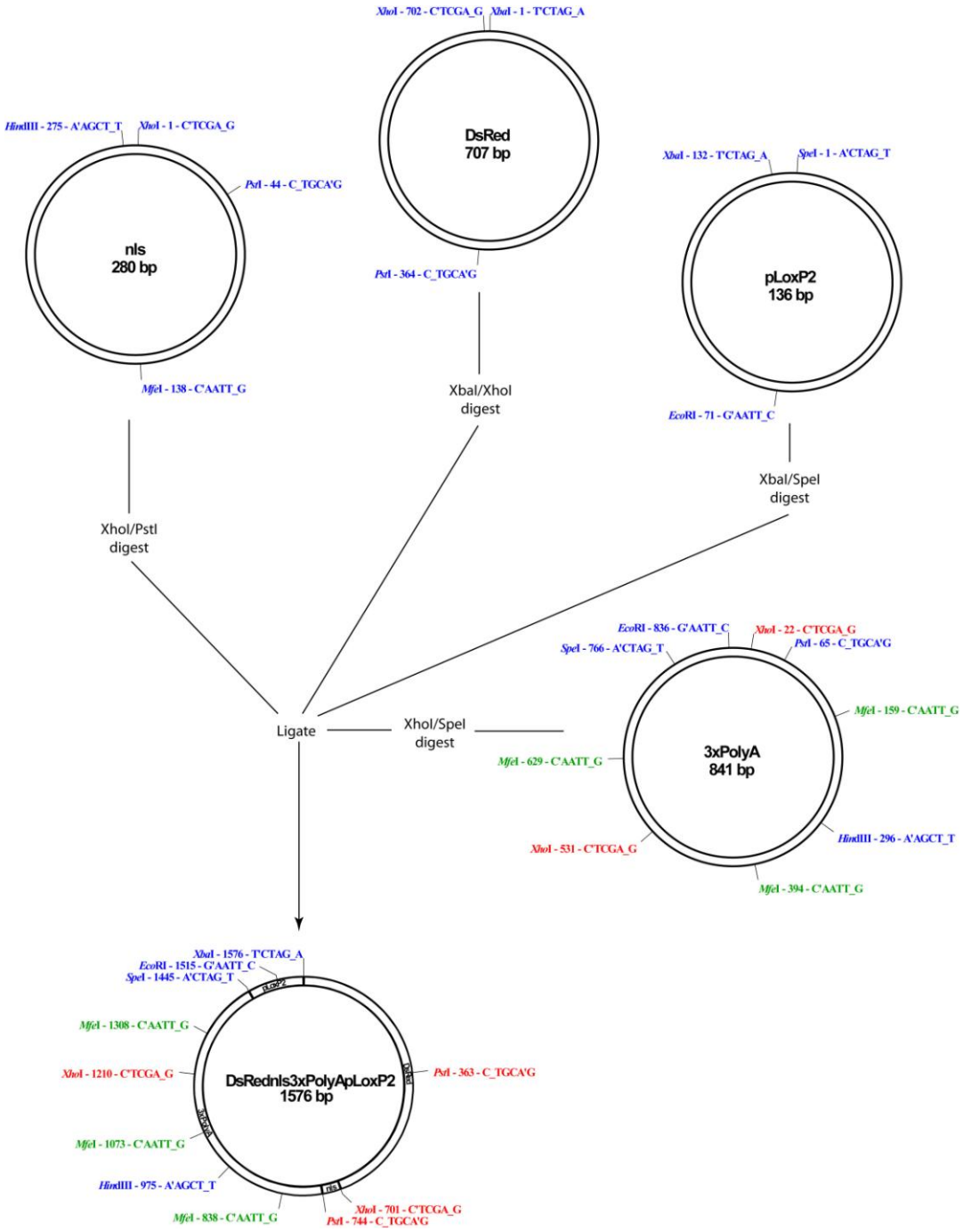

Figure 5.4a *Construction of the Ermin-DTR targeting vector. The first step in construction was a 4-way ligation step combining the 280bp nls, the 707bp DsRed from pIRES-DsRed2, the 136bp pLoxP2 and the 3xPolyA from Sox10GFPDTA to make DsRed·nls-3xPolyApLoxP2*

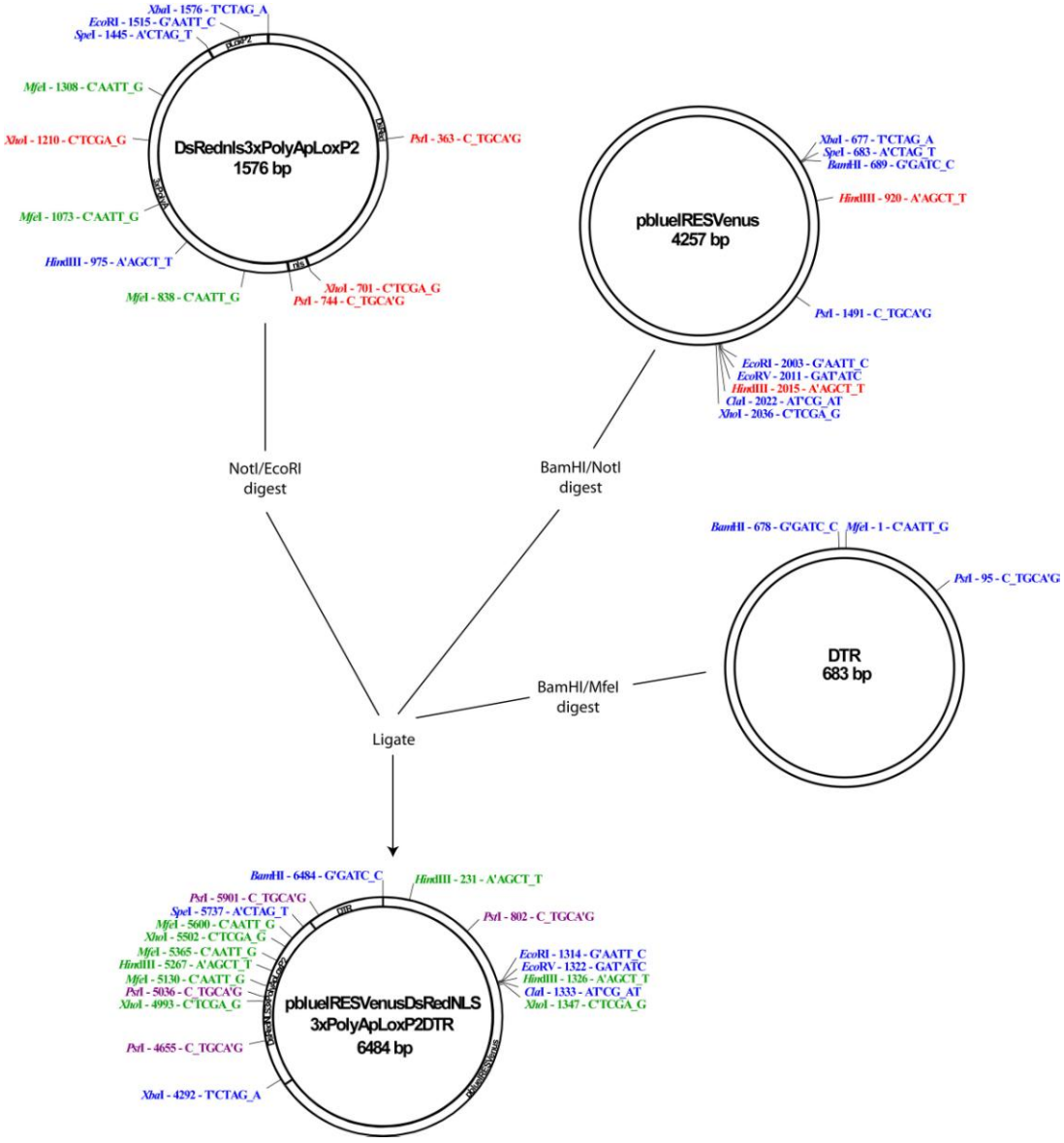

Figure 5.4b *Construction of the Ermin-DTR targeting vector. The second step in construction was a triple ligation step combining 1576bp DsRed·nls-3xPolyApLoxP2 produced from the previous ligation, the 4257bp pblueIRESVenus and the 683bp DTR from the DTR-TOPO to make pblueIRESVenusDsRed·nls-3xPolyApLoxP2DTR*

of the Venus sequence ClaI, blunting with T4 DNA Polymerase and further digesting with EcoRV. The *polyAfrt-Kan-frt* cassette was removed from the vector backbone by digesting with SpeI, blunting with T4 DNA Polymerase and further digesting with EcoRV as described in **2.5.1.3**. The resulting DNA fragments were ligated to produce *ΔDsRed2·nls-STOPΔ DTR·IRES·Venus- polyA·frt-Kan-frt* (**Fig. 5.4c**).

The final step involved the addition of the *Ermin* homology regions at either end of the construct, and the insertion of the construct into the *ΔpBluePacAsc* vector. For the final ligation, the 5' homology region was amplified by PCR from purified *Ermin* BAC DNA, adding *PacI* and *NotI* sites to the flanks (forward primer, 5'- TTA ATT AAG CTT CCT GAG AGC ACA CTA TG-3'; reverse primer, 5'-GCG GCC GCC TGA GGT CTG ATT TAA GGA CGC-3'). This PCR product was isolated and cloned directly into pCRII-TOPO® to make 5' Hom. The 3' homology region was also amplified by PCR from purified *Ermin* BAC DNA, adding *AscI* and *SalI* sites to the flanks (forward primer, 5'-GTC GAC GCC TGA AGA TGA GAA GAT CCT CA-3'; reverse primer, 5'-GGC GCG CCG GGA GAA ACA CAA GCA CTG TAA C-3'). The PCR product was isolated and cloned into pCRII-TOPO® to make 3' Hom. Both 5' Hom and 3' Hom were fully sequenced to ensure that their sequences were correct. To create the final targeting vector *ΔDsRed2·NLS-STOPΔDTR·IRES·VenusSTOP·frt-Kan-frt* was excised from pbluescript by digesting the purified DNA with NotI and SalI. The *pBluePacAsc* vector was constructed by modifying the multiple cloning site of *pBluescript* to add *PacI* and *AcsI* restriction sites (gift from N. Kessaris and M. Grist). *pBluePacAsc* vector DNA was cut with PacI and AscI and then ligated with the purified 5' *Hom*, 3' *Hom* and *ΔDsRed2·NLS-*

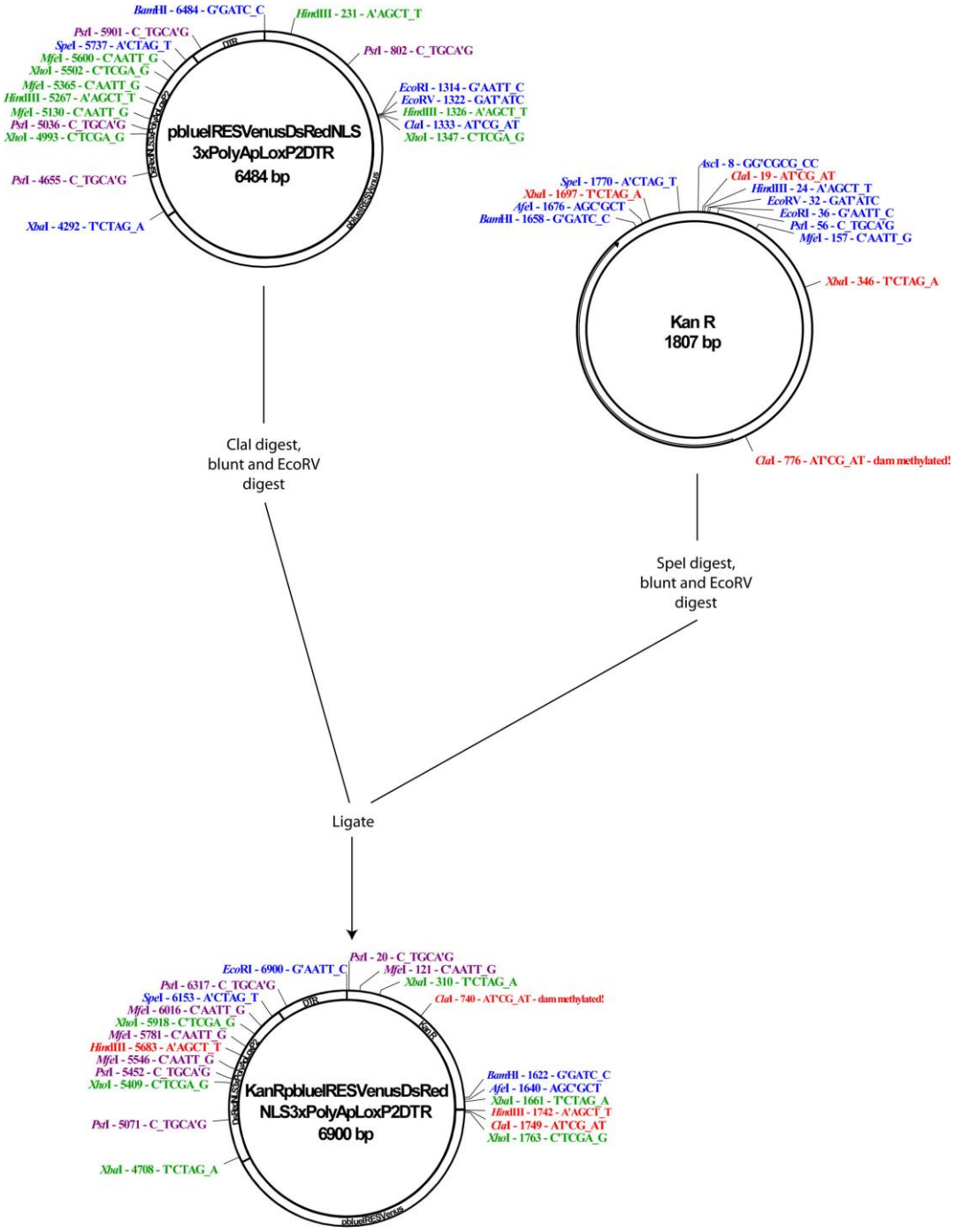

Figure 5.4c *Construction of the Ermin-DTR targeting vector. The third step in construction was a double ligation step combining 6484bp pblueIRESVenusDsRed·nls-3xPolyApLoxP2DTR produced from the previous ligation and the 1807bp Kan R to make KanRpblueIRESVenusDsRed·nls-3xPolyApLoxP2DTR.*

STOPΔDTR·IRES·VenusSTOP·frt-Kan-frt to make the final targeting vector (**Fig 5.4d**).

All cloning steps were verified by digesting DNA from transformed bacteria using restriction enzymes followed by gel electrophoresis. When the targeting vector was complete, it was linearized from the vector backbone by digesting with the restriction enzymes PacI and AscI, purified and electroporated into EL250 bacteria containing the modified *Ermin* BAC.

5.2.3 BAC modification

The BAC vector (pBACe3.6; **Fig. 5.5a**) contains an SV40 and a CMV promoter as well as a loxP site which might interfere with some downstream applications of the gene of interest. Therefore the mouse genomic fragment with the transgene must first be isolated before microinjection. As the final recombined *Ermin* BAC DNA sequence contains internal NotI, EcoRI and BamHI sites, it cannot be from the BAC vector using its existing cloning sites. For that reason, homologous recombination was first carried out in EL250 bacteria containing the *Ermin* BAC, in order to replace a 2618bp region from pBACe3.6 with an ampicillin selection cassette and an additional PISceI restriction enzyme site. The targeting vector for this step (pPISceAmp; **Fig. 5.5b**) was a gift from N. Kessaris and P. Iannarelli. Recombination was carried out according to the protocol outlined in Chapter 2. Ampicillin resistant colonies were verified to contain the modified *Ermin* BAC by restriction enzyme digestion of the BAC DNA with PacI and PmeI (**Fig. 5.6**).

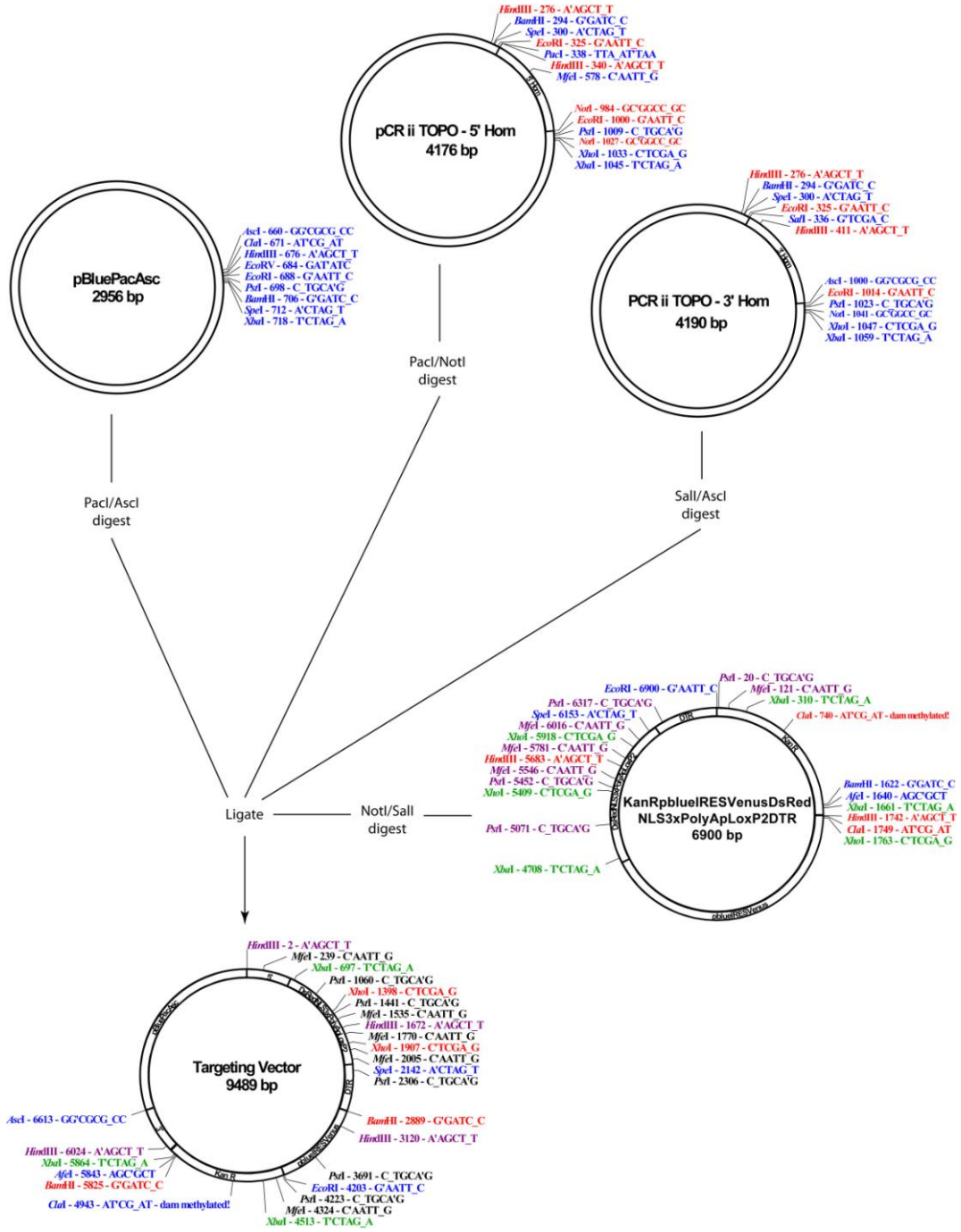

Figure 5.4d *Construction of the Ermin-DTR targeting vector. The final step in construction was a 4-way ligation step combining the 2878bp pBluePacAsc, the 646bp ermin 5' Hom, the 664bp ermin 3' Hom and the 5301bp KanRpblueIRESVenusDsRed·nls-3xPolyApLoxP2DTR fragments produced from the previous ligation to make the targeting vector.*

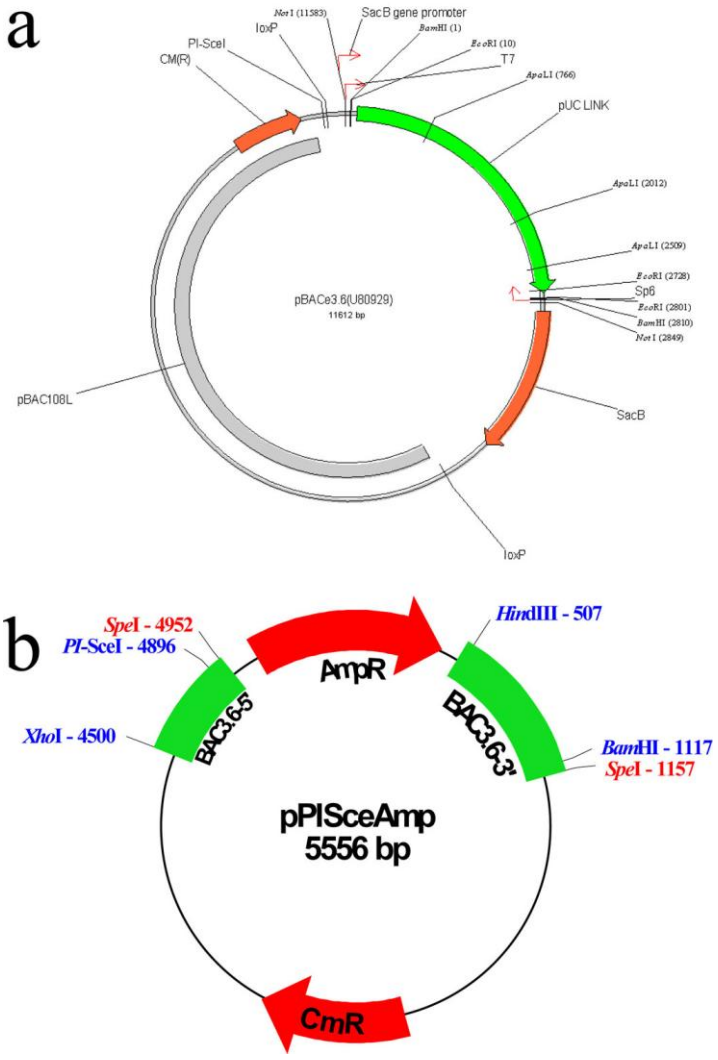

Figure 5.5 *Schematic depicting the pBACe3.6 vector, into which the genomic BAC insert was cloned between the two EcoRI sites removing the intervening 2618bp (a). The orange arrows show the antibiotic resistant sites, the green arrow the region that the gene of interest is inserted and the small red arrows the sites that the T7 and Sp6 primers cut for genotyping purposes (a). Recombination with the targeting vector pPISeAmp introduced an ampicillin resistance cassette (red arrow) to the BAC insert (b). The restriction sites are also indicated around the periphery (a, b).*

The second BAC modification inserted the final targeting vector. Part of the coding region of exon I in the *Ermin* gene was replaced with the linearized targeting vector (**Fig. 5.6**). Homologous recombination in bacteria was carried out as described in **2.5.2.1** and bacteria containing the recombined DNA sequence had acquired Kanamycin resistance. Next, the kanamycin resistance cassette was removed from the recombined clones by transient induction of *flpe* in EL250 cells using arabinose as described in **2.5.2.1**. The final recombined *Ermin* BAC DNA product was found to be correct by PFGE following restriction enzyme digestion again with PmeI (**Fig. 5.7**).

5.2.4 Generation of ErminΔdsred·STOPΔDTR·IRES·VENUS-STOP (Ermin-DTR) transgenic mice

5.2.4.1 Introduction of the recombinant BAC DNA into mouse ova

The modified *Ermin-DTR* BAC clone was liberated from the vector backbone with pISceI and purified by PFGE as described in **2.6.1**. Purified *Ermin-DTR* BAC DNA was quantified by PFGE (**Fig. 5.8**) as per section **2.6.1** and injected into fertilized mouse ova at a concentration of around 200ng/µl. All pronuclear injections were carried out by U. Dennehy as described in **2.6.2**.

5.2.5 Characterising the expression of the Ermin∆dsred-STOP∆DTR-IRES-Venus-STOP transgene in each founder line

Three rounds of micro-injection generated 7 *Ermin-DTR* transgenic mice, as determined by successful PCR amplification of the *Venus* sequence from genomic

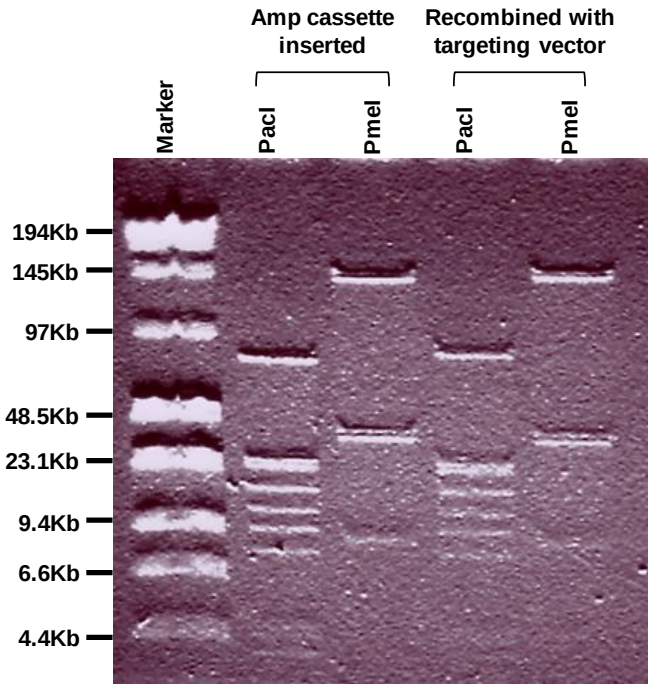

Figure 5.6 *PFGE analysis of DNA Ermin BAC following the 2 recombination events: first to remove unwanted sequences from the pBACe3.6 vector backbone and insertion of an ampicillin resistance cassette, and second to insert the targeting vector. The DNA was digested with PacI and PmeI.*

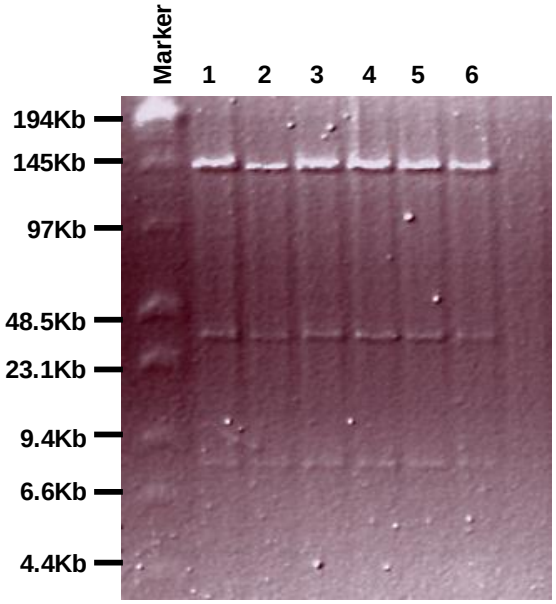

Figure 5.7 *PFGE analysis of Ermin BAC DNA following arabinose treatment to remove the kanamycin resistance cassette. The DNA was digested PmeI. All 6 clones selected were correct.*

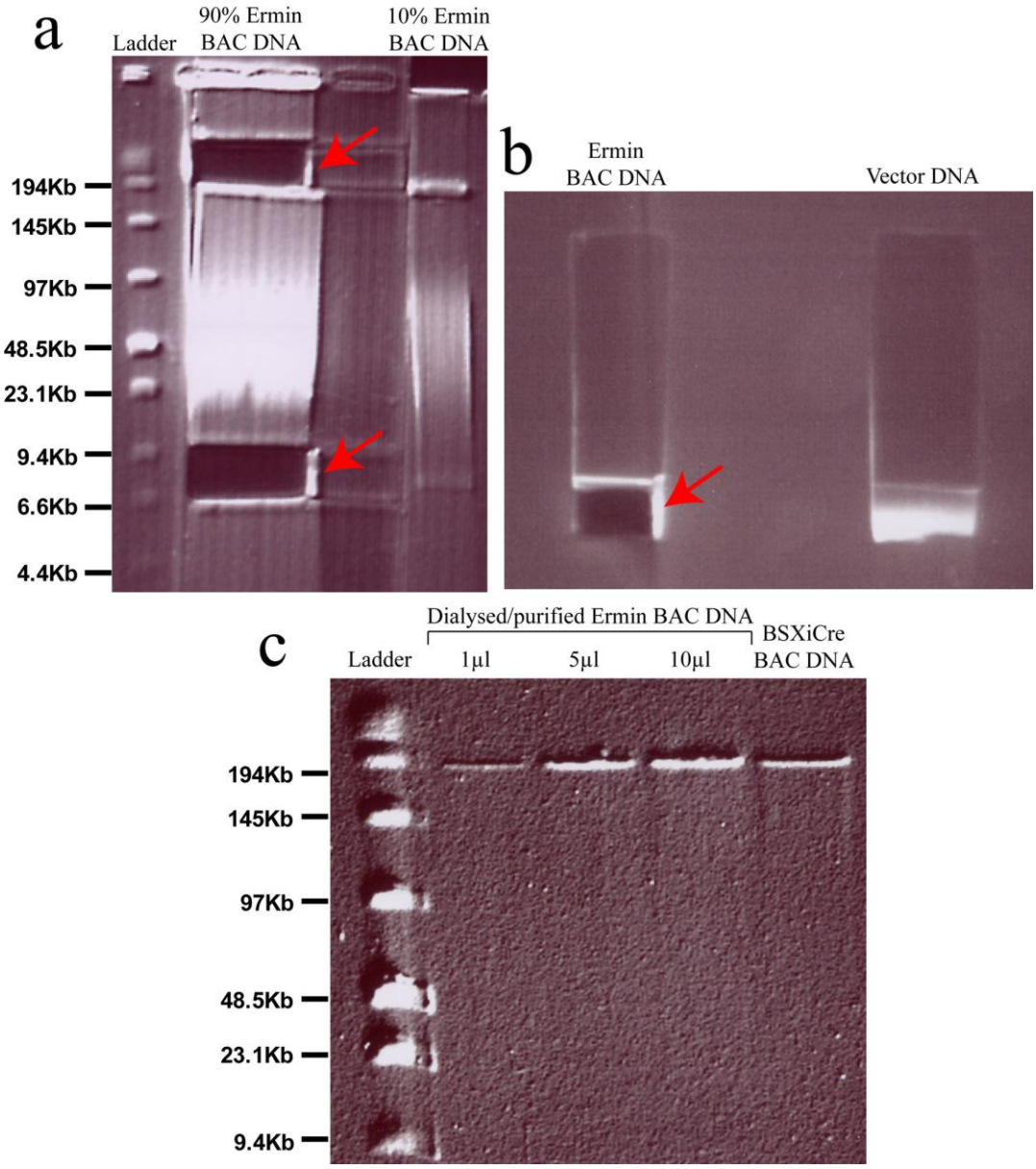

Figure 5.8 *Ermin BAC DNA linearization and purification. (a) 90% and 10% of Ermin BAC DNA were subjected to PFGE. The DNA required for microinjection and the vector DNA (red arrows) were excised from the gel prior to ethidium bromide staining. (b) The Ermin BAC DNA and the vector DNA were run on 4% (w/v) LMP agarose gel. The BAC DNA insert band was cut away from the gel (red arrow), which was then stained with ethidium bromide. (c) Following dialysis, 1µl, 5µl and 10µl of the Ermin BAC DNA was subjected to PFGE along with a quantity of BSX-iCre BAC DNA that has previously been used for microinjection.*

DNA as described in **2.2.1**. In order to screen for the correct expression of the transgene and demonstrate that it can functionally recombine, each founder mouse was crossed with an *Emx1-iCre* transgenic mouse. ~50% of SOX10+ cells and ~40% of PDGFRα+ cells in the corpus callosum and motor cortex of adult mice are derived from the Emx1+ cortical stem cells embryonically (Kessaris et al., 2006, Psachoulia et al., 2009 – Chapter 4). Therefore in the progeny of these crosses, Cre Recombinase will be active in all Emx1+ cells and should induce recombination of the *Ermin-DTR* transgene in the DNA of all Emx1+ stem cells (**Fig. 2.2**), excising the *DsRed* coding sequence and the *STOP* sequence. In the adult brain (cortex and corpus callosum), when the *Ermin* gene is expressed by all mature, myelinating oligodendrocytes, we would expect ~50% of the oligodendrocytes to express DsRed (not recombined) and ~ 50% to express Venus (recombined by *Emx1-Cre*).

All seven founders successfully passed the transgene onto their offspring (PCR genotyping). Coronal brain sections from P50 mice were processed for immunohistochemistry to detect DsRed and Venus protein expression. Offspring from five of the founders had no detectable DsRed+ or Venus+ cells (data not shown). In tissue from offspring of the sixth founder, a few faint DsRed+ cells could be seen, but no Venus+ expression, indicating that the transgene had not recombined in this mouse and that the transgene was not efficiently expressed (data not shown). Progeny from the seventh founder had poor DsRed expression but importantly, robust expression of Venus, indicating successful recombination of the transgene (**Fig. 5.9**). Therefore, the seventh founder was selected for more detailed analysis and will now be referred to as the *Ermin-DTR* transgenic mouse.

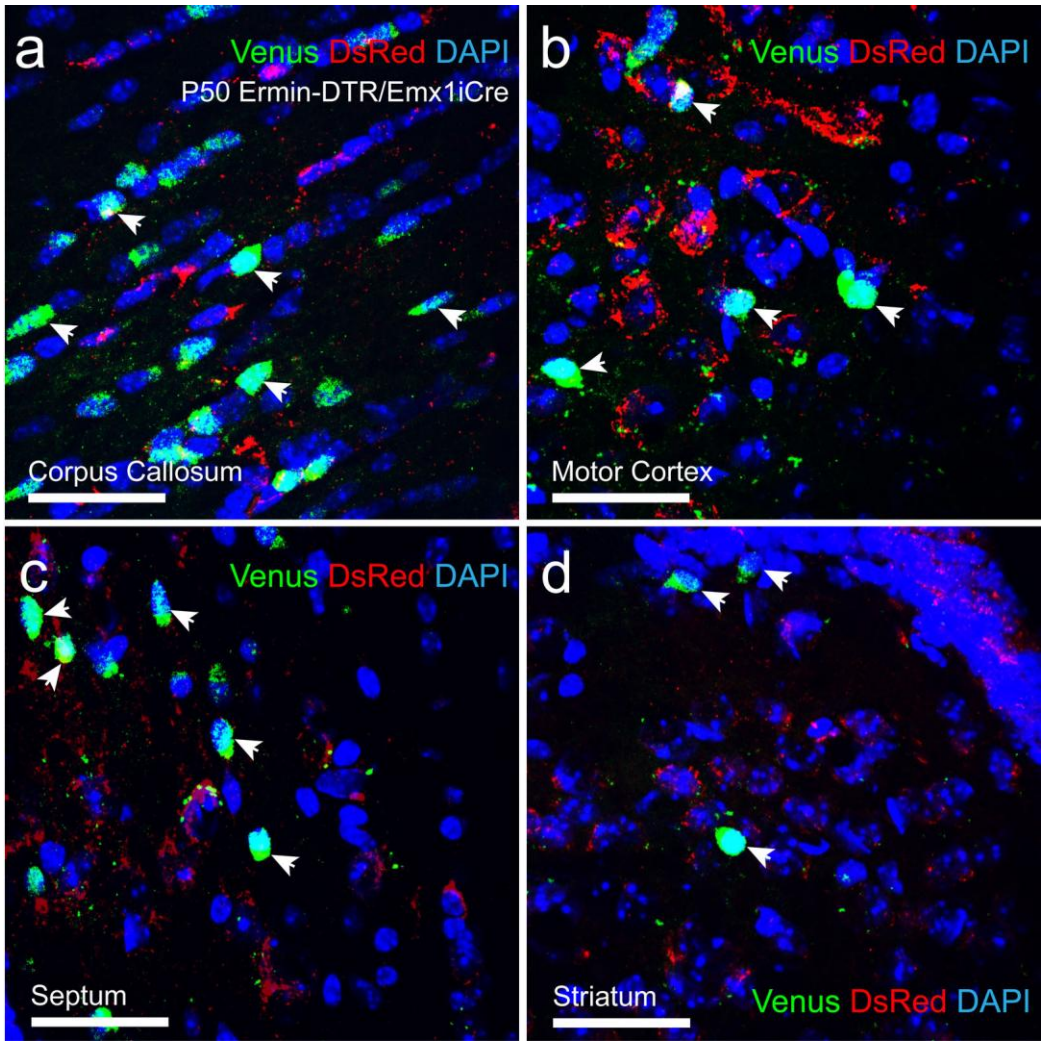

Figure 5.9 *Expression of DsRed and Venus protein in the forebrain of adult Ermin-DTR/Emx1-iCre transgenic mice. Coronal brain sections from P50 Ermin-DTR/Emx1-iCre transgenic mice were immunolabelled to detect Venus and DsRed. Venus+ cells (arrowheads) were found in the corpus callosum (a), motor cortex (b), septum (c), and striatum (d). Clearly labelled DsRed+ cells were not detected in any of the regions examined.*

At P50 DsRed was weakly expressed in the callosal white matter of *Ermin-DTR* transgenic mice. Furthermore, the red fluorescence did not appear to be localized to the nucleus as would be expected if the NLS was functional. Additionally, clear DsRed staining was absent from the grey matter (**Fig. 5.9a, b**). In contrast, in the corpus callosum, a substantial number of Venus+ cells were detected, which presumably correspond to the Emx1-derived oligodendrocytes. Adult Emx1-derived oligodendrocytes are found dorsally and are rarely present in the ventral brain (Kessaris et al., 2006). Appropriately, Venus+ cells were found in small numbers in the dorsal striatum and dorsal septum (**Fig. 5.9c, d**) but were absent from more ventral parts of these structures (data not shown).

As the distribution of the Venus cells appeared correct in all brain regions examined, the molecular identity of the Venus+ cells was investigated. For this, brain sections of P50 *Ermin-DTR/Emx1-iCre* transgenic mice were immunolabelled with antibodies against Venus (anti-GFP) and either the differentiated oligodendrocyte marker CC1, the oligodendroglial lineage marker OLIG2 or the oligodendrocyte progenitor marker NG2. In the corpus callosum, Venus expression co-localized with CC1 (**Fig. 5.10a**) and OLIG2 (**Fig. 5.10b**) but never with NG2 (**Fig. 5.10c**). The proportion of Venus+ cells that expressed each of these three markers was quantified relative to the total number of Venus+ cells. 100% of Venus+ cells in the corpus callosum expressed CC1 and OLIG2, indicating that Venus is exclusively expressed by oligodendrocyte lineage cells and, in particular, by differentiated oligodendrocytes (**Fig. 5.10d**).

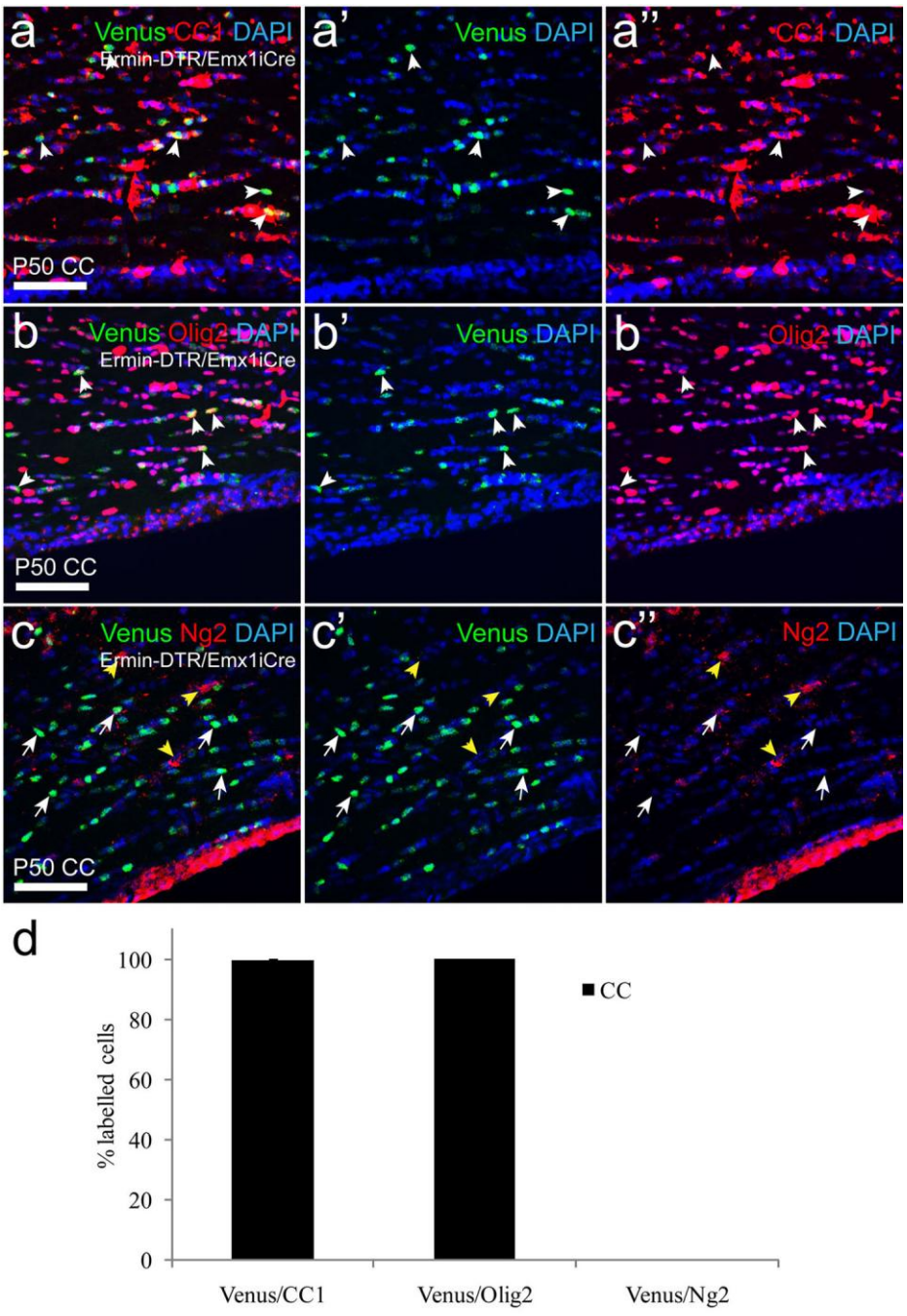

Figure 5.10 *Venus+ cells in the corpus callosum of Ermin-DTR/Emx1-iCre transgenic mice. Brain sections from P50 Ermin-DTR/Emx1-iCre transgenic mice were immunolabelled with antibodies against Venus and CC1 (a), OLIG2 (b) and NG2 (c). Double positive cells (white arrowheads) were detected in the corpus callosum when stained with GFP and CC1 or OLIG2. No GFP+ cells (white arrowheads) co-labelled with NG2 (yellow arrowheads). The proportion (%) of Venus+ cells that co-expressed either CC1, OLIG2 or NG2 was quantified (d).*

In the motor cortex, the identity of Venus+ cells was similarly restricted to oligodendrocytes. Venus+ cells were labelled solely for Olig2 and CC1, but NG2+/Venus+ double-positive cells were not found (**Fig. 5.11**).

Collectively, these data indicate that Venus expression is appropriately restricted to oligodendrocytes in the adult brain. However we would expect Venus to be expressed by ~half of all oligodendrocytes present in the corpus callosum and motor cortex in *Ermin-DTR/Emx1-iCre* transgenic mice. To confirm this, I examined brain sections from P50 *Ermin-DTR/Emx1-iCre* transgenic mice already stained to detect Venus and CC1 protein expression (**Fig. 5.12a, b**). 54% ± 9% of all CC1+ cells in the corpus callosum were Venus+/CC1+ cells compared with 37% ± 10% in the motor cortex (**Fig. 5.12**). Therefore, while the DsRed component of the transgene cannot be used, the *Ermin-DTR* transgene is correctly expressed by oligodendrocytes and recombines successfully in the presence of iCre to permit expression of Venus.

5.2.6 Testing DTR expression in the Ermin-DTR/Emx1-iCre transgenic mice

The correct expression of DTR in the *Ermin-DTR/Emx1-iCre* transgenic mice is presently being examined by Dr. Ian McKenzie.

5.3 Discussion

This study generated a transgenic mouse that, after recombination, correctly expressed a fluorescent protein (Venus) and possibly the human diphtheria toxin receptor under the control of the E*rmin* promoter. This transgenic mouse should

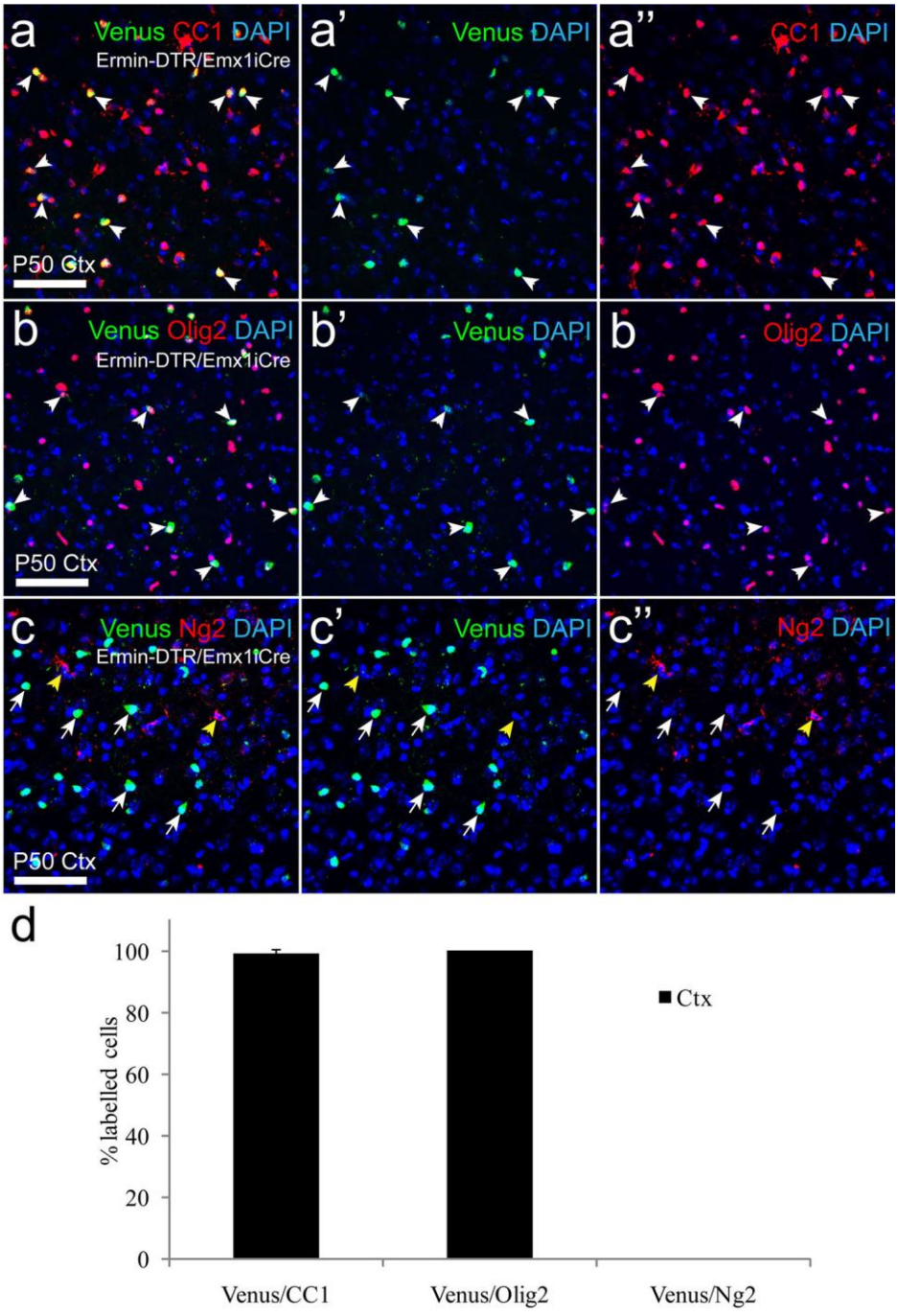

Figure 5.11 *Venus+ cells in the motor cortex of Ermin-DTR/Emx1-iCre transgenic mice. Brain sections from P50 Ermin-DTR/Emx1-iCre transgenic mice were immunolabelled with antibodies against Venus and CC1 (a), Olig2 (b) and Ng2 (c). Double positive cells (white arrowheads) were detected in the motor cortex when stained with GFP and CC1 or OLIG2. No GFP+ cells (white arrowheads) co-labelled with NG2 (yellow arrowheads). The proportion (%) of Venus+ cells that co-expressed either CC1, OLIG2 or NG2 was quantified (d).*

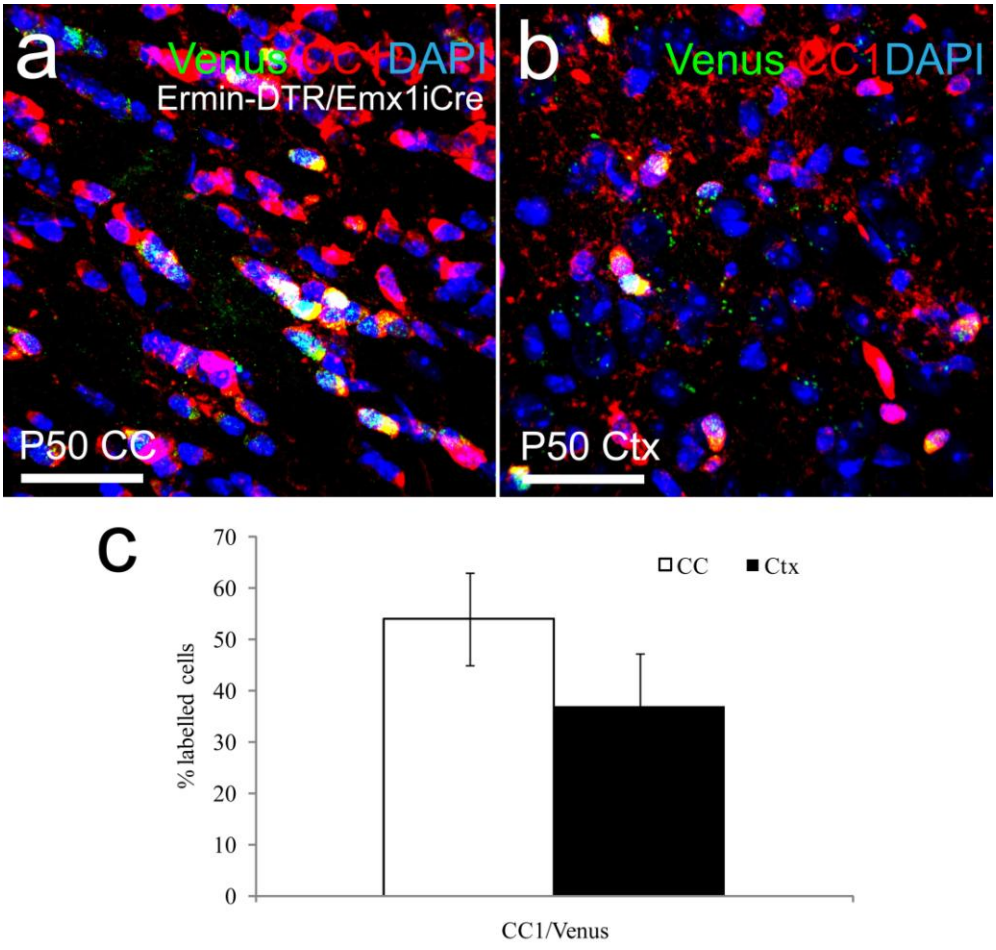

Figure 5.12 *Venus labelling in CC1+ cells of Ermin-DTR/Emx1iCre transgenic mice. The corpus callosum (a) and motor cortex (b) of adult (P50) mice were stained with antibodies against Venus (green) and CC1 (red). The proportion of all CC1+ cells present in the two brain regions that co-expressed Venus was quantified from confocal scans (c).*

potentially permit oligodendrocyte-specific labelling and, after diphtheria toxin administration, killing of myelinating oligodendrocytes.

The *Ermin-DTR* transgenic mouse generated failed to express DsRed effectively. This could result from a combination of factors. Firstly, DsRed is less bright than Venus. Secondly, failure of the NLS meant that the protein was not concentrated in the nucleus of the cell resulting in weak DsRed signal and thirdly, there may only be a low level of activity of the Ermin promoter in adult mice. The limited DsRed expression detected in the white matter showed evidence of cytoplasmic and not nuclear-specific expression as was expected due to the presence of the *NLS* sequence in the transgene, indicative of a defective NLS. Ermin transcription, like that of many mature oligodendrocyte genes, may only occur at a low level in adulthood resulting in a low level of transgene expression. In any case, the failure to detect DsRed expression in oligodendrocytes is a small drawback considering that DsRed was the least necessary component of the construct, only included as a marker of all oligodendrocytes, which can instead be achieved by antibody labelling.

This transgenic will be a very useful tool for addressing a number of different questions. For instance, if *Ermin-DTR* transgenic mice are crossed to mice that express an inducible form of Cre recombinase under the control of an oligodendrocyte progenitor cell specific promoter, e.g. *PDGFRα-CreER*^{T2} transgenic mice, it would be possible to limit recombination of the transgene to adult OLPs and selectively ablate adult born oligodendrocytes. Tamoxifen would be given to adult, double heterozygous offspring, which would activate Cre in adult OLPs and induce a

DNA recombination event. Initially this will result in no visible change in the CNS. However all new cells produced from these recombined adult OLPs, that subsequently differentiate to become mature myelinating Ermin+ oligodendrocytes will become labeled with Venus and express human DTR. Subsequently, these mice will be traced for various periods of time to observe the accumulation of newly generated, functionally myelinating oligodendrocytes in the CNS. To test the importance of these cells to adult CNS function, DT could be administered at various periods following tamoxifen treatment. As 17% of all oligodendrocytes in the corpus callosum are generated between P45 and P135 (Rivers *et al*., 2008) ablating these cells may cause visible motor and detectable cognitive impairments.

As was hypothesized in Chapter 3 and in **5.1**, adult oligodendrogenesis may be an important component of motor learning and memory. Therefore the rate of oligodendrogenesis could be compared between *Ermin-DTR/PDGFRα-CreER*^{T2} transgenic mice that were regularly housed and those that have been provided access to a running wheel (as previously – Chapter 3). A third group of mice could be provided with a more complex running wheel representing a more complex motor test that requires more practice for the mouse to become proficient (Liebetanz *et al*., 2006). An example of such an experiment is described in Figure 5.13. The plan would be to ablate oligodendrocytes generated from OLPs during the motor learning period, by DT administration, and determine whether that has an impact on motor performance when mice are re-exposed to the same task.

Similar to the running wheel experiment, using this transgenic mouse to eliminate

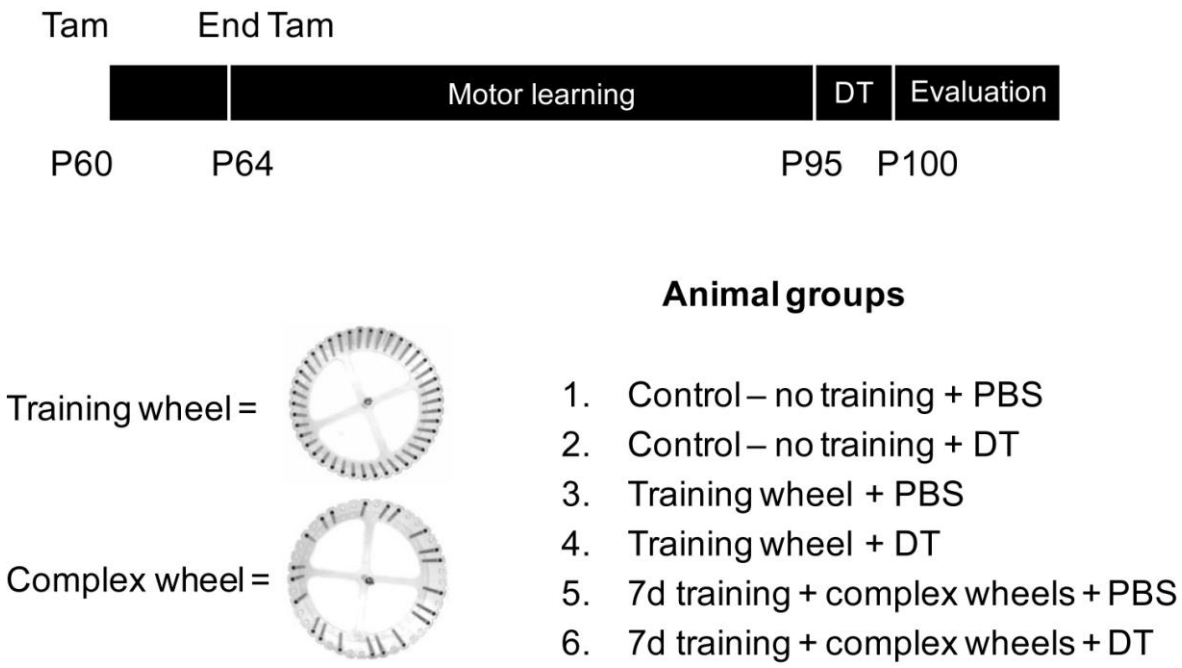

Figure 5.13 *An experimental plan for complex motor learning. Tamoxifen would be administered at P60 and motor training commenced at P64. All trained mice would initially run on the training wheel, which has regular rung spacing as shown in the above schematic. Training wheel mice will continue under these conditions until P95. Training and complex wheel mice will run on the training wheel for 7 days and subsequently on a wheel that has increasingly complex patterns of rung spacing as shown in the schematic. Mice that would be trained using the complex wheel would have the rung spacing altered every week of the training period. From P95 to P100, mice will be given either DT or PBS before their running performance is re-evaluated.*

adult-born oligodendrocytes generated prior to or during a multitude of other behavioral tasks, could shed light on the function of adult oligodendrogenesis and indicate how significant role it plays in memory formation/retention and brain plasticity. Additionally, crossing this transgenic mouse line with another that induces recombination in neural stem/progenitor cells would specifically identify oligodendrocytes derived from these cells in the adult brain by Venus labelling and could also be used to remove these cells from the adult brain.

Chapter 6: Final Discussion

Oligodendrocyte progenitor cells (OLPs), also known as 'NG2 cells', persist in the adult brain in great abundance (~5% of brain cells) and are distributed more-or-less evenly throughout the brain. Until recently it was presumed that the function of these adult OLPs was to act as a reservoir for the production of new myelinating oligodendrocytes in order to replace those that are lost as a result of injury, disease or ageing.

My studies have generated strong evidence for the production of myelinating oligodendrocytes in apparently healthy, young adult mice. This could contribute to some forms of neural plasticity, for example motor learning and memory. I have also shown that the differentiation rate of adult OLPs decreases with age, but nevertheless new oligodendrocytes are still being produced even in mice aged P240 +100d. This could be important for the maintenance of myelination with age.

Interestingly, adult OLPs were also found to generate a small proportion of projection neurons in the anterior piriform cortex. The functional importance of this finding is still unknown. However, it does reflect the multiplicity of roles that adult OLPs can serve in the CNS.

OLP contribution to brain plasticity was directly addressed by the behavioural testing of adult mice. This study showed that OLPs respond to exercise that requires inter-hemispherical communication, thus presumably involving the corpus callosum, by stimulating the generation of oligodendrocytes in this brain region. Though this observation requires further confirmation, it raises the possibility that OLPs might contribute to brain plasticity during adulthood. To address this directly, I generated a transgenic mouse that will allow labelling and conditional ablation of adult-born oligodendrocytes. Though characterization of this mouse was not completed during the timeframe of this PhD, initial evidence suggests correct expression of the transgene (*Ermin-loxDsRedSTOPlox-DTR-IRESVenus*) and encourages us to believe that this transgenic tool will be useful for behavioural tests aimed at assesing the involvement of adult-born oligodendrocytes in brain function and plasticity.

These new and unexpected functional roles of OLPs in the adult brain would be expected to require the generation of a substantial number of new oligodendrocytes through proliferation of OLPs. Though it is known that adult OLPs proliferate *in vivo*, their rate of proliferation and how this changes with age was not previously examined. Therefore, I investigated the cell cycle kinetics of OLPs by cumulative administration of two different thymidine analogues, BrdU and EdU. Strikingly, OLPs were found to proliferate even in very old age (P540+100d) both in the brain grey matter (motor cortex) and the white matter (corpus callosum). In addition, a linear relationship between cell cycle time and age was determined for OLPs present in the motor cortex, which allows prediction of the cell cycle of cortical OLPs at any given postnatal age. Both BrdU and EdU cumulative labelling experiments showed

that Tc is greater in the grey than in the white matter and increases with age due to longer cell cycle arrest at the G0 or G1 phase rather than a slower S phase. Furthermore, the decrease in OLP proliferation rate with age was roughly parallel to the decrease in their rate of production of new oligodendrocytes. This finding suggests that if OLPs could be triggered to proliferate more rapidly in the aged brain, they could potentially generate more oligodendrocytes and therefore respond more productively to demyelination. Whether the change in proliferation and differentiation rates of OLPs is an intrinsic phenomenon or else depends on extracellular signals is yet to be determined.

Using both BrdU and EdU, I detected two sub-populations of OLPs. A proportion of OLPs (20-50%) did not undergo cell division even after 50 days of EdU/BrdU administration, indicating the existence of a quiescent OLP population, which persists throughout life in both the grey and white matter. The splitting of OLPs into two populations has already been suggested by other OLP characteristics, such as electrical activity and the ability to fire action potentials in response to a depolarizing stimulus (Chittajallu *et al*., 2004; Karadottir *et al*., 2008), formation of glutamatergic synapses with un-myelinated axons (Kukley *et al*., 2007; Ziskin *et al*., 2007), as well as their developmental origins (Kessaris *et al*., 2006). The latter was directly addressed in this study but failed to show any relevance between proliferating behaviour and embryonic origins of forebrain OLPs. However, the other characteristics that split OLPs into two sub-populations remain to be correlated with their differing cycling behaviour.

Overall, the findings of this study emphasize the potential importance of OLPs in the healthy adult brain and the variety of roles that OLPs serve to preserve normal brain function and integrity throughout life. While their chief role in adulthood is to act as a source of new myelinating oligodendrocytes, the fact that they also seem capable of generating certain projection neurons does raise the possibility that it might become possible to manipulate OLPs in order to enhance their pluripotent properties for a variety of repair processes in neurodegenerative diseases. Enhancing their proliferation rate or steady-state numbers could conceivably improve some types of learning and/or memory. While this is highly speculative at present, it is an exciting prospect that should stimulate a lot of further work on adult myelinogenesis.

Reference List

Aguirre AA, Chittajallu R, Belachew S, Gallo V (2004) NG2-expressing cells in the subventricular zone are type C-like cells and contribute to interneuron generation in the postnatal hippocampus. J Cell Biol 165:575-589.

Bacus SS, Goldschmidt R, Chin D, Moran G, Weinberg D, Bacus JW (1989) Biological grading of breast cancer using antibodies to proliferating cells and other markers. Am J Pathol 135:783-792.

Baird GS, Zacharias DA, Tsien RY (2000) Biochemistry, mutagenesis, and oligomerization of DsRed, a red fluorescent protein from coral. Proc Natl Acad Sci U S A 97:11984-11989.

Baron W, Shattil SJ, Ffrench-Constant C (2002) The oligodendrocyte precursor mitogen PDGF stimulates proliferation by activation of alpha(v)beta3 integrins. EMBO J 21:1957-1966.

Barres BA, Raff MC (1993) Proliferation of oligodendrocyte precursor cells depends on electrical activity in axons. Nature 361:258-260.

Barres BA, Raff MC (1999) Axonal control of oligodendrocyte development. J Cell Biol 147:1123-1128.

Bartzokis G, Beckson M, Lu PH, Nuechterlein KH, Edwards N, Mintz J (2001) Age-related changes in frontal and temporal lobe volumes in men: a magnetic resonance imaging study. Arch Gen Psychiatry 58:461-465.

Bartzokis G, Lu PH, Tingus K, Mendez MF, Richard A, Peters DG, Oluwadara B, Barrall KA, Finn JP, Villablanca P, Thompson PM, Mintz J (2008) Lifespan trajectory of myelin integrity and maximum motor speed. Neurobiol Aging.

Baumann N, Pham-Dinh D (2001) Biology of oligodendrocyte and myelin in the mammalian central nervous system. Physiol Rev 81:871-927.

Bengtsson SL, Nagy Z, Skare S, Forsman L, Forssberg H, Ullen F (2005) Extensive piano practicing has regionally specific effects on white matter development. Nat Neurosci 8:1148-1150.

Bergles DE, Roberts JD, Somogyi P, Jahr CE (2000) Glutamatergic synapses on oligodendrocyte precursor cells in the hippocampus. Nature 405:187-191.

Bowley MP, Cabral H, Rosene DL, Peters A (2010) Age changes in myelinated nerve fibers of the cingulate bundle and corpus callosum in the rhesus monkey. J Comp Neurol 518:3046-3064.

Boyke J, Driemeyer J, Gaser C, Buchel C, May A (2008) Training-induced brain structure changes in the elderly. J Neurosci 28:7031-7035.

Bravo R, Macdonald-Bravo H (1987) Existence of two populations of cyclin/proliferating cell nuclear antigen during the cell cycle: association with DNA replication sites. J Cell Biol 105:1549-1554.

Bravo R, Frank R, Blundell PA, Macdonald-Bravo H (1987) Cyclin/PCNA is the auxiliary protein of DNA polymerase-delta. Nature 326:515-517.

Bretscher A, Edwards K, Fehon RG (2002) ERM proteins and merlin: integrators at the cell cortex. Nat Rev Mol Cell Biol 3:586-599.

Brockschnieder D, Sabanay H, Riethmacher D, Peles E (2006) Ermin, a myelinating oligodendrocyte-specific protein that regulates cell morphology. J Neurosci 26:757-762.

Bruno S, Darzynkiewicz Z (1992) Cell cycle dependent expression and stability of the nuclear protein detected by Ki-67 antibody in HL-60 cells. Cell Prolif 25:31-40.

Buch T, Heppner FL, Tertilt C, Heinen TJ, Kremer M, Wunderlich FT, Jung S, Waisman A (2005) A Cre-inducible diphtheria toxin receptor mediates cell lineage ablation after toxin administration. Nat Methods 2:419-426.

BUNGE MB, BUNGE RP, RIS H (1961) Ultrastructural study of remyelination in an experimental lesion in adult cat spinal cord. J Biophys Biochem Cytol 10:67-94.

BUNGE RP (1968) Glial cells and the central myelin sheath. Physiol Rev 48:197-251.

Butt AM, Kiff J, Hubbard P, Berry M (2002) Synantocytes: new functions for novel NG2 expressing glia. J Neurocytol 31:551-565.

Cai J, Qi Y, Hu X, Tan M, Liu Z, Zhang J, Li Q, Sander M, Qiu M (2005) Generation of oligodendrocyte precursor cells from mouse dorsal spinal cord independent of Nkx6 regulation and Shh signaling. Neuron 45:41-53.

Calver AR, Hall AC, Yu WP, Walsh FS, Heath JK, Betsholtz C, Richardson WD (1998) Oligodendrocyte population dynamics and the role of PDGF in vivo. Neuron 20:869-882.

Cha JH, Chang MY, Richardson JA, Eidels L (2003) Transgenic mice expressing the diphtheria toxin receptor are sensitive to the toxin. Mol Microbiol 49:235-240.

Chang A, Nishiyama A, Peterson J, Prineas J, Trapp BD (2000) NG2-positive oligodendrocyte progenitor cells in adult human brain and multiple sclerosis lesions. J Neurosci 20:6404-6412.

Chehrehasa F, Meedeniya AC, Dwyer P, Abrahamsen G, Mackay-Sim A (2009) EdU, a new thymidine analogue for labelling proliferating cells in the nervous system. J Neurosci Methods 177:122-130.

Chen H, Kohno K, Gong Q (2005) Conditional ablation of mature olfactory sensory neurons mediated by diphtheria toxin receptor. J Neurocytol 34:37-47.

Chittajallu R, Aguirre A, Gallo V (2004) NG2-positive cells in the mouse white and grey matter display distinct physiological properties. J Physiol 561:109-122.

Curtis R, Cohen J, Fok-Seang J, Hanley MR, Gregson NA, Reynolds R, Wilkin GP (1988) Development of macroglial cells in rat cerebellum. I. Use of antibodies to follow early in vivo development and migration of oligodendrocytes. J Neurocytol 17:43-54.

Dai X, Qu P, Dreyfus CF (2001) Neuronal signals regulate neurotrophin expression in oligodendrocytes of the basal forebrain. Glia 34:234-239.

Dai X, Lercher LD, Clinton PM, Du Y, Livingston DL, Vieira C, Yang L, Shen MM, Dreyfus CF (2003) The trophic role of oligodendrocytes in the basal forebrain. J Neurosci 23:5846-5853.

Dawson MR, Polito A, Levine JM, Reynolds R (2003) NG2-expressing glial progenitor cells: an abundant and widespread population of cycling cells in the adult rat CNS. Mol Cell Neurosci 24:476-488.

Dayer AG, Cleaver KM, Abouantoun T, Cameron HA (2005) New GABAergic interneurons in the adult neocortex and striatum are generated from different precursors. J Cell Biol 168:415-427.

Dimou L, Simon C, Kirchhoff F, Takebayashi H, Gotz M (2008) Progeny of Olig2-expressing progenitors in the gray and white matter of the adult mouse cerebral cortex. J Neurosci 28:10434-10442.

Driemeyer J, Boyke J, Gaser C, Buchel C, May A (2008) Changes in gray matter induced by learning--revisited. PLoS One 3:e2669.

du MS, Guillaud P, Camus E, Seigneurin D, Brugal G (1991) Ki-67 labeling in postmitotic cells defines different Ki-67 pathways within the 2c compartment. Cytometry 12:455-463.

Du Y, Dreyfus CF (2002) Oligodendrocytes as providers of growth factors. J Neurosci Res 68:647-654.

Dubois-Dalcq M, Behar T, Hudson L, Lazzarini RA (1986) Emergence of three myelin proteins in oligodendrocytes cultured without neurons. J Cell Biol 102:384-392.

Dupree JL, Mason JL, Marcus JR, Stull M, Levinson R, Matsushima GK, Popko B (2004) Oligodendrocytes assist in the maintenance of sodium channel clusters independent of the myelin sheath. Neuron Glia Biol 1:179-192.

Engel U, Wolswijk G (1996) Oligodendrocyte-type-2 astrocyte (O-2A) progenitor cells derived from adult rat spinal cord: in vitro characteristics and response to PDGF, bFGF and NT-3. Glia 16:16-26.

Ffrench-Constant C, Raff MC (1986) Proliferating bipotential glial progenitor cells in adult rat optic nerve. Nature 319:499-502.

Fields RD (2008) White matter in learning, cognition and psychiatric disorders. Trends Neurosci 31:361-370.

Fiore M, Triaca V, Amendola T, Tirassa P, Aloe L (2002) Brain NGF and EGF administration improves passive avoidance response and stimulates brain precursor cells in aged male mice. Physiol Behav 77:437-443.

Fogarty M, Richardson WD, Kessaris N (2005) A subset of oligodendrocytes generated from radial glia in the dorsal spinal cord. Development 132:1951-1959.

Fruttiger M, Karlsson L, Hall AC, Abramsson A, Calver AR, Bostrom H, Willetts K, Bertold CH, Heath JK, Betsholtz C, Richardson WD (1999) Defective oligodendrocyte development and severe hypomyelination in PDGF-A knockout mice. Development 126:457-467.

Fulton D, Paez PM, Campagnoni AT (2009) The multiple roles of myelin protein genes during the development of the oligodendrocyte. ASN Neuro.

Gaglia P, Bernardi A, Venesio T, Caldarola B, Lauro D, Cappa AP, Calderini P, Liscia DS (1993) Cell proliferation of breast cancer evaluated by anti-BrdU and anti-Ki-67 antibodies: its prognostic value on short-term recurrences. Eur J Cancer 29A:1509-1513.

Gallo V, Zhou JM, McBain CJ, Wright P, Knutson PL, Armstrong RC (1996) Oligodendrocyte progenitor cell proliferation and lineage progression are regulated by glutamate receptor-mediated K+ channel block. J Neurosci 16:2659-2670.

Gasparini G, Boracchi P, Verderio P, Bevilacqua P (1994) Cell kinetics in human breast cancer: comparison between the prognostic value of the cytofluorimetric S-phase fraction and that of the antibodies to Ki-67 and PCNA antigens detected by immunocytochemistry. Int J Cancer 57:822-829.

Ge WP, Zhou W, Luo Q, Jan LY, Jan YN (2009) Dividing glial cells maintain differentiated properties including complex morphology and functional synapses. Proc Natl Acad Sci U S A 106:328-333.

Geha S, Pallud J, Junier MP, Devaux B, Leonard N, Chassoux F, Chneiweiss H, Daumas-Duport C, Varlet P (2010) NG2+/Olig2+ cells are the major cycle-related cell population of the adult human normal brain. Brain Pathol 20:399-411.

Gensert JM, Goldman JE (1997) Endogenous progenitors remyelinate demyelinated axons in the adult CNS. Neuron 19:197-203.

Gerdes J, Dallenbach F, Lennert K, Lemke H, Stein H (1984) Growth fractions in malignant non-Hodgkin's lymphomas (NHL) as determined in situ with the monoclonal antibody Ki-67. Hematol Oncol 2:365-371.

Gerdes J, Li L, Schlueter C, Duchrow M, Wohlenberg C, Gerlach C, Stahmer I, Kloth S, Brandt E, Flad HD (1991) Immunobiochemical and molecular biologic characterization of the cell proliferation-associated nuclear antigen that is defined by monoclonal antibody Ki-67. Am J Pathol 138:867-873.

Goto K, Kurihara T, Takahashi Y, Kondo H (1990) Expression of genes for the myelin-specific proteins in oligodendrocytes in vivo demands the presence of axons. Neurosci Lett 117:269-274.

Gould E, Reeves AJ, Graziano MS, Gross CG (1999) Neurogenesis in the neocortex of adult primates. Science 286:548-552.

Guo F, Ma J, McCauley E, Bannerman P, Pleasure D (2009) Early postnatal proteolipid promoter-expressing progenitors produce multilineage cells in vivo. Journal of Neuroscience 29:7256-7270.

Guo F, Maeda Y, Ma J, Xu J, Miers L, Vaccarino F, Pleasure D (2010) Pyramidal neurons are generated from oligodendroglial progenitor cells in adult piriform cortex. Journal of Neuroscience (pending).

Haberly LB (2001) Parallel-distributed processing in olfactory cortex: new insights from morphological and physiological analysis of neuronal circuitry. Chem Senses 26:551-576.

Hall A, Giese NA, Richardson WD (1996) Spinal cord oligodendrocytes develop from ventrally derived progenitor cells that express PDGF alpha-receptors. Development 122:4085-4094.

Hasan KM, Kamali A, Kramer LA, Papnicolaou AC, Fletcher JM, Ewing-Cobbs L (2008) Diffusion tensor quantification of the human midsagittal corpus callosum subdivisions across the lifespan. Brain Res 1227:52-67.

Heldin CH, Westermark B, Wasteson A (1981) Platelet-derived growth factor. Isolation by a large-scale procedure and analysis of subunit composition. Biochem J 193:907-913.

Hoch RV, Soriano P (2003) Roles of PDGF in animal development. Development 130:4769-4784.

Horner PJ, Power AE, Kempermann G, Kuhn HG, Palmer TD, Winkler J, Thal LJ, Gage FH (2000) Proliferation and differentiation of progenitor cells throughout the intact adult rat spinal cord. J Neurosci 20:2218-2228.

Houweling AR, Brecht M (2008) Behavioural report of single neuron stimulation in somatosensory cortex. Nature 451:65-68.

Huber D, Petreanu L, Ghitani N, Ranade S, Hromadka T, Mainen Z, Svoboda K (2008) Sparse optical microstimulation in barrel cortex drives learned behaviour in freely moving mice. Nature 451:61-64.

Hudson LD, Friedrich VL, Jr., Behar T, Dubois-Dalcq M, Lazzarini RA (1989) The initial events in myelin synthesis: orientation of proteolipid protein in the plasma membrane of cultured oligodendrocytes. J Cell Biol 109:717-727.

Imfeld A, Oechslin MS, Meyer M, Loenneker T, Jancke L (2009) White matter plasticity in the corticospinal tract of musicians: a diffusion tensor imaging study. Neuroimage 46:600-607.

Jin K, Sun Y, Xie L, Batteur S, Mao XO, Smelick C, Logvinova A, Greenberg DA (2003) Neurogenesis and aging: FGF-2 and HB-EGF restore neurogenesis in hippocampus and subventricular zone of aged mice. Aging Cell 2:175-183.

Jordan C, Friedrich V, Jr., Dubois-Dalcq M (1989) In situ hybridization analysis of myelin gene transcripts in developing mouse spinal cord. J Neurosci 9:248-257.

Kaplan MR, Meyer-Franke A, Lambert S, Bennett V, Duncan ID, Levinson SR, Barres BA (1997) Induction of sodium channel clustering by oligodendrocytes. Nature 386:724-728.

Kaplan MR, Cho MH, Ullian EM, Isom LL, Levinson SR, Barres BA (2001) Differential control of clustering of the sodium channels Na(v)1.2 and Na(v)1.6 at developing CNS nodes of Ranvier. Neuron 30:105-119.

Karadottir R, Cavelier P, Bergersen LH, Attwell D (2005) NMDA receptors are expressed in oligodendrocytes and activated in ischaemia. Nature 438:1162-1166.

Karadottir R, Hamilton NB, Bakiri Y, Attwell D (2008) Spiking and nonspiking classes of oligodendrocyte precursor glia in CNS white matter. Nat Neurosci 11:450-456.

Keirstead HS, Levine JM, Blakemore WF (1998) Response of the oligodendrocyte progenitor cell population (defined by NG2 labelling) to demyelination of the adult spinal cord. Glia 22:161-170.

Kessaris N, Fogarty M, Iannarelli P, Grist M, Wegner M, Richardson WD (2006) Competing waves of oligodendrocytes in the forebrain and postnatal elimination of an embryonic lineage. Nat Neurosci 9:173-179.

Kippert A, Trajkovic K, Fitzner D, Opitz L, Simons M (2008) Identification of Tmem10/Opalin as a novel marker for oligodendrocytes using gene expression profiling. BMC Neurosci 9:40.

Klein C, Krämer EM, Cardine AM, Schraven B, Brandt R, Trotter J (2002) Process outgrowth of oligodendrocytes is promoted by interaction of Fyn kinase with the cytoskeletal protein Tau. J Neurosci 22(3):698-707.

Knapp PE, Bartlett WP, Skoff RP (1987) Cultured oligodendrocytes mimic in vivo phenotypic characteristics: cell shape, expression of myelin-specific antigens, and membrane production. Dev Biol 120:356-365.

Kokoeva MV, Yin H, Flier JS (2005) Neurogenesis in the hypothalamus of adult mice: potential role in energy balance. Science 310:679-683.

Kondo T, Raff M (2000) Oligodendrocyte precursor cells reprogrammed to become multipotential CNS stem cells. Science 289:1754-1757.

Kuhlbrodt K, Herbarth B, Sock E, Hermans-Borgmeyer I, Wegner M (1998) Sox10, a novel transcriptional modulator in glial cells. J Neurosci 18:237-250.

Kuhn HG, Dickinson-Anson H, Gage FH (1996) Neurogenesis in the dentate gyrus of the adult rat: age-related decrease of neuronal progenitor proliferation. J Neurosci 16:2027-2033.

Kukley M, Capetillo-Zarate E, Dietrich D (2007) Vesicular glutamate release from axons in white matter. Nat Neurosci 10:311-320.

Kukley M, Kiladze M, Tognatta R, Hans M, Swandulla D, Schramm J, Dietrich D (2008) Glial cells are born with synapses. FASEB J 22:2957-2969.

Lasiene J, Matsui A, Sawa Y, Wong F, Horner PJ (2009) Age-related myelin dynamics revealed by increased oligodendrogenesis and short internodes. Aging Cell 8:201-213.

Laursen LS, ffrench-Constant C (2007) Adhesion molecules in the regulation of CNS myelination. Neuron Glia Biol 3:367-375.

Lee EC, Yu D, Martinez d, V, Tessarollo L, Swing DA, Court DL, Jenkins NA, Copeland NG (2001) A highly efficient Escherichia coli-based chromosome engineering system adapted for recombinogenic targeting and subcloning of BAC DNA. Genomics 73:56-65.

Levine JM, Beasley L, Stallcup WB (1986) Localization of a neurectoderm-associated cell surface antigen in the developing and adult rat. Brain Res 392:211-222.

Levine JM, Stallcup WB (1987) Plasticity of developing cerebellar cells in vitro studied with antibodies against the NG2 antigen. J Neurosci 7:2721-2731.

Levine JM, Stincone F, Lee YS (1993) Development and differentiation of glial precursor cells in the rat cerebellum. Glia 7:307-321.

Levison SW, Young GM, Goldman JE (1999) Cycling cells in the adult rat neocortex preferentially generate oligodendroglia. J Neurosci Res 57:435-446.

Liebetanz D, Merkler D (2006) Effects of commissural de- and remyelination on motor skill behaviour in the cuprizone mouse model of multiple sclerosis. Exp Neurol 202:217-224.

Lin SC, Bergles DE (2002) Physiological characteristics of NG2-expressing glial cells. J Neurocytol 31:537-549.

Lin SC, Bergles DE (2004) Synaptic signaling between GABAergic interneurons and oligodendrocyte precursor cells in the hippocampus. Nat Neurosci 7:24-32.

Lin SC, Huck JH, Roberts JD, Macklin WB, Somogyi P, Bergles DE (2005) Climbing fiber innervation of NG2-expressing glia in the mammalian cerebellum. Neuron 46:773-785.

Liu A, Han YR, Li J, Sun D, Ouyang M, Plummer MR, Casaccia-Bonnefil P (2007) The glial or neuronal fate choice of oligodendrocyte progenitors is modulated by their ability to acquire an epigenetic memory. J Neurosci 27:7339-7343.

Lu QR, Yuk D, Alberta JA, Zhu Z, Pawlitzky I, Chan J, McMahon AP, Stiles CD, Rowitch DH (2000) Sonic hedgehog--regulated oligodendrocyte lineage genes encoding bHLH proteins in the mammalian central nervous system. Neuron 25:317-329.

Lytle JM, Chittajallu R, Wrathall JR, Gallo V (2009) NG2 cell response in the CNP-EGFP mouse after contusive spinal cord injury. Glia 57:270-285.

Mabbott DJ, Noseworthy M, Bouffet E, Laughlin S, Rockel C (2006) White matter growth as a mechanism of cognitive development in children. Neuroimage 33:936-946.

Magavi SS, Leavitt BR, Macklis JD (2000) Induction of neurogenesis in the neocortex of adult mice. Nature 405:951-955.

Marin-Husstege M, Muggironi M, Liu A, Casaccia-Bonnefil P (2002) Histone deacetylase activity is necessary for oligodendrocyte lineage progression. J Neurosci 22:10333-10345.

Maslov AY, Barone TA, Plunkett RJ, Pruitt SC (2004) Neural stem cell detection, characterization, and age-related changes in the subventricular zone of mice. J Neurosci 24:1726-1733.

Matz MV, Fradkov AF, Labas YA, Savitsky AP, Zaraisky AG, Markelov ML, Lukyanov SA (1999) Fluorescent proteins from nonbioluminescent Anthozoa species. Nat Biotechnol 17:969-973.

McTigue DM, Tripathi RB (2008) The life, death, and replacement of oligodendrocytes in the adult CNS. J Neurochem 107:1-19.

Mikoshiba K, Okano H, Tamura T, Ikenaka K (1991) Structure and function of myelin protein genes. Annu Rev Neurosci 14:201-217.

Nagai T, Ibata K, Park ES, Kubota M, Mikoshiba K, Miyawaki A (2002) A variant of yellow fluorescent protein with fast and efficient maturation for cell-biological applications. Nat Biotechnol 20:87-90.

Nishiyama A, Lin XH, Giese N, Heldin CH, Stallcup WB (1996) Interaction between NG2 proteoglycan and PDGF alpha-receptor on O2A progenitor cells is required for optimal response to PDGF. J Neurosci Res 43:315-330.

Nishiyama A, Lin XH, Giese N, Heldin CH, Stallcup WB (1996) Co-localization of NG2 proteoglycan and PDGF alpha-receptor on O2A progenitor cells in the developing rat brain. J Neurosci Res 43:299-314.

Nishiyama A (2007) Polydendrocytes: NG2 cells with many roles in development and repair of the CNS. Neuroscientist 13:62-76.

Nishiyama A, Komitova M, Suzuki R, Zhu X (2009) Polydendrocytes (NG2 cells): multifunctional cells with lineage plasticity. Nat Rev Neurosci 10:9-22.

Nowakowski RS, Lewin SB, Miller MW (1989) Bromodeoxyuridine immunohistochemical determination of the lengths of the cell cycle and the DNA-synthetic phase for an anatomically defined population. J Neurocytol 18:311-318.

Nussbaum JL, Espinosa de los MA, Pari FM, Doerr-Schott J, Roussel G, Neskovic NM (1988) A morphological and biochemical study of the myelin-like membrane structures formed in cultures of pure oligodendrocytes. Int J Dev Neurosci 6:395-408.

Orentas DM, Hayes JE, Dyer KL, Miller RH (1999) Sonic hedgehog signaling is required during the appearance of spinal cord oligodendrocyte precursors. Development 126:2419-2429.

Park J, Liu B, Chen T, Li H, Hu X, Gao J, Zhu Q, Qiang B, Yuan J, Peng X, Qiu M (2008) Disruption of Nectin-Like 1 cell adhesion molecule leads to delayed axonal myelination in the CNS. J Neurosci 28(48):12815-12819

Pena LL, Nieto AI, Perez-Alenza D, Cuesta P, Castano M (1998) Immunohistochemical detection of Ki-67 and PCNA in canine mammary tumors: relationship to clinical and pathologic variables. J Vet Diagn Invest 10:237-246.

Poncet C, Soula C, Trousse F, Kan P, Hirsinger E, Pourquie O, Duprat AM, Cochard P (1996) Induction of oligodendrocyte progenitors in the trunk neural tube by ventralizing signals: effects of notochord and floor plate grafts, and of sonic hedgehog. Mech Dev 60:13-32.

Pringle N, Collarini EJ, Mosley MJ, Heldin CH, Westermark B, Richardson WD (1989) PDGF A chain homodimers drive proliferation of bipotential (O-2A) glial progenitor cells in the developing rat optic nerve. EMBO J 8:1049-1056.

Pringle NP, Mudhar HS, Collarini EJ, Richardson WD (1992) PDGF receptors in the rat CNS: during late neurogenesis, PDGF alpha-receptor expression appears to be restricted to glial cells of the oligodendrocyte lineage. Development 115:535-551.

Pringle NP, Richardson WD (1993) A singularity of PDGF alpha-receptor expression in the dorsoventral axis of the neural tube may define the origin of the oligodendrocyte lineage. Development 117:525-533.

Pringle NP, Yu WP, Guthrie S, Roelink H, Lumsden A, Peterson AC, Richardson WD (1996) Determination of neuroepithelial cell fate: induction of the oligodendrocyte lineage by ventral midline cells and sonic hedgehog. Dev Biol 177:30-42.

Psachoulia K, Jamen F, Young KM, Richardson WD (2009) Cell cycle dynamics of NG2 cells in the postnatal and ageing brain. Neuron Glia Biol 5:57-67.

Quallo MM, Price CJ, Ueno K, Asamizuya T, Cheng K, Lemon RN, Iriki A (2009) Gray and white matter changes associated with tool-use learning in macaque monkeys. Proc Natl Acad Sci U S A 106:18379-18384.

Raff MC, Miller RH, Noble M (1983) A glial progenitor cell that develops in vitro into an astrocyte or an oligodendrocyte depending on culture medium. Nature 303:390-396.

Ramesh V (2004) Merlin and the ERM proteins in Schwann cells, neurons and growth cones. Nat Rev Neurosci 5:462-470.

Reynolds R, Hardy R (1997) Oligodendroglial progenitors labeled with the O4 antibody persist in the adult rat cerebral cortex in vivo. J Neurosci Res 47:455-470.

Reynolds R, Dawson M, Papadopoulos D, Polito A, Di Bello IC, Pham-Dinh D, Levine J (2002) The response of NG2-expressing oligodendrocyte progenitors to demyelination in MOG-EAE and MS. J Neurocytol 31:523-536.

Richardson WD, Pringle N, Mosley MJ, Westermark B, Dubois-Dalcq M (1988) A role for platelet-derived growth factor in normal gliogenesis in the central nervous system. Cell 53:309-319.

Richardson WD, Smith HK, Sun T, Pringle NP, Hall A, Woodruff R (2000) Oligodendrocyte lineage and the motor neuron connection. Glia 29:136-142.

Richter-Landsberg C, Gorath M (1999) Developmental regulation of alternatively spliced isoforms of mRNA encoding MAP2 and tau in rat brain oligodendrocytes during culture maturation. J Neurosci Res 56:259-270.

Rivers LE, Young KM, Rizzi M, Jamen F, Psachoulia K, Wade A, Kessaris N, Richardson WD (2008) PDGFRA/NG2 glia generate myelinating oligodendrocytes and piriform projection neurons in adult mice. Nat Neurosci 11:1392-1401.

Rowitch DH, Lu QR, Kessaris N, Richardson WD (2002) An 'oligarchy' rules neural development. Trends Neurosci 25:417-422.

Saito M, Iwawaki T, Taya C, Yonekawa H, Noda M, Inui Y, Mekada E, Kimata Y, Tsuru A, Kohno K (2001) Diphtheria toxin receptor-mediated conditional and targeted cell ablation in transgenic mice. Nat Biotechnol 19:746-750.

Salter MG, Fern R (2005) NMDA receptors are expressed in developing oligodendrocyte processes and mediate injury. Nature 438:1167-1171.

Saneto RP, de VJ (1985) Characterization of cultured rat oligodendrocytes proliferating in a serum-free, chemically defined medium. Proc Natl Acad Sci U S A 82:3509-3513.

Scholz J, Klein MC, Behrens TE, Johansen-Berg H (2009) Training induces changes in white-matter architecture. Nat Neurosci 12:1370-1371.

Schwartz BR, Pinkus G, Bacus S, Toder M, Weinberg DS (1989) Cell proliferation in non-Hodgkin's lymphomas. Digital image analysis of Ki-67 antibody staining. Am J Pathol 134:327-336.

Scott RJ, Hall PA, Haldane JS, van NS, Price Y, Lane DP, Wright NA (1991) A comparison of immunohistochemical markers of cell proliferation with experimentally determined growth fraction. J Pathol 165:173-178.

Shapiro LA, Ng KL, Kinyamu R, Whitaker-Azmitia P, Geisert EE, Blurton-Jones M, Zhou QY, Ribak CE (2007) Origin, migration and fate of newly generated neurons in the adult rodent piriform cortex. Brain Struct Funct 212:133-148.

Shen S, Li J, Casaccia-Bonnefil P (2005b) Histone modifications affect timing of oligodendrocyte progenitor differentiation in the developing rat brain. J Cell Biol 169:577-589.

Shen S, Sandoval J, Swiss VA, Li J, Dupree J, Franklin RJ, Casaccia-Bonnefil P (2008) Age-dependent epigenetic control of differentiation inhibitors is critical for remyelination efficiency. Nat Neurosci 11:1024-1034.

Shen S, Liu A, Li J, Wolubah C, Casaccia-Bonnefil P (2008) Epigenetic memory loss in aging oligodendrocytes in the corpus callosum. Neurobiol Aging 29:452-463.

Sherman DL, Brophy PJ (2005) Mechanisms of axon ensheathment and myelin growth. Nat Rev Neurosci 6:683-690.

Shi J, Marinovich A, Barres BA (1998) Purification and characterization of adult oligodendrocyte precursor cells from the rat optic nerve. J Neurosci 18:4627-4636.

Shields SA, Blakemore WF, Franklin RJ (2000) Schwann cell remyelination is restricted to astrocyte-deficient areas after transplantation into demyelinated adult rat brain. J Neurosci Res 60:571-578.

Siitonen SM, Kallioniemi OP, Isola JJ (1993) Proliferating cell nuclear antigen immunohistochemistry using monoclonal antibody 19A2 and a new antigen retrieval technique has prognostic impact in archival paraffin-embedded node-negative breast cancer. Am J Pathol 142:1081-1089.

Sim FJ, Zhao C, Penderis J, Franklin RJ (2002) The age-related decrease in CNS remyelination efficiency is attributable to an impairment of both oligodendrocyte progenitor recruitment and differentiation. J Neurosci 22:2451-2459.

Simons M, Trotter J (2007) Wrapping it up: the cell biology of myelination. Curr Opin Neurobiol 17:533-540.

Soula C, Danesin C, Kan P, Grob M, Poncet C, Cochard P (2001) Distinct sites of origin of oligodendrocytes and somatic motoneurons in the chick spinal cord: oligodendrocytes arise from Nkx2.2-expressing progenitors by a Shh-dependent mechanism. Development 128:1369-1379.

Srinivas S, Watanabe T, Lin CS, William CM, Tanabe Y, Jessell TM, Costantini F (2001) Cre reporter strains produced by targeted insertion of EYFP and ECFP into the ROSA26 locus. BMC Dev Biol 1:4.

Stallcup WB, Beasley L (1987) Bipotential glial precursor cells of the optic nerve express the NG2 proteoglycan. J Neurosci 7:2737-2744.

Sturrock RR (1980) Myelination of the mouse corpus callosum. Neuropathol Appl Neurobiol 6:415-420.

Suzuki N, Bekkers JM (2006) Neural coding by two classes of principal cells in the mouse piriform cortex. J Neurosci 26:11938-11947.

Tamura Y, Kataoka Y, Cui Y, Takamori Y, Watanabe Y, Yamada H (2007) Multi-directional differentiation of doublecortin- and NG2-immunopositive progenitor cells in the adult rat neocortex in vivo. Eur J Neurosci 25:3489-3498.

Taveggia C, Feltri ML, Wrabetz L (2010) Signals to promote myelin formation and repair. Nat Rev Neurol 6:276-287

Tekki-Kessaris N, Woodruff R, Hall AC, Gaffield W, Kimura S, Stiles CD, Rowitch DH, Richardson WD (2001) Hedgehog-dependent oligodendrocyte lineage specification in the telencephalon. Development 128:2545-2554.

Toschi L, Bravo R (1988) Changes in cyclin/proliferating cell nuclear antigen distribution during DNA repair synthesis. J Cell Biol 107:1623-1628.

Tropepe V, Craig CG, Morshead CM, van der Kooy D (1997) Transforming growth factor-alpha null and senescent mice show decreased neural progenitor cell proliferation in the forebrain subependyma. J Neurosci 17:7850-7859.

Trotter J, Karram K, Nishiyama A (2010) NG2 cells: Properties, progeny and origin. Brain Res Rev.

Ullen F, Forsman L, Blom O, Karabanov A, Madison G (2008) Intelligence and variability in a simple timing task share neural substrates in the prefrontal white matter. J Neurosci 28:4238-4243.

Vallstedt A, Klos JM, Ericson J (2005) Multiple dorsoventral origins of oligodendrocyte generation in the spinal cord and hindbrain. Neuron 45:55-67.

van HP, Calver AR, Richardson WD (2001) Control of progenitor cell number by mitogen supply and demand. Curr Biol 11:232-241.

Watanabe M, Toyama Y, Nishiyama A (2002) Differentiation of proliferated NG2-positive glial progenitor cells in a remyelinating lesion. J Neurosci Res 69:826-836.

Wegner M (2001) Expression of transcription factors during oligodendroglial development. Microsc Res Tech 52:746-752.

Wilkins A, Chandran S, Compston A (2001) A role for oligodendrocyte-derived IGF-1 in trophic support of cortical neurons. Glia 36:48-57.

Wilkins A, Majed H, Layfield R, Compston A, Chandran S (2003) Oligodendrocytes promote neuronal survival and axonal length by distinct intracellular mechanisms: a novel role for oligodendrocyte-derived glial cell line-derived neurotrophic factor. J Neurosci 23:4967-4974.

Wilson SS, Baetge EE, Stallcup WB (1981) Antisera specific for cell lines with mixed neuronal and glial properties. Dev Biol 83:146-153.

Wolf SA, Kronenberg G, Lehmann K, Blankenship A, Overall R, Staufenbiel M, Kempermann G (2006) Cognitive and physical activity differently modulate disease progression in the amyloid precursor protein (APP)-23 model of Alzheimer's disease. Biol Psychiatry 60:1314-1323.

Wolswijk G, Noble M (1989) Identification of an adult-specific glial progenitor cell. Development 105:387-400.

Wolswijk G, Riddle PN, Noble M (1991) Platelet-derived growth factor is mitogenic for O-2Aadult progenitor cells. Glia 4:495-503.

Wolswijk G, Noble M (1992) Cooperation between PDGF and FGF converts slowly dividing O-2Aadult progenitor cells to rapidly dividing cells with characteristics of O-2Aperinatal progenitor cells. J Cell Biol 118:889-900.

Woodruff RH, Fruttiger M, Richardson WD, Franklin RJ (2004) Platelet-derived growth factor regulates oligodendrocyte progenitor numbers in adult CNS and their response following CNS demyelination. Mol Cell Neurosci 25:252-262.

Wren D, Wolswijk G, Noble M (1992) In vitro analysis of the origin and maintenance of O-2Aadult progenitor cells. J Cell Biol 116:167-176.

Young KM, Mitsumori T, Pringle N, Grist M, Kessaris N, Richardson WD (2010) An Fgfr3-iCreER(T2) transgenic mouse line for studies of neural stem cells and astrocytes. Glia 58:943-953.

Zahr NM, Rohlfing T, Pfefferbaum A, Sullivan EV (2009) Problem solving, working memory, and motor correlates of association and commissural fiber bundles in normal aging: a quantitative fiber tracking study. Neuroimage 44:1050-1062.

Zeller NK, Behar TN, Dubois-Dalcq ME, Lazzarini RA (1985) The timely expression of myelin basic protein gene in cultured rat brain oligodendrocytes is independent of continuous neuronal influences. J Neurosci 5:2955-2962.

Zhang B, Cao Q, Guo A, Chu H, Chan YG, Buschdorf JP, Low BC, Ling EA, Liang F (2005) Juxtanodin: an oligodendroglial protein that promotes cellular arborization and 2',3'-cyclic nucleotide-3'-phosphodiesterase trafficking. Proc Natl Acad Sci U S A 102:11527-11532.

Zhao M, Momma S, Delfani K, Carlen M, Cassidy RM, Johansson CB, Brismar H, Shupliakov O, Frisen J, Janson AM (2003) Evidence for neurogenesis in the adult mammalian substantia nigra. Proc Natl Acad Sci U S A 100:7925-7930.

Zhu X, Hill RA, Nishiyama A (2008) NG2 cells generate oligodendrocytes and gray matter astrocytes in the spinal cord. Neuron Glia Biol 4:19-26.

Zhu X, Bergles DE, Nishiyama A (2008) NG2 cells generate both oligodendrocytes and gray matter astrocytes. Development 135:145-157.

Ziskin JL, Nishiyama A, Rubio M, Fukaya M, Bergles DE (2007) Vesicular release of glutamate from unmyelinated axons in white matter. Nat Neurosci 10:321-330.

Appendix I

Media and Solutions

Blocking solution	10% (v/v) sheep or horse serum, 0.1% (v/v) Triton X-100 in PBS
Denhardt's Solution	1% Ficoll 400, 1% polyvinylpyrrolidine, 1% bovine serum albumin
EDTA	0.5M Na_2EDTA, pH8.0
EdU reaction cocktail	For 500µl: 43µl 10x reaction buffer, 20µl $CuSO_4$, 1.2µl Alexa Fluor® 647 azide, 5µl 10x reaction buffer additive, dH_2O
Extraction Buffer	100mM Tris-HCl pH8.5, 5mM EDTA pH8.0, 200mM NaCl, 0.2% SDS
LB (1 litre)	10g bacto-tryptone, 5g yeast extract, 10g NaCl
MABT	0.5M maleic acid, 0.75M NaCl, 1M NaOH, 0.5% Tween-20

Microinjection Buffer	1M Tris-HCl pH7.5, 0.5M EDTA pH8.0, 5M NaCl
NBT	1g 4-nitro blue tetrazolium chloride crystals, 7ml dimethyl formamide, 3ml dH_2O
P1 Solution	50mM glucose, 25mM Tris pH8.0, 10mM EDTA pH8.0
P2 Solution	0.2N NaOH, 1% SDS
P3 Solution	0.3M Potassium Acetate, 11.5% w/v glacial acetic acid
PBS	0.2 M phosphate, 1.5 M NaCl, pH7.5
10x PCR Buffer	500mM KCl, 100mM Tris-HCL pH9.0, 1% (v/v) Triton X-100
Protease K	10mM Tris pH8, 0.1M EDTA pH8, 0.5% SDS
Salt solution	2M NaCl, 50mM EDTA, 100mM Tris-HCl pH7.5, 50mM $NaH_2PO_42H_2O$, 50mM Na_2HPO_4, DEPC treated
SATO	DMEM-Glutamax medium (Invitrogen) supplemented with: 100µg/ml Transferrin (Sigma), 100µg/ml BSA (Sigma), 60ng/ml Progesterone (Sigma), 40ng/ml Sodium selenite (Sigma), 16µg/ml Putrescine (Sigma), 5µg/ml Insulin (Sigma), 1x Penicillin/Streptomycin (Invitrogen), 10ng/ml bFGF (Invitrogen), 10ng/ml CNTF (Peprotech EC Ltd), 10ng/ml PDGF-AA (R & D Systems Europe), 1ng/ml NT3 (Peprotech EC Ltd), 10µM Forskolin (Enzo), 5µg/ml N-acetyl-L-cysteine (Sigma), 1x B27 Supplement (Invitrogen)
SSC	3.0 M NaCl, 0.3 M sodium citrate, pH7.0

Staining Buffer	0.1M NaCl, 0.05M $MgCl_2$, 0.1M Tris pH9.5, 0.01% Tween-20
TAE	400mM Tris, 1mM EDTA, 0.35% glacial acetic acid
TBE	45mM Tris-borate, 1mM EDTA pH8.0
TE	5mM Tris pH7.5, 2.5mM EDTA pH8
Wash solution	50% formamide, 1x SSC, 0.1% Tween-20